THERMOMECHANICAL TRAINING AND CHARACTERIZATION OF NI-TI-HF AND NI-TI-HF-CU HIGH TERMPERATURE SHAPE MEMEORY ALLOYS

by

Chantz Michael Denowh

A thesis submitted in partial fulfillment
of the requirements for the degree

of

Master of Science

in

Mechanical Engineering

MONTANA STATE UNIVERSITY
Bozeman, Montana

April 2011

APPROVAL

of a thesis submitted by

Chantz Michael Denowh

This thesis has been read by each member of the thesis committee and has been found to be satisfactory regarding content, English usage, format, citation, bibliographic style, and consistency and is ready for submission to The Graduate School.

Dr. David A. Miller

Approved for the Department of Mechanical and Industrial Engineering

Dr. Christopher H.M. Jenkins

Approved for The Graduate School

Dr. Carl A. Fox

STATEMENT OF PERMISSION TO USE

In presenting this thesis in partial fulfillment of the requirements for a master's degree at Montana State University, I agree that the Library shall make it available to borrowers under rules of the Library.

If I have indicated my intention to copyright this thesis by including a copyright notice page, copying is allowable only for scholarly purposes, consistent with "fair use" as prescribed in the U.S. Copyright Law. Requests for permission for extended quotation from or reproduction of this thesis in whole or in parts may be granted only by the copyright holder.

Chantz Michael Denowh

April 2011

DEDICATION

I would like to dedicate this work to my Grandmother Doris Erickson. Since I've been a little kid, Grams has always encouraged me to follow whatever path my heart desires. And win or lose, she has always let me know how proud she is of me. They say the people you grow up around make you into the person you are today, and I strongly believe without Grams in my life I wouldn't be where I am today. I thank God for putting her in my life, and hope she always knows how much I love her.

TABLE OF CONTENTS

TABLE OF CONTENTS – CONTINUED

LIST OF TABLES

LIST OF FIGURES

Figure Page

LIST OF FIGURES – CONTINUED

Figure Page

LIST OF FIGURES - CONTINUED

Figure Page

LIST OF FIGURES - CONTINUED

Figure Page

LIST OF FIGURES - CONTINUED

Figure Page

LIST OF EQUATIONS

Equation Page

ABSTRACT

Nickel-Titanium (NiTi) is the most commonly used Shape Memory Alloy (SMA) for actuator applications. Typical SMA actuators use changes in temperature to initiate solid to solid phase transformations resulting in macroscopic material deformations; though NiTi is limited to temperature changes below 100°C. This eliminates high temperature applications of NiTi actuators. To expand the design window of SMAs, many high temperature NiTi based SMAs have been developed by adding ternary elements to the NiTi matrix. The additions result in degradation of the shape memory behaviors and their usefulness as actuators is still in question. The purpose of this research is to characterize and train two recently developed high temperature SMAs, $NiTi_{29.7}Hf_{20}$ and $NiCu_5Ti_{29.7}Hf_{20}$, to determine their effectiveness as linear actuators.

Shape memory effect (SME) and superelastic tests were used to characterize the materials behavior followed by thermomechanical training at a constant stress. The SME test resulted in no martensite detwinning plateau and a non-linear stress-strain curve implying the simultaneous occurrence of slip and martensite reorientation. The superelastic tests also show an austenitic yield stress above 600 MPa. Thermomechanical training resulted in small amounts of plastic strain growth, and the development of two-way shape memory (TWSM). The TWSM results were fitted using the Bo & Lagoudas model, and is capable of predicting the actuation strains at other stresses. The results support the conclusion that hafnium distorts martensite slip planes, and $(Ti,Hf)_2Ni$ and $(Ti,Hf)_3Ni_4$ precipitates form during aging and annealing. The distorted slip planes cause slip and martensite reorientation to occur simultaneously. This develops a strong stress field during training within the first few cycles. The stress field develops TWSM, but limits further plastic growth and TWSM development. The precipitate formation increases material strength, as seen in the superelastic loading, but also embrittles the material. Thermomechanical training of an annealed specimen resulted in a brittle failure after several thermal cycles due to the growth of particulate size during annealing. The two alloys are ideally suited for high temperature actuators. TWSM was trained into the material and the transformation temperatures are higher than that of NiTi, but low enough to avoid annealing and problematic creep temperatures.

.

INTRODUCTION

Over the past few decades, interest in using Shape Memory Alloys (SMAs) as high force/displacement actuators has increased because of their small size, simplicity, and low weight; making SMAs ideal to replace pneumatic, hydraulic, and solenoid actuator systems of today. Their acceptance as a viable actuator though is hindered by a lack understanding of SMA behavior, no set standards for training, and only functioning in certain temperature environments.

Shape memory alloys are thermoelastic materials that experience a diffusionless or displacive, solid to solid, reversible phase transformation from a high temperature austenitic phase to a low temperature martensitic phase. Alloys that are categorized as shape memory alloys include AuCd, InTl, CuZn, CuAlNi, CuZnAl, NiTi, and Fe-based alloys among others, with nickel-titanium (NiTi) being the most common and the concentration of this research. The two phenomena that categorize a material as a shape memory alloy are the shape memory effect and superelasticity. The shape memory effect is where the alloy is capable of recovering deformations from its low temperature martensite phase by heating into the high temperature austenite phase. Superelasticity takes place in the high temperature, austenite phase where the alloy can have large, non-linear deformations (up to 18%) thru a stress induced phase transformation and recover these deformations upon unloading (Otsuka & Wayman, 1998).

To become an actuator, a SMA must go through a process called training. By training, the alloy memorizes specific configurations through transformation by activating a temperature change, inducing a stress state, or a combination of the two

(Becker, 2010). This transformation can generate substantial forces and displacements (500 MPa at 4-8% strain), and has the ability to repeatedly recover these strains while the forces are still being applied (Tobushi, Ohashi, Saida, Hori, & Shirai, 1992). NiTi is the most commonly used shape memory alloy for a variety of reasons. Other alloys, such as CuZnAl, CuAlNi, and Fe-based alloys have reduced shape memory properties and difficulties during wire production. NiTi also has excellent corrosion resistance (Mertmann & Vergani, 2008). The downside to NiTi is it is limited to applications below 100 °C (Otsuka & Wayman, 1998). This reduces the applications for NiTi to low temperatures, and decreases the actuation response speed due to the length of time it takes to reach the martensite transformation temperature.

To expand the use of NiTi above temperatures of 100 °C, and aid in the development of a faster response actuator, additional ternary elements are added to the NiTi matrix which results in increased transformation temperatures. These alloys are called high temperature shape memory alloys. Many Ni-Ti-X (X being the additional element) high temperature shape memory alloys have been developed including X - Zr, Hf, Pd, Pt in different atomic weight percent combinations. The ternary elements Zr and Hf take the place of titanium while Pd and Pt are substituted for nickel. The addition of these elements has favorable outcomes for the transformation temperatures, but there are also unavoidable consequences (Otsuka & Wayman, 1998; Wojcik, 2009). Typically, there is a reduction of shape memory properties, and the austenite transformation temperatures of some element combinations are now high enough that creep and annealing become problematic (Kumar & Lagoudas, 2010).

New high temperature SMAs are developed regularly, but the usefulness of the alloy as an actuator is difficult to gage because there is no standard for characterizing and training SMAs into actuators. The purpose of the following work is expand on a characterization and training procedure developed for NiTi SMA actuators by M. Becker and D.A Miller to high temperature alloys (Becker, 2010). Two newly developed high temperature SMAs, $NiTi_{29.7}Hf_{20}$ and $NiCu_5Ti_{29.7}Hf_{20}$ at. wt%, were first characterized by shape memory effect and superelastic tests to find material parameters for thermomechanical training. The alloys were then thermomechanically trained into actuators by thermal cycles under a constant applied stress and the resulting actuation strains were fit to model commonly used to for NiTi actuators. The transformation temperatures were then analyzed to predict if creep or annealing was likely to occur.

BACKGROUND

Initial Discovery

A general definition of a Shape Memory Alloy (SMA) is a metallic alloy that can undergo martensitic phase transformations as a result of applied thermomechanical loads, and are capable of recovering permanent strains when heated above a certain temperature (Patoor, Lagoudas, Entchev, Brinson, & Gao, 2006). Nickel-Titanium (NiTi) is the most common SMA and is the main area of interest in this work. For a NiTi alloy to exhibit shape memory and superelastic properties, it must contain 49.5 – 57% nickel by at. wt% as shown in Figure 1. Above or below these limits, the alloy no longer exhibits its unique thermomechanical properties. NiTi has a very ordered atomic packing structure with alternating nickel to titanium atoms. From Figure 1, a NiTi SMA can also have combinations of Ti_2Ni and $TiNi_3$ based on composition and temperature. The different phase relationships of Nickel and Titanium have been known for some time, but the discovery of their unique properties occurred relatively recently.

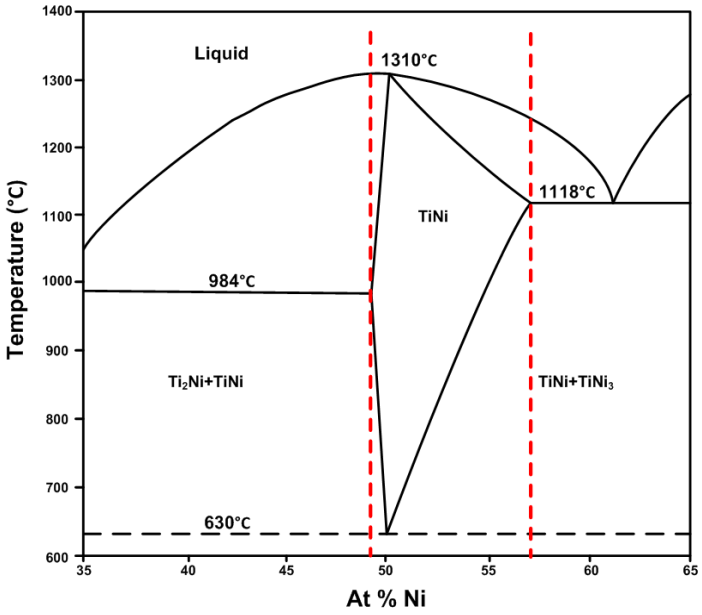

Figure 1: Condensed phase diagram of nickel-titanium, red lines signify where shape memory phenomena occur (based from Massalski, T.B., Binary Alloy Phase Diagrams)

William J. Buehler discovered nickel-titanium's shape memory properties in 1959 while researching different materials for use on the nose cone of the U.S. Navy's Polaris reentry vehicle. For this project, he cast an equiatomic nickel-titanium alloy and named the new material system NITINOL for **Ni**ckel **Ti**tanium **N**aval **O**rdnance **L**aboratory. The discovery of NITINOL's unique properties came later when after arc-casting several NITINOL bars, Buehler purposefully dropped a cooled bar to quickly test the damping capacity of the alloy. Disappointed in the dull thud the cold bar made, he also dropped the other bars that were still cooling. He noticed the warm bars rang "brilliantly," which he immediately recognized as a major atomic structural change (Kauffman & Mayo, 1996). The change in the acoustic properties of the NITINOL bars Buehler noticed was the reversible transformation of the material from austenite to martensite.

Austenite / Martensite Crystalline Structure

Austenite, the high temperature, parent phase has an ordered body centered cubic crystal structure as shown in Figure 2 (titanium represented by smaller, grey spheres). With this packing structure, the austenite phase contains 6 slip planes, each with 2 directions resulting in 12 slip systems.

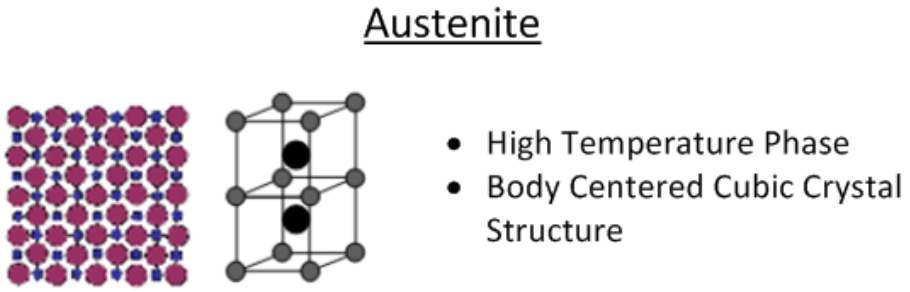

Figure 2: Austenite crystal structure (Volk & Lagoudas, 2005)

The low temperature martensite phase has a monoclinic, twinned crystal structure with 24 variants. Twinned martensite occurs in individual grains where rows of atoms form a mirror image across a twin boundary as shown in Figure 3. All 24 martensite variants are possible in a NiTi material system, and with no applied stress they will align themselves in the easiest manner by twinning. But they can be aligned with the application of an applied stress by a shear-like mechanism called detwinning. When a stress is applied and the crystalline structure detwinns, the mirror images across the twin boundary align (see Figure 3). The mirror images align in the grains internal lattice; this allows grains to internally change while the interface between grains remains the same. It is important to note that no change in the crystal structure occurs, rather a reorientation of the lattice. This implies twinning is different from slip. Both twinning and slip

involve a shearing of the lattice, but slip occurs on individual lattice planes and may be many times larger than the lattice spacing. Deformation by twinning is uniformly distributed over a volume. The atoms only move a fraction of an interatomic spacing relative to each other. Even with only moving a fraction of an interatomic space, a material that is heavily twinned, such as NiTi, will have large macroscopic deformations (Reed-Hill & Abbaschian, 1992).

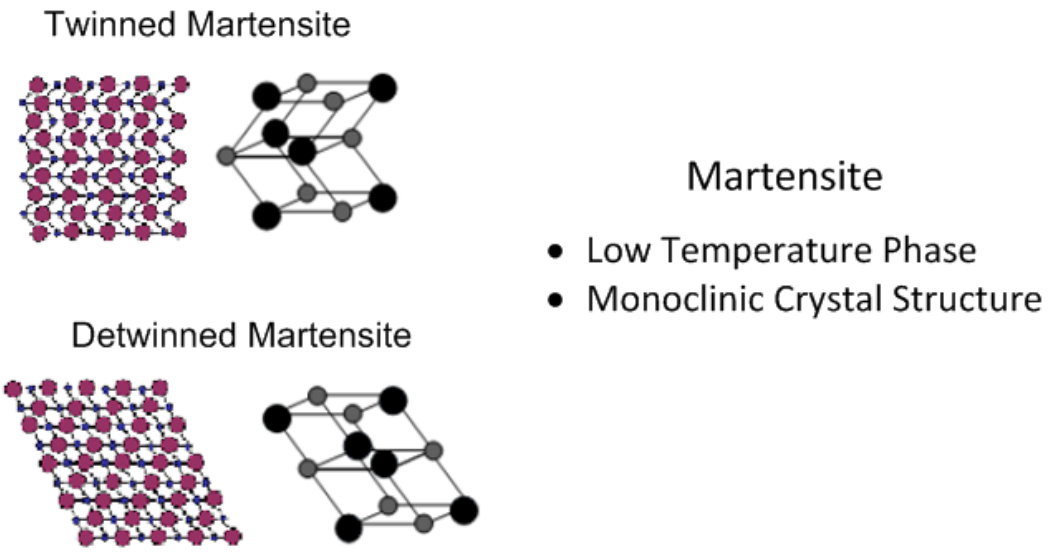

Figure 3: Martensite crystal structure (Volk & Lagoudas, 2005)

The martensite detwinning process is best illustrated by a stress-strain diagram as shown in Figure 4. Initially the twinned martensite behaves elastically (region 1 of Figure 4), until it reaches a critical value where detwinning occurs in region 2. The reason detwinning occurs before any slip is the interfacial energy between twin boundaries is much smaller when compared to grain boundaries (Reed-Hill & Abbaschian, 1992). Large strains ranging from 4 to 6% are possible during detwinning

with no increase in stress (Y. N. Liu, Liu, & Van Humbeeck, 1998). Once the martensite is fully detwinned, it behaves elastically again as in region 3. This is the elasticity of the detwinned martensite. After further loading, the detwinned martensite will plastically deform by slip as in region 4. The values of elastic modulus for regions 1 and 3 vary from test to test, but the modulus of region 3 is generally lower than region 1. The method of deformation in region 3 isn't well established, but generally assumed to have continued martensite detwinning which lowers the modulus (Y. Liu & Xiang, 1998).

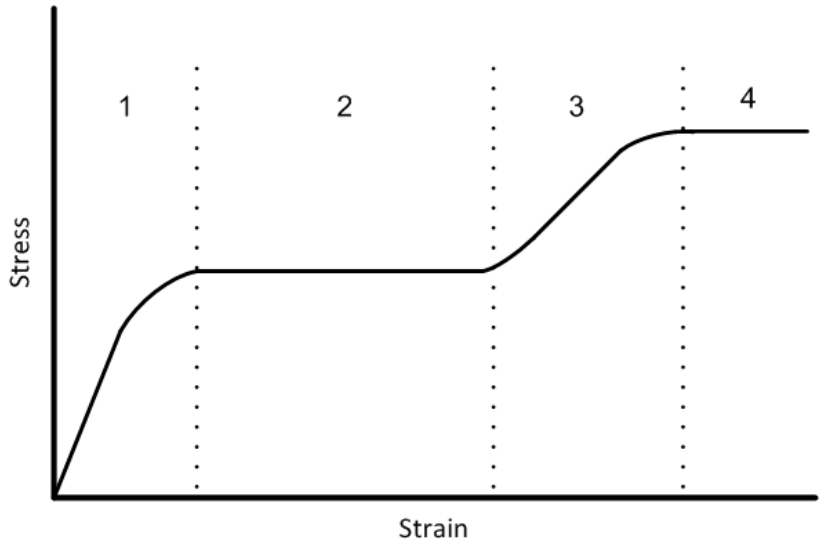

Figure 4: Martensite stress vs. strain

Shape Memory Alloys as Thermoelastic Materials

The driving force behind the forward phase transformation, austenite to martensite, and the reverse transformation, martensite to austenite, is the free-energy of the material system. When the temperature of a SMA is raised or lowered at some point it will pass through an equilibrium temperature separating the stability ranges of the two

phases as seen in Figure 5. When the temperature reaches this equilibrium point, the free energy of the SMA will be lowered if it changes phase. The free energy difference is the driving force for the transformation (Reed-Hill & Abbaschian, 1992). A latent heat is also absorbed or released during the transformation depending on a forward or reverse transformation. The forward transformation (austenite to martensite) releases heat while the reverse transformation (martensite to austenite) absorbs it. An increase or decrease in stress also effects at what temperature a transformation takes place. An increase in internal stress locks in the crystal variants, so it takes more energy (higher temperature) to drive the phase change. During the phase transformations, the displacement of the individual atoms is small relative to their neighbors. There is no change in composition and no diffusion required to complete the transformation; thus the phase change is not time dependent and practically instantaneous.

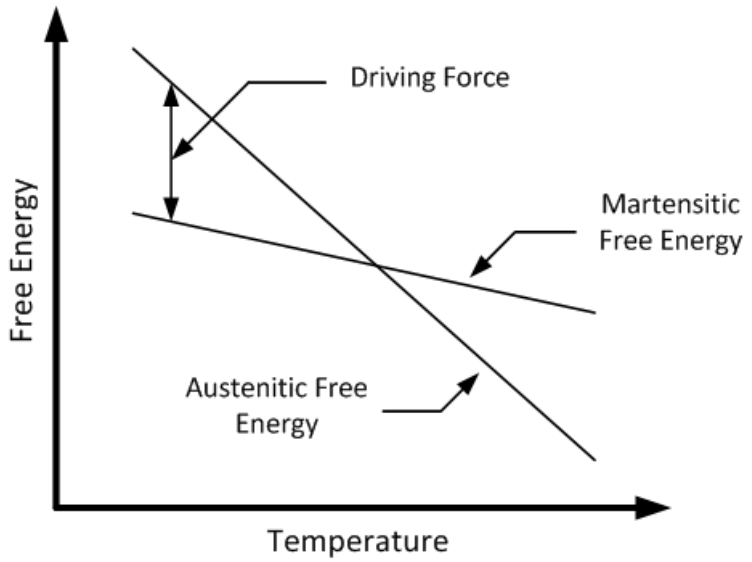

Figure 5: Temperature dependence of free energies for the martensitic and austenitic phases (D. Miller, 2000)

Since the phase changes depend on thermal and elastic conditions, they are easily visualized on a stress/temperature space diagram as shown in Figure 6. The equilibrium transformation temperatures are split into an austenite/martensite start temperature (A_s / M_s) and austenite/martensite finish temperature (A_f / M_f). The start temperature designates the temperature the martensite or austenite will start forming while the finish temperature signifies when the SMA is completely one phase. In a perfect crystalline structure, the start and finish temperatures would be the same (Figure 5), but discontinuities, dislocations, and stacking faults inherent in any material system cause the material to transform non-uniformly; thus resulting in the start and finish temperatures. The critical temperature lines shown in Figure 6 represent the typical trend for phase transformations zones. Austenite and martensite transformation zones are not always parallel, and in some cases can overlap depending on the alloy and processing. As previously stated, an increase in stress will also increase the temperature required to drive the phase transformation; a noticeable trend in Figure 6. There are also two dotted lines included in the stress-temperature space that signify detwinning start (σ_{ds}) and detwinning finish (σ_{df}). Once the material crosses the detwinning start stress, it will start to accumulate permanent strain from detwinned martensite which is not recovered from unloading. The red lines in Figure 6 represent the different loading paths for an SMA. Each loading path exhibits different thermomechanical behaviors and are discussed in detail in the next section.

The transformation temperatures are a function of the alloy's composition and processing (Patoor, et al., 2006). The transformation temperatures of the NiTi alloy

system are very sensitive to the slightest change in composition. A deviation of 0.1 at. wt% can change the transformation temperature by 10°C (Fuentes, Gumpel, & Strittmatter, 2002). The transformation temperatures vary widely, but literature agrees the alloy's usefulness is limited to 100°C (Otsuka & Wayman, 1998). Internal defects can also affect the transformation temperatures. Cold working will act to increase the transformation temperatures by creating more defects in the material. Annealing thus decreases transformation temperatures by relieving internal stresses and defects.

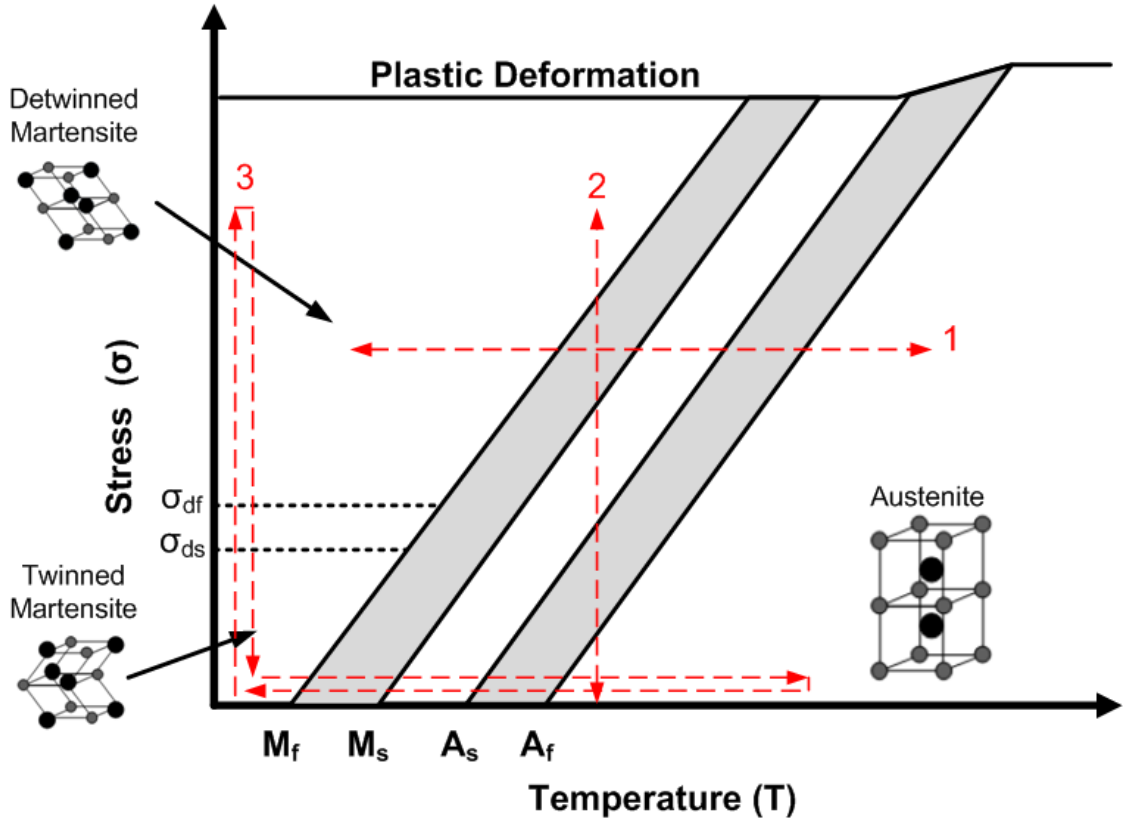

Figure 6: Stress-temperature phase space

Loading Paths

Isobaric Thermal Cycles

Loading path 1 in Figure 6 illustrates isobaric thermal cycles, or thermally cycling the material at a constant stress. The phase transformations along this path are induced by changes in temperature only. The loading path and a typical strain-temperature diagram for isobaric thermal cycles is shown in Figure 7a and Figure 7b respectively with the critical points labeled in each figure. Following the path in Figure 7a, the material cools down from austenite and reaches point (a) which signifies the martensite start temperature. The material then continues to cool and transform with a positive net strain to point (b) which is the martensite finish temperature. At this point, the material is 100% martensite. Important to note is between martensite start and finish, the material contains both martensite and austenite. For the reverse transformation the material is heated to point (c), the austenite start temperature, and the material transforms with a negative net strain until it is completely austenite at point (d).

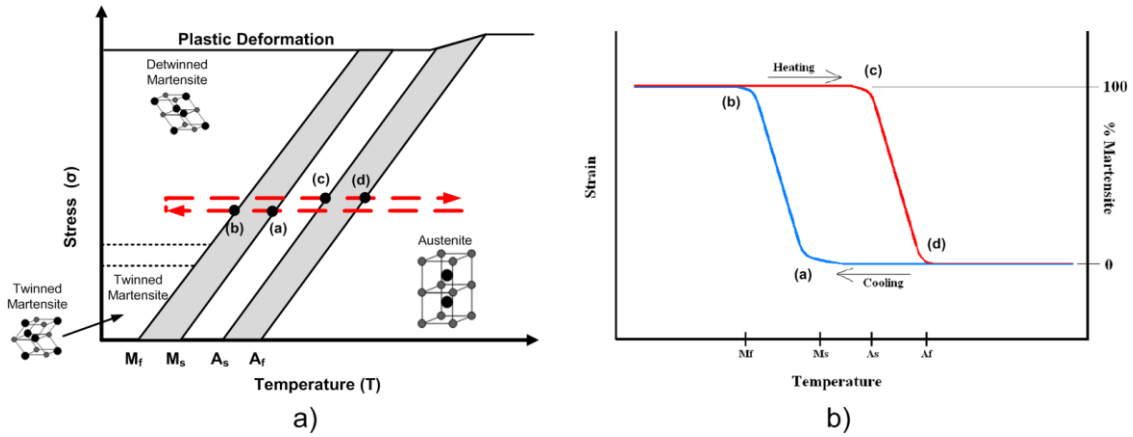

Figure 7: Isobaric thermal cycles loading path b) Isobaric strain-temperature

Superelasticity

Superelasticity (also known as pseudoelasticity) is represented on Figure 6 by loading path 2. Superelasticity allows for large, recoverable deformations from stress inducing martensite at a constant temperature. Figure 8b shows a typical stress-strain diagram for the superelastic effect. From Figure 8a, the material begins as 100% austenite. As it is loaded it will reach point (a), the martensite start temperature. Between points (a) and (b), there is a large plateau in the stress-strain diagram where strain increases with a small increase in stress. This deformation plateau is from the formation of stress induced martensite, and can result in a recoverable deformation of 5 to 7% (Miyazaki, Imai, Igo, & Otsuka, 1986; Yoon & Yeo, 2008) . When the stress is released, there is an initial elastic response of martensite from point (b) to (c) until the austenite start point is reached at (c). At this point, the martensite starts to transform back to austenite from point (c) to (d). At point (d), austenite finish, the material is once again 100% austenite and elastically returns to zero stress.

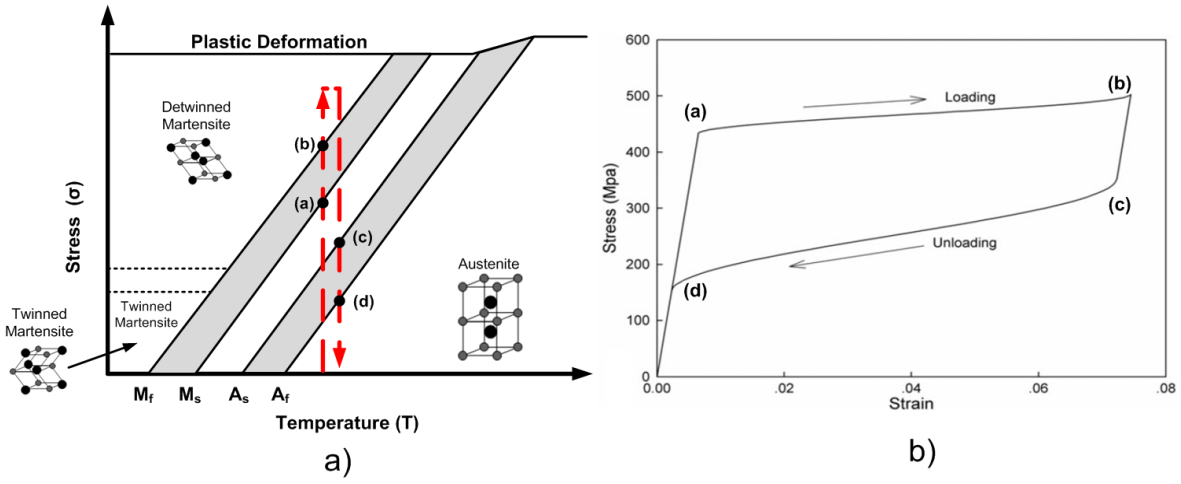

Figure 8: a) superelastic loading path b) superelastic stress-strain diagram (Zhou & Yoon, 2006)

Whether or not a NiTi SMA will exhibit superelasticity in the form of stress induced martensite depends on composition and processing. NiTi alloys with nickel content of 51 at wt% or higher exhibit superelasticity, but alloys with lower nickel content do not. Also, a NiTi SMA with a high amount of cold work would only exhibit superelasticity after heat treatment. This is due to raising the critical stress for slip by annealed the material; the material can reach a higher stress and induce martensite before it starts to plastically deform (Otsuka & Shimizu, 1986).

Shape Memory Effect

The shape memory effect (SME), loading path 3 in Figure 6, allows a SMA to recover a deformation from detwinning by activating a phase change into austenite. The process of one way shape memory effect is illustrated in Figure 9. A SMA starts as twinned martensite. It is then loaded to cause some or all of the martensite to detwinn resulting in a deformation. After the load is released, this deformation remains. It is recovered by heating the SMA into austenite. As the SMA transforms to austenite under stress free conditions, the deformation is recovered. Then as the material cools, it changes phase back into its original twinned martensite length. The loading path diagram and stress-strain diagram in Figure 10a and Figure 10b respectively shows the SME in more detail. Point (a) represents the detwinning start stress. Between points (a) and (b), a large deformation created. After point (b), the material is unloaded and the deformation is recovered by reheating through points (e) and (f). The detwinning martensite can lead to deformations of to 6-8%, which can then be recovered by reheating (Pappas, Bollas,

Parthenios, Dracopoulos, & Galiotis, 2007). If the SMA is constrained during the transformation from detwinned martensite to austenite, stresses as large as 700 MPa in some alloys are possible (Pappas, et al., 2007).

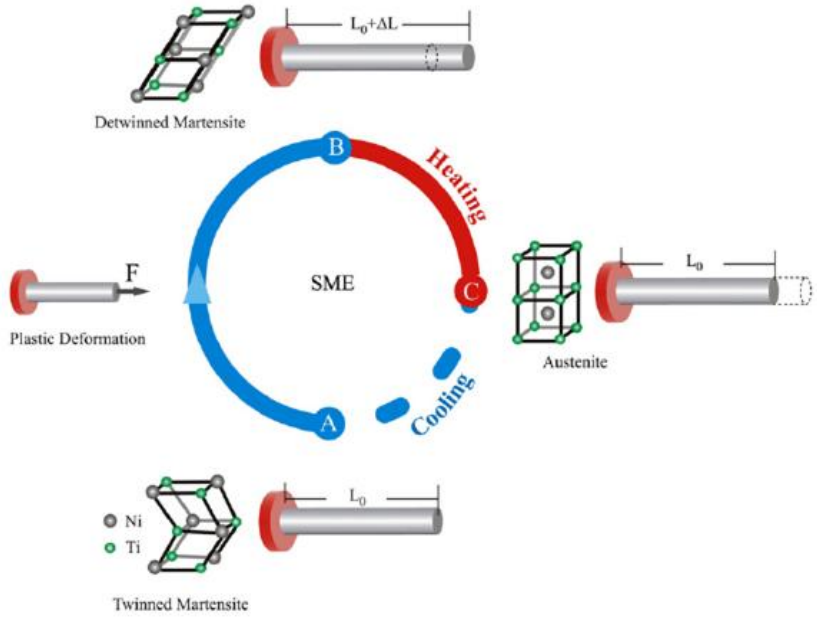

Figure 9: Shape memory effect (Pappas, et al., 2007)

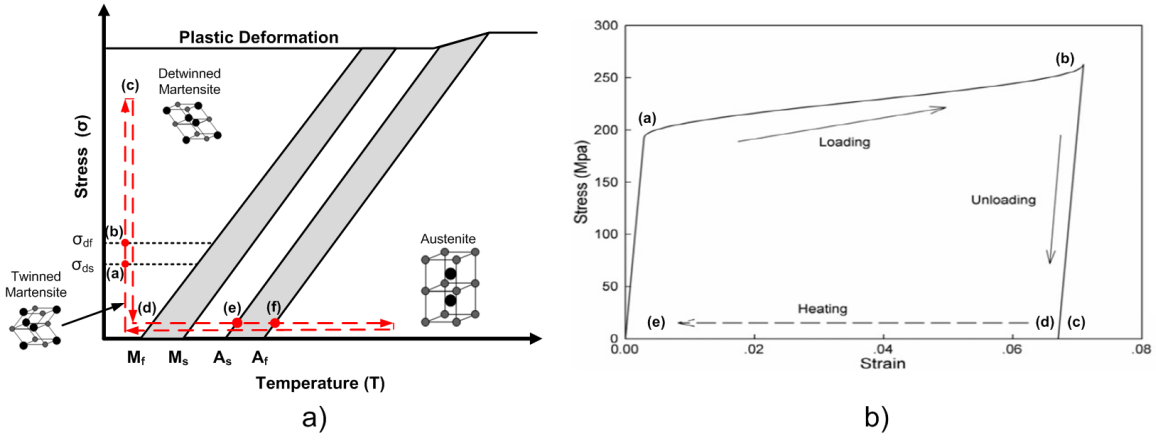

Figure 10: a) SME loading path b) Shape memory effect stress-strain diagram (Zhou & Yoon, 2006)

Two-way Shape Memory Effect

The shape memory effect described in the previous section is also known as one-way shape memory because it has a one-time deformation recovery. For an actuator, the SMA is "taught" or "trained" to remember both a hot and cold shape; this is known as two-way shape memory (TWSM). There are several methods for training a SMA and they will be discussed further in the next section, but the mechanism that causes the TWSM is the same. The purpose of training is to develop a local internal stress field and dislocation structure by plastically deforming the material. The dislocation structure guides the formation of martensite variants into preferred orientations. Since the dislocation structure forces the martensite to form in the same orientations every time, the net change in length will be the same for each phase transformation. The dislocations structure remains unchanged during repeated phase transformations; however, temperatures high enough for annealing will erode the dislocations and decay the TWSM (Becker, 2010; Y. O. Liu & McCormick, 1990; D. A. Miller & Lagoudas, 2000).

Thermomechanical Training

Training is required to develop the dislocation structure for two-way shape memory in a SMA. The reason for training and why a SMA is not immediately used as an actuator is large, non-recoverable strains are prone to develop in the material during a mechanical or thermal cycle. This phenomenon is known as Transformation Induced Plasticity (TrIP). Numerous studies have shown thermomechanical training is a viable method of eliminating or "saturating" TrIP (Becker, 2010; Lahoz, Gracia-Villa, &

Puertolas, 2002; Y. N. Liu, et al., 1998; D. Miller, 2000; Wada & Liu, 2008). The TrIP during training is usually large in the initial cycles, but begins to decline as the number of cycles increases. In this way, the TrIP "saturates" by continuous mechanical or thermal cycles and stable two-way memory effect is achieved. During training, full transformations from the two phases are required. Partial transformations into either phase will generate path dependence in the material effecting the resulting actuation strain. If SMA is properly trained by full transformations, the path dependence created by a partial transformation is reset by a full transformation and the SMA returns to its previously trained state (Wada & Liu, 2008). Physically, the partial transformations have little effect on the previously established dislocation structure.

Isobaric Training

The three methods used to train a SMA for positive TWSM each plastically deform the SMA by a mechanical or thermal cycle. Loading paths 1-3 in Figure 6 represent three methods of training. Loading path 1, isobaric thermal cycling, has been investigated heavily (Lahoz, et al., 2002; Luo & Abel, 2007; D. A. Miller & Lagoudas, 2000; Padula et al.) and is a popular thermomechanical training method as discussed later in this section. For this method, a SMA is loaded below the martensite plastic yield stress and then thermally cycles between martensite and austenite. A typical strain-temperature curve for isobaric training it pictured in Figure 11 where the amount of TrIP decreases after each cycle. It is predicted that at the end of each cycle, an increasing fraction of martensite is retained from dislocations increasing the local stress state. This retention constitutes a part of the plastic strain after each cycle. As long as the applied stress is not

larger than the yield stress of martensite, plastic slip of thermally induced martensite will not occur. This suggests the TrIP present during training is a combination of martensite retention and plastic deformation of the martensite phase (McCormick & Liu, 1994; D. A. Miller & Lagoudas, 2000). Saturation of the plastic strains occurs from the material reaching the maximum amount of retained martensite it can retain.

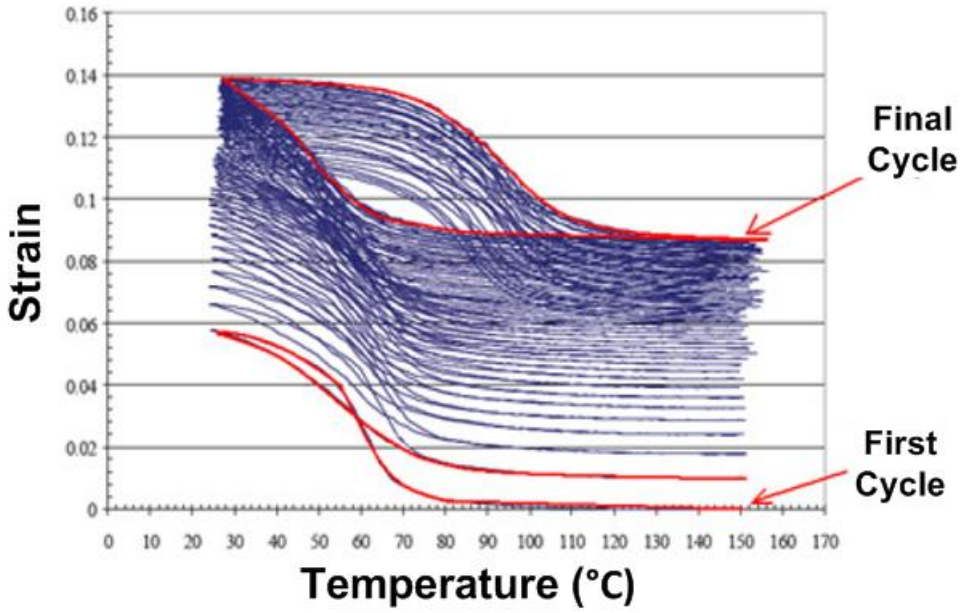

Figure 11: Typical strain-temperature diagram for isobaric training

It is well documented that a higher training stress results in higher two-way actuation strains for isobaric training. Recently, it was also shown that training temperatures also play a role in the amount of actuation strain after training. Tests performed by Padula, et al. (Padula, et al.) reveal higher training stresses and temperatures result in higher initial plastic strain after the second cycle of training as shown in Figure 12. A higher temperature and stress causes a higher initial plastic strain, but not necessarily a higher transformation (actuation) strain as demonstrated in Figure

13. Here, the upper cycle temperature increases the transformation strain to a certain point for this alloy system. Further temperature increases result in a lowering of the transformation strain. The authors attribute these effects to factors that promote the development of texture (martensite variants aligned along the loading direction) and the amount of retained martensite after reaching the upper training temperature. They concluded higher temperatures and lower stresses produce less retained martensite upon heating, and a higher training temperature favors the formation of martensite variants along the loading direction. However, no conclusions could be drawn for the mechanism causing the transformation strains to decrease at the highest training temperatures (Figure 13). Also, no available literature has yet shown that for a specific stress, an increase in training temperature will result in an increase in final actuation strain after TrIP has saturated. The initial TrIP may be larger, but the different training temperatures may reach the same end actuation stress.

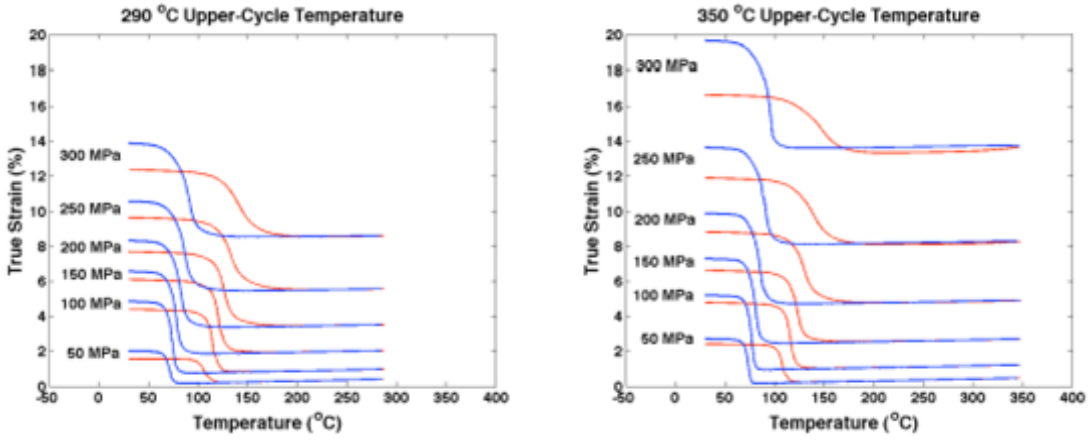

Figure 12: Effect of training temperature during isobaric training at 290°C and 350°C for the second cycle of training for NiTi 55 wt% Ni (Padula, et al.)

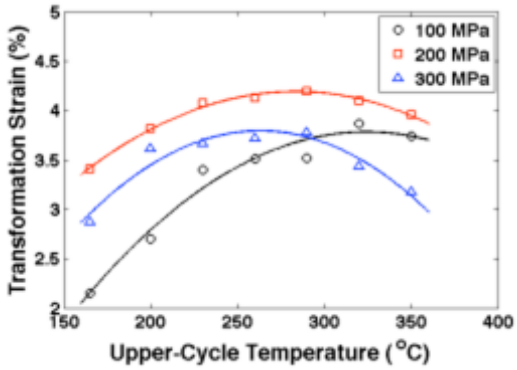

Figure 13: Effect of training temperature on transformation strain during isobaric training after second cycle of training for NiTi 55 wt% Ni (Padula, et al.)

Superelastic Training

The second method for training TWSM is by stress inducing martensite from the austenitic region (loading path 2 in Figure 6). Here, the SMA is heated into the austenite phase. Once in austenite, the SMA is loaded until martensite is stress induced; then unloaded back to zero stress. This cycle is also known as the superelastic effect as discuss earlier. A typical stress-strain curve of this type of training is shown in Figure 14. After each cycle, the stress required to stress induce martensite is reduced and some amount of plastic strain is retained. The plastic strain is a combination of martensite which is "locked" in by stress concentrations around the dislocations generated by training. These dislocations keep some of the material as martensite even at zero stress and above the A_f temperature (Lim & McDowell, 1994). Superelastic training is completed when plastic strain no longer accumulates after each cycle at zero stress.

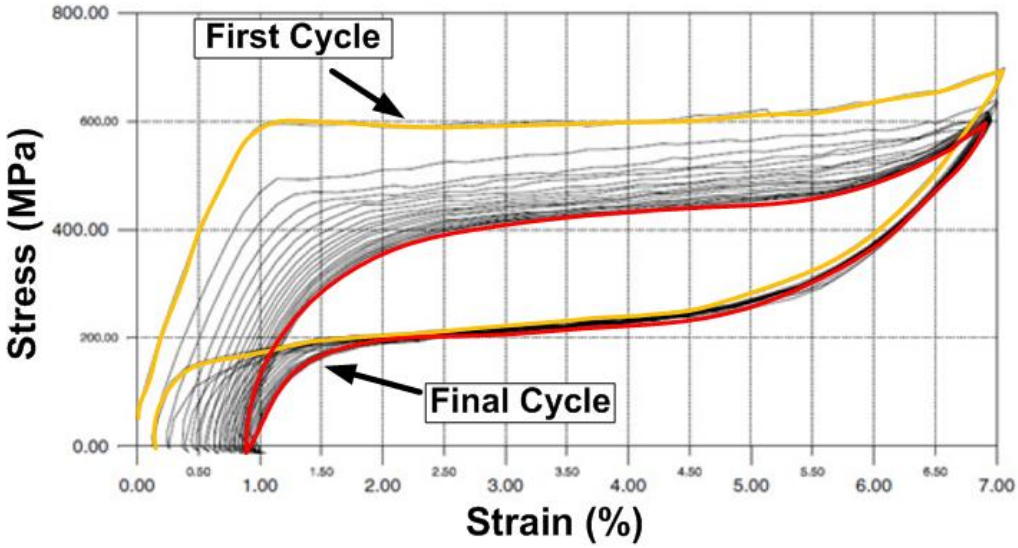

Figure 14: Stress-strain diagram of stress-induced martensite (superelastic) loading (Becker, 2010)

Martensite Deformation Training

The third method of thermomechanical training is martensite deformation followed by reheating to recover a portion of the plastic strain; loading path 3 on Figure 6. The SMA is loaded to or past the martensite detwinning stress and then unloaded. Next it's heated above A_f to recover a portion of the plastic strain; also known as the shape memory effect as discussed previously. This process is repeated until the amount of transformation strain achieved saturates as shown in Figure 15. Martensite deformation creates internal plastic deformations which in turn creates a directional stress field. The directional stress field directs where martensite is formed and results in TWSM (Y. N. Liu, et al., 1998). Of the three methods, martensite deformation training results in the highest amount of actuation strain when fully trained. This is due to the dislocation development through the detwinning process and plastic slip of the martensitic microstructure generating a higher preferential ordering of the martensite

variants, and a higher two-way strain than the other training methods (D. A. Miller & Lagoudas, 2000).

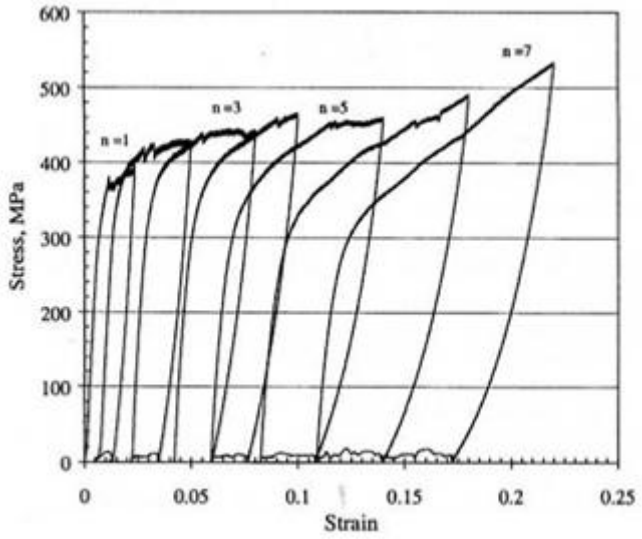

Figure 15: Stress-strain diagram of martensite deformation training (D. A. Miller & Lagoudas, 2000)

Advantages of Isobaric Training

The following work uses the isobaric training method for the thermomechanical training of all test specimens. The reasoning behind this decision is the strain-temperature response of this training method is more suitable for a temperature activated actuator. In current and envision SMA actuator applications, a change in temperature is used to activate the actuation. Training by changing the temperature of the material is then the logical choice. It is also seen as the most economic way to mass produce actuators. Training by superelastic or SME methods require more steps and time to complete each training cycle which incurs a higher cost.

Factors Affecting Training Results

How a SMA is processed will also affect the amount of TWSM achieved during training. This is especially significant in SMA wires which go through multiple drawings to get to standard wire diameters. The multiple drawings impart large amounts of plastic deformation and creates a texturing in the wires that causes thermomechanical properties to differ from cast parts. Literature has shown an increase in cold work develops smaller two-way strain and total accumulated TrIP during training (D. A. Miller & Lagoudas, 2001). On the opposite side, annealing develops higher amounts of TrIP during training and higher TWSME (Becker, 2010). The difference between cold work and annealing is best shown by comparing the isobaric training strain vs. temperature diagrams of an as-received (high cold worked) and annealed NiTi wire as in Figure 16. Figure 16a is the as-received (high cold work) wire, and Figure 16b is the same wire, annealed at 450 °C for 1 hour. The as-received wire yielded low amounts of TrIP during training and almost no TWSM compared to the annealed wire.

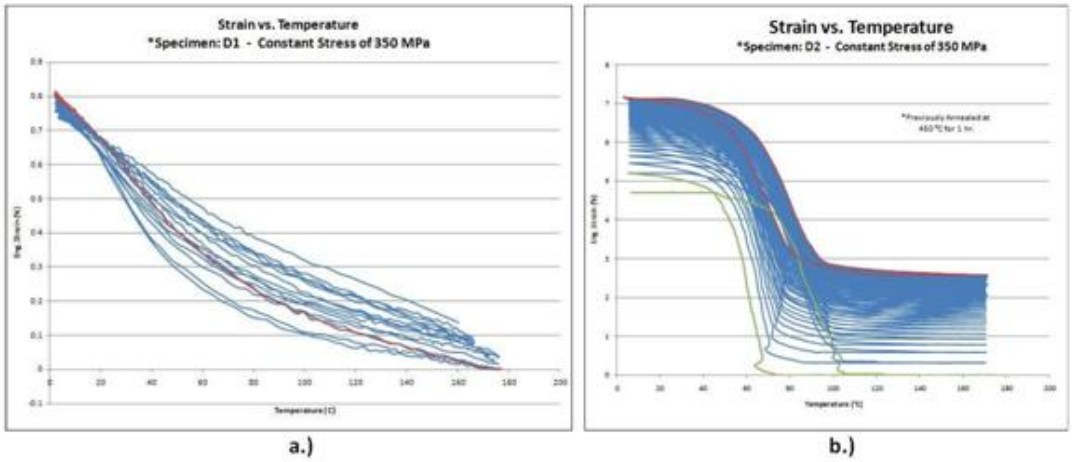

Figure 16: Constant stress thermal cycle training at 350 MPa; a.) As-received NiTi Wire b.) NiTi Wire, Annealed at 450ºC for 1 hr. (Becker, 2010)

Ternary and High Temperature Shape Memory Alloys

As discussed in previous sections, the thermomechanical properties of NiTi can be tailored by changing the ratio of nickel to titanium or by additional processing. A second method is to add a ternary alloy. One important alloy compositions available today is Ni-Ti-Cu. The addition of copper does not appreciabley change the transformation temperatures of the alloy, but does change the transformation type of the lattice. This in turn creates a smaller temperature hysteresis which further decreases with increasing copper content (see Figure 7b, the gap between M_s and A_s closes). A smaller temperature hysteresis is beneficial for an actuator because less of a temperature change is required to activate the actuator. Other properties improved by Cu include thermal stability, damping properties, and workability of the alloy when copper content is lower than 8%. The addition of Niobium into NiTi raises the A_s temperature significantly when the alloy is deformed in the martensitic state thus increasing the temperature hysteresis. This makes the Ni-Ti-Nb alloy system useful for coupling applications where a large temperature hysteresis is beneficial (Chastaing et al., 2006; Otsuka & Ren, 1999).

While ternary addition of Cu has beneficial effects on some thermomechancial properties of NiTi, it does not help with the fact NiTi SMAs are useful at temperatures below 100°C only (Otsuka & Wayman, 1998). This in turn limits NiTi to lower temperature environments. Also, in a warmer environment a NiTi actuator response speed is lowered or requires external cooling because of the difficulty in reaching the martensite transformation temperature. To address these problems, many high temperature shape memory alloys have been developed including Ni-Ti-(Zr, Hf, Pd, Pt).

Zirconium (Zr) and Hafnium (Hf) are attractive because they are relatively less expensive than Palladium (Pd) or Platinum (Pt). Palladium and Platinum though do produce higher transformation temperatures on the range of 400°C to 500°C (Kumar & Lagoudas, 2010; Panduranga, Shin, & Carman, 2006) as compared to Hafnium and Zirconium's range of 250°C to 350°C (Wojcik, 2009). One problem encountered in high temperature SMA actuators with transformation temperatures as high as 500°C is creep occurring simultaneously with phase transformations. This has been found to significantly impact an actuator's performance (Kumar & Lagoudas, 2010). Because of the price and creep considerations for Pt and Pd, the favorable choices for high temperature SMAs are Hf and Zr. Of these two, Hf is preferred because it affects the transformation temperatures to a larger degree than Zr (Otsuka & Wayman, 1998; Wojcik, 2009).

Numerous studies have been conducted on high temperature SMAs containing Hf. All studies came to the conclusion that precipitates of either $(Ti,Hf)_3Ni_4$ or $(Ti,Hf)_2Ni$ play an important role on the materials behavior (Meng et al., 2008; Meng, Fu, Cai, Li, & Zhao, 2009). The matrix of a NiTiHf alloy has a relatively low strength for slip without additional processing. Hf causes the interplanar distance of certain slip planes to be larger than that of equiatomic NiTi in the martensitic phase. This makes slip on certain planes easier than that of NiTi. Other studies on Hf SMAs have confirmed that dislocation slip and martensite variant reorientation almost occur simultaneously during the deformation of martensite (Chastaing, et al., 2006; Meng, et al., 2008). During extended exposures to high temperatures, such as during aging or annealing, $(Ti,Hf)_3Ni_4$ or $(Ti,Hf)_2Ni$ precipitates form. These precipitates form along grain boundaries and

increased aging or annealed times will further increase the size of the precipitates. Both precipitates have the same effect of introducing strong internal stress fields which substantially strengthens the material's matrix and makes the shear mechanism of detwinning difficult.

Overview of SMA Models

The last thirty years have seen numerous publications in the area of modeling the complex behaviors of SMAs. A series of recent papers by Patoor et al. (Patoor, et al., 2006) and Lagoudas et al. (Lagoudas et al., 2006) summarized the basic modeling of SMA single crystals and polycrystals respectively; with the latter reviewing the notable models of the past three decades. The authors concluded that models usually fit in one of two categories: micromechanical models or phenomenological models.

Micromechanical models try to predict SMA behavior by taking into account the granular microstructure of polycrystalline SMAs. These are based on the assumption that if the microstructure is known, it is feasible to expand modeling results of a single crystal SMA and solve boundary value problems in a polycrystalline material. The limitations of this approach are it is impossible to exactly represent the microstructure or possible to solve boundary value problems for a sufficient number of grains to represent a three-dimensional problem. For more information on micromechanical models, see the work of Gao and Brinson (Gao & Brinson, 2002), Lu and Weng (Lu & Weng, 1998), and Patoor et al. (Patoor, Eberhardt, & Berveiller, 1996).

Phenomenological models use continuum mechanics and internal state variables to detail microstructural changes during phase transformations. These models will usually assume a macroscopic energy function that depends on the state of internal variables. Evolution equations are then formed for the internal state variables. The internal state variables and the evolution equations are based off parameters determined by experimental observations. The SMA behavior is then determined from the internal state variables and by satisfying the second law of thermodynamics. There are numerous phenomenological models describing a SMAs superelastic behavior (Tanaka, Kobayashi, & Sato, 1986; Tanaka, Nishimura, Hayashi, Tobushi, & Lexcellent, 1995), martensite detwinning (Juhasz, Schnack, Hesebeck, & Andra, 2002; Lagoudas & Shu, 1999), and the cyclic loading with TrIP (Bo & Lagoudas, 1999a, 1999b; Lagoudas & Bo, 1999; Lagoudas & Entchev, 2004; Lexcellent, Leclercq, Gabry, & Bourbon, 2000; Tanaka, et al., 1995). For this work, the model presented in the four paper series by Bo & Lagoudas and Lagoudas & Bo is used to model the actuation strains of SMA actuators. Unlike the other micromechanical and phenomenological mentioned, the model by Bo & Lagoudas can track the evolution of transformation and plastic strains during phase transformations under various applied cyclic loads. The cyclic loads can be either thermally or stress induced. This is ideally suited for the current work since the amount of transformation strain at a certain stress is the same as the actuation strain for that stress. Previous studies have found strong agreement between experimental and model results (Becker, 2010; Lagoudas, et al., 2006). The Bo & Lagoudas model was also expanded to three dimensions by Lagoudas & Entchev (Lagoudas & Entchev, 2004), but is not necessary

for the current one dimensional work. The development and implementation of the Bo & Lagoudas model used for this research will be discussed in the following section.

A large amount of research has been invested into phenomenological models because they are easy to implement by numerical methods and FEA. The framework of the governing equations for a SMA model are similar to the equations describing rate-independent plasticity; therefore, the return-mapping algorithms originally intended for rate-independent plasticity can be applied to SMAs (Lagoudas, et al., 2006). For more information on the current research on return mapping algorithms used for SMAs models, see the work of Qidwai and Lagoudas (Qidwai & Lagoudas, 2000), Govindjee and Miehe (Govindjee & Miehe, 2001), and Auricchio (Auricchio, 2001). The return mapping algorithms are easily implemented into FEM codes and have been used to investigate the use of SMAs as structural components (Lagoudas, et al., 2006).

Thermomechanical Modeling of Polycrystalline SMAs Under Cyclic Loading

General Information

Bo & Lagoudas split the description of their model into four parts: theoretical derivations, material characterization, cyclic deformations and TWSM, and minor hysteresis loops. Part one, theoretic derivations, details the development of a generic form of the Gibbs free energy over a representative volume element (RVE), and the internal state variables that govern the Gibbs free energy. The Gibbs free energy is the backbone of the model since the free energy governs the phase transformation. The Gibbs free energy is a combination of the elastic potential energy and chemical energy

over the RVE. The most generic form of the free energy is shown in Equation 1 (for more information on the formulation of this equation see (Bo & Lagoudas, 1999a). This equation is a function of two independent variables, the applied stress tensor and temperature, and five internal state variables: martensitic volume faction, macroscopic transformation strain, macroscopic plastic strain, the back stress, and the drag stress. The back stress is the average of the local stress over the RVE. The local stresses are the result of microstructural changes caused by both phase transformation and plastic deformations. These local stresses, induced by the microstructural changes, may also create a substantial overall energy change in the RVE. This is taken into account by the drag stress, which represents the elastic interaction strain energy due to the creation of martensitic variants. The purpose of the back and drag stress is to represent an average measure of the effect of the current microstructural changes on the phase transformation (Bo & Lagoudas, 1999a).

Equation 1: General form of Gibbs free energy for a polycrystalline SMA

$$- \; 0- \qquad 0- \; 0 \; - \; 0+ \; 0 \; h+$$

S_{ijkl}	average effective elastic compliance	E^{o}_{ij}	macroscopic elastic strain due to Σ
Σ_{ij}	applied stress tensor	E^{p}_{ij}	macroscopic plastic strain
ξ	martensitc volume fraction	E^{m}_{ij}	macroscopic transformation strain
α_{ij}	back stress tensor	E^{θ}	thermal strain
η	drag stress	G^{ch}_{o}	average Gibbs chemical free energy per unit mass
c	specific heat	G^{p}	interacton energy induced by plastic strains in austenitic phase
s_o	specific entropy	T	current tempeature

In Equation 1, the internal state variables are all either functions of, or integrated with respect to, the martensitic volume fraction (ξ). This is because the phase transformations of SMAs are non-diffusive (not time dependent). Therefore, the phase transformation can only be possible and limited by changing the martensitic volume fraction. This implies the other internal state variables all depend and evolve with the martensitic volume fraction. Also, the evolution equations of the other internal state variables can be integrated in terms of the martensitic volume fraction to obtain an evolution equation as a function of martensitic volume fraction. This simplifies the evolution laws of the internal state variables, but also makes them loading path dependent because the transformation of martensite variants depends on the applied load and temperature (Bo & Lagoudas, 1999a).

The evolution equation for the martensitic volume fraction (ξ) is obtained by introducing a dissipation potential and applying the second law of thermodynamics to the Gibbs free energy equation (Equation 1). The second law places the restriction that the rate of entropy increase must be greater than the entropy input rate. The model for cyclic loading of SMAs must satisfy this law, and more specifically, satisfy the local form of the second law known as the Clausius-Duhem inequality. One criteria of satisfying the Clausius-Duhem inequality is the material must obey the dissipation inequality or the Kelvin inequality stated in Equation 2. The thermodynamic force conjugate for the dissipation inequality is also stated in Equation 2 (Lubliner, 1990).

Equation 2: Dissipation inequality and the thermodynamic force conjugate to ξ_α

$$\underline{\quad}$$

ξ	internal state variables	p	thermodynamic force conjugate
D	local dissapation rate		

After some manipulation and applying the Clausius-Duhem inequality, the dissipation inequality results in the following using Equation 1.

Equation 3: Dissipation inequality for SMAs

$$\underline{\quad} \qquad \underline{\quad} \qquad \underline{\quad}$$

E_{ij}	total strain tensor	s	entropy
$\acute{\eta}$	local dissapation rate	ξ	martensitic volume fraction

As stated previously, the other internal state variables evolve with the martensitic volume fraction (ξ). So in Equation 3, the variation of the Gibbs free energy (G) with respect to the other internal state variables is included in the variation of G with respect to the martensitic volume fraction. For the inequality in Equation 3 to hold true, each part of the equation must simultaneous satisfy the inequality. With this, the following constitutive equations can be written:

Equation 4: Total strain tensor including elastic, thermal, plastic, and transformation strain

$$\underline{\quad}$$

Equation 5: Specific entropy

Equation 6: Local internal dissipation rate

where π is the thermodynamic force conjugate to ξ and Σ_{ij}^{eff} is the thermodynamic force conjugate to E_{ij}^{m} given by:

Equation 7: Thermodynamic force conjugate to the martensitic volume fraction (ξ)

Equation 8: Thermodynamic force conjugate to E_{ij}^{m}

The main point to take away in the development of the above constitutive equations is they all came from satisfying the second law of thermodynamics with the functional form of the Gibbs free energy for polycrystalline SMAs. In other words, a functional form for the Gibbs free energy for polycrystalline SMAs was derived as a function of two independent variables, the applied stress tensor and temperature, and five internal state variables: martensitic volume faction, macroscopic transformation strain, macroscopic plastic strain, the back stress, and the drag stress. This form of the Gibbs free energy was then used to satisfy the second law of thermodynamics; more specifically

the Clausius-Duhem inequality. The dissipation inequality must also hold true to satisfy the Clausius-Duhem inequality. From this, certain forms of constitutive equations were derived and used to determine the evolution laws for the five internal state variables. Detailed formulation of the evolution equations for the internal state variables are beyond the scope of this work, but for completeness the evolution equations and the methods of determining their material parameters are detailed in the next section.

Evolution Equations and Material Parameters

The evolution equation for the martensitic volume fraction is shown in Equation 9. It is a function of the thermodynamic force conjugate (π), and the material parameter Y. Y is a measure of the internal dissipation due to microstructural changes that happen during the phase transformation. The phase transformations produce a latent heat that is either endothermic or exothermic depending on a forward or reverse transformation, and can be captured by a Digital Scanning Calorimeter (DSC) test of the material. Using the measured latent heat from the DSC test, the change in specific entropy (Δs) and material parameter Y can be measured (Lagoudas & Bo, 1999).

Equation 9: Evolution of martensitic volume fraction

ϕ	transformation function	Y	material parameter
π	thermodynamic force conjugate to ξ		

The evolution of the transformation strain (Equation 10) is mainly a function o the applied strain (or stress). During the forward transformation (austenite to martensite), the variant(s) the martensite form are in orientations favoring the applied stress. In the reverse transformation, there is only one possible variant of austenite, but the sequence of which martensite variants transform is dependent on the strain or applied stress. This evolution equation contains no material parameters and is simply loading dependent (Bo & Lagoudas, 1999a).

Equation 10: Evolution of transformation strain

$$\dot{H} = \dot{\Sigma}$$

H^{cur}	current max uniaxial transformation strain	Σ	applied von Mises stress
$E^{m\text{-}max}$	uniaxial transformation strain at reverse transformation	Σ^{eff}	effective von Mises stress

The evolution of the plastic strain (Equation 11) is dependent on the applied stress, the current plastic strain, and the martensitic volume fraction (ξ). The rate of which plastic strain increases will slow with the accumulation of plastic strain. The material constant r_1 captures this. The larger the value of r_1, the plastic strain rate decrease faster. D^p accounts for the fact plastic strains do not form uniformly during the cyclic transformations, and z is a hardening function for the accumulated plastic strain. The material constants depend on the detwinned martensitic volume fraction and form a

non-linear differential equation that is easily solved with numerical algorithms (Bo & Lagoudas, 1999b).

Equation 11: Evolution of plastic strains

$$\dot{D}^p$$

D^p	accounts for non-uniform plastic strains	z	hardening function involving three material constants: d_0, d_1, and d_2
r_1	material constant		
ξ^d	detwinned martensitic volume fraction		

The back and drag stress control the transformation hardening. This implies they evolve with the residual stress left by dislocations and defects in the material after cyclic loadings. The evolution laws for the back and drag stress (Equation 12 and Equation 13 respectively) include a number of material constants. These material constants are accounting for the different dislocations and inclusions that are imparted into the material during cyclic transformations. D_o accounts for the elastic strain energy per unit volume of inclusion embedded in an infinite medium, and parameter D_1 is used to describe the TWSME. D_3 and m_1 together describe the loading path for the drag stress while D_5 and m_2 do the same for the drag stress. The last two parameters, D_2 and D_4, are used to account for the self-induced effect during phase transformations for the drag and back stress respectively. The self-induced effect is also known as the "autocatalytic" effect. The autocatalytic effect can be thought of as a chain reaction where once the energy is reached to induce a phase change, the material transforms and the energy state in the material system is reduced (Bo & Lagoudas, 1999b; Lagoudas & Bo, 1999).

The material parameters listed above are all determined by curve fits of experimental data. Parameters m_1, D_1, D_2, and D_3, are obtained from the experimental applied stress vs. current maximum uniaxial transformation strain. The other parameters m_2, D_4, and D_5, are obtained from the experimental strain-temperature hysteresis curve, like the one shown in Figure 7b. An important note is the parameters are used for both trained and untrained SMAs, but will have different values.

Equation 12: Evolution of back stress

$$\dot{\alpha} = \frac{2}{3} D_1 \dot{\varepsilon}^{pl} - D_2 \alpha \left| \dot{\varepsilon}^{pl} \right| - D_3 \alpha \left| \dot{\varepsilon}^{tr} \right|$$

$$\dot{\varepsilon}^{tr} = \left(\frac{H^{cur}}{H} \right)^{m_1} \dot{\varepsilon}$$

H^{cur}	current max uniaxial transformation strain	D_1, D_2, D_3, m_1	Material constants
H	maxium uniaxial transformation strain		

Equation 13: Evolution of drag stress

$$\dot{R} = D_0 \left| \dot{\varepsilon}^{pl} \right| - D_4 R \left| \dot{\varepsilon}^{pl} \right| - D_5 R \left| \dot{\varepsilon}^{tr} \right|^{m_2}$$

D_0, D_4, D_5, m_2	Material constants

In summary, there are nine physical constants, ten material parameters for phase transformations, five parameters for evolution of plastic strains, and two parameters for evolution of back and drag stresses are required to describe the full behavior of a SMA in

this model. The constants and parameters are listed in Table 2. One of the advantages to this model over others is the use of ten material parameters to describe the phase transformation. Previous models only used five. By the addition of another five parameters, this model can now be used to describe the thermally induced phase transformations under variable applied load and TWSM.

Table 1: Physical constants and material parameters characterizing the phase transformation and evolution of internal state variables (Bo & Lagoudas, 1999b; Lagoudas & Bo, 1999)

Physical constants of austenitic and martensitc phases (9)			
	E^A , E^M		Young's modulus of austenite and martensite, respectively
	ν^A , ν^M		Poisson ratio of austenite and martensite, respectively
	α^A , α^M		Thermal expansion coefficients of austenite and martensite, respectively
	ρc^A , ρc^M		Specific heat of austenite and martensite, respectively
	$\rho \Delta s_0$		Difference of the specific entropy between martensite and austenite
Material parameters characterizing phase transfromation (10)			
	H		Maximum transformation strain
	Y		Total hysteresis of a SMA in a complete transforamtion cycle
	M^{os}		Martensitic start phase transformation temperature
	D_1, D_2, D_3, m_1		Transformation hardening parameters relted to back stress
	D_4, D_5, m_2		Transformation hardening parameters related to drag stress
Parameters related to the evolution of plastic strains (5)			
	D^p, r_1, d_0, d_1, d_2		
Parameters governing the evolution of the back and drag stress (2)			
	λ_1, λ_2		

Another advantage of this model over others is it can describe all the behaviors of a SMA (one-way SME, superelasticity, transformation temperatures, etc.). Part four of

the papers series also models minor hysteresis loops, but is not of interest for this work. Since stress dependence has been introduced into the evolution of the transformation strain, it can model thermally induced phase transformations at various applied loads. Also, the loading history is accounted for by the evolution of the back and drag stress due to the number of loading cycles. This way the model can also account for the training of an SMA. So given the temperature history and total strain (or stress), the cyclic thermomechanical response can be predicted.

Modeling Actuation Strains

The end goal of using the Bo & Lagoudas model for the following work is to model the TWSM achieved by thermomechanical training. The training and TWSM performed in this experiment is in 1-D, so the equations from the Bo & Lagoudas model can also be simplified to 1-D. To model the TWSME from thermomechanical training, the two areas of interest are the back stress (Equation 14) and the effective stress (Equation 15) for 1-D.

Equation 14: Back stress in 1-D

Equation 15: Effective stress in 1-D

In Equation 15, the effective stress is the driving force behind the transformation. When the transformation is completed, the driving force no longer exists and the effective stress goes to zero. In other words, as the SMA completes the reverse transformation to martensite, the martensitic volume fraction (ξ) goes to one and the effective stress goes to zero. Then Equation 14 and Equation 15 can be combined to yield the following:

Equation 16: Combination of effective and back stress at $\xi = 1$

$$\overline{\overline{\Sigma}} = \overline{\overline{\beta}}$$

With this equation, it is now possible to curve fit a transformation strain (H^{cur}) vs. applied stress (Σ) graph for the material parameters D_1, D_2, D_3, m_1, and H at an applied uniaxial stress Σ. The material parameters are important for two reasons. First, the parameters are important for actuation design because they can be used to predict the maximum transformation strain (actuation strain) at other stresses. Secondly, the parameter values can be compared to other SMAs to gain a better understanding of which external factor controls each parameter. The long term purpose of using this model is not to repeatedly determine material parameters from data, but to predict the actuation strains of an SMA before it is ever trained. By understanding how the material parameters change with changing training stress and temperature, it is possible to predict and train actuation strains to fit a specific design window.

Equation 16 will be used extensively in the remainder of the work so a deeper understanding of what the material parameters represent is required. The parameters m_1,

D_3, and H are accounting for the initial and accumulated material heterogeneity built up from repeated phase transformations. In other words, they account for the hardening of the material. The parameter m_1 defines the shape of the transformation strain (H^{cur}) vs. applied stress (Σ) curve, and experiments have shown setting m_1 to 1.8 fits almost all H^{cur} vs. Σ curves. D_3 is the heterogeneity back stress and is another mathematical construct to define the shape of the H^{cur} vs. Σ curve. The maximum transformation strain, H, is the maximum possible actuation strain at any stress level based off the H^{cur} vs. Σ curve. Parameter $D_{1,}$ the two-way drag stress, accounts for the residual stresses created from training. Graphically, this parameter defines where the actuation strain intersects the H^{cur} axis (x-axis). The last parameter, D_2, accounts for the autocatalytic effect as described earlier. This parameter is included in the model to completely account for all energy changes possible in the RVE of a SMA. Experimentally; however, this effect is not observed. So for the curve fits performed in this work, the value of D_2 is set to zero.

EXPERIMENTAL PROCEDURE

Problem Definition

The purpose of this research was to characterize and train two high temperature SMAs for use as actuators. The characterization used SME and superelastic tests to determine training stresses and temperatures. Training was performed by isobaric thermal cycles. After training, the tests specimens were actuated at lower stresses to evaluate actuation strains vs. stress. The actuation strain vs. stress data also provided the transformation temperatures at various stresses. The transformation temperatures were then used to evaluate the potential of creep and annealing in the actuators. Finally, the actuation strain vs. stress data was fit to the model by Bo & Lagoudas to predict other actuation strains and give a deeper insight on the material parameters of this model.

The motivation for this research was to find a feasible high temperature SMA actuator. Low temperature SMA actuators are effective if used in temperatures below 100°C. This limits the environments and applications of SMA actuators. Also, a thermally induced actuator will have a long response time in higher temperatures or require external cooling to cause the reverse transformation to martensite. There is little data available in literature on the two alloys used in this research; especially in the form of training methods and resulting actuation strains. A full characterization and prediction of actuation strains resulting from isobaric training is crucial for design and implementation of the two high temperature alloys. The alloys will be of even further if the model by Bo & Lagoudas is capable of predicting their behavior and implemented

into FEA code. To this end, the following research details the characterization, thermomechanical training, actuation strains, and modeling of two high temperature SMA actuators for use as linear actuators.

Testing Materials

The two high temperature SMA alloys used in this research were $NiTi_{29.7}Hf_{20}$ and $NiCu_5Ti_{29.7}Hf_{20}$ at. wt%. The test specimens were supplied from NASA-Glenn Research Center (NASA-GRC) in Cleveland, Ohio. Little information accompanied the two alloys when received, but it is known they were aged at 500°C for three hours after casting. They were machined by CNC lathes to reduce the cross section for testing. Nominal diameter of the tests specimens was approximately 6.30 mm, but varied from bar to bar. Shown in Figure 17 is an example of the tests specimens for both alloys. The two alloys were tested and trained in the as-received (as-machined from NASA-GRC) or annealed condition. The annealing process took place in a Barnstead Thermolyne 1300 furnace, model FB1315M. They were annealed at 450 °C for one hour, and then allowed to cool in ambient temperature air. The alloys are indistinguishable in the as machined (received) condition, but turn different colors after the annealing process. As seen in Figure 17a, the $NiTi_{29.7}Hf_{20}$ turns a bright blue typical of annealed titanium while the $NiCu_5Ti_{29.7}Hf_{20}$, Figure 17b, had a greenish tint from the copper.

Figure 17: a) As-received and annealed $NiTi_{29.7}Hf_{20}$ b) As-received and annealed $NiCu_5Ti_{29.7}Hf_{20}$

Experimental Setup

All experimental testing was performed using an Instron 5882 load frame with a 100 kN load cell. The Instron used an Instron 5800 Controller in conjunction with a Merlin graphical user interface. The Merlin GUI was used to create the loading profiles needed for the material characterization and thermomechanical training. An Epsilon #3448-0050-020 high temperature furnace model extensometer with a 0.5 inch gage length and ±0.1 inch travel was used for strain measurements (Figure 18). The Instron was equipped with the clamshell furnace picture in Figure 19. The furnace used two 120V resistive heating elements to control the temperature of the specimens. The clamshell furnace and heating elements were fitted around the tests specimen after it was loading into the Instron load frame as seen in Figure 20. Also shown in Figure 20 is the exposed junction type “K” thermocouple used to monitor the specimen temperature.

Thin copper wire was used to tie the bead of the thermocouple directly to the samples. Special care was taken to not let the copper wire tough the bead of the thermocouple. Thermally conductive past (Omegatherm 201) was used to cover the thermocouple bead for electrical insulation and to ensure good thermal conduction with the specimen.

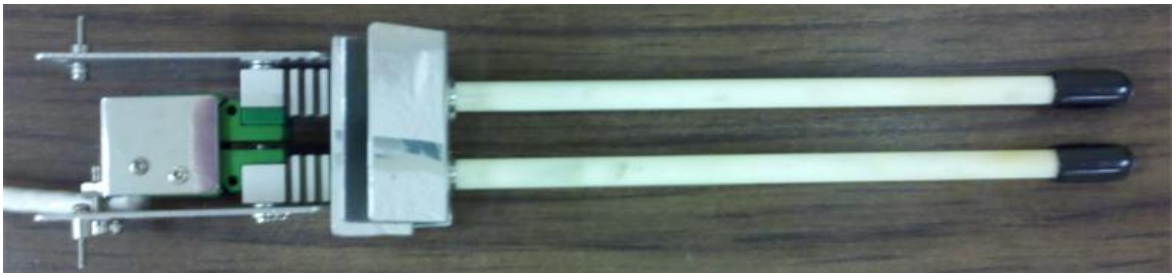

Figure 18: High temperature extensometer

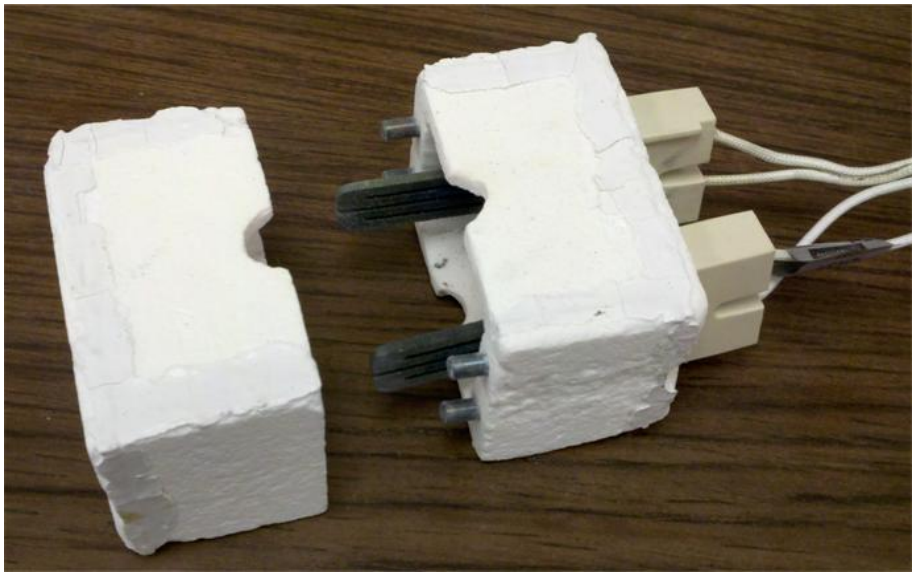

Figure 19: Clamshell furnace

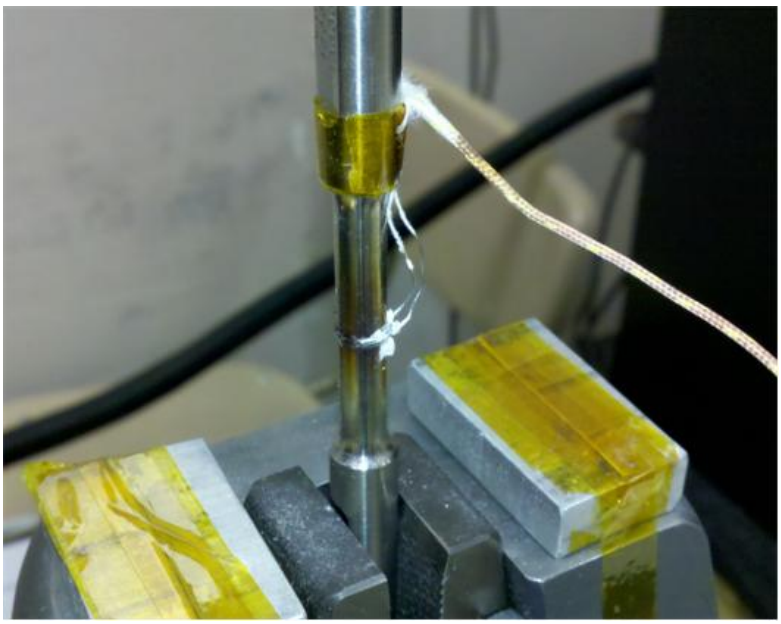

Figure 20: Instron and thermocouple attachment

The complete test setup including the extensometer, clamshell furnace, and thermocouple fitted to the Instron is shown below in Figure 21.

Figure 21: Instron 5882 load frame

The data acquisition and temperature control was performed using LabVIEW and a National Instruments USB-6221 16 bit, 16 input data acquisition system (DAQ). The load cell, extensometer, and thermocouple signals were connected directly to the DAQ and the thermocouple signal was used to control the voltage input to the 120V resistive heating elements to ensure a uniform heating/cooling ramp up/down. A uniform ramp up/down is important to ensure uniform and controlled heating of the test specimens. Because of the high temperatures reached during the characterization and training of high temperature SMAs, extensive testing was performed on the furnace and heating elements to obtain equations relating temperature signal vs. power output. The equations for the ramp up/down are shown in Equation 17 and Equation 18 respectively. These ramps were activated and disabled at 200°C. Before 200°C, a constant voltage of 1.75V was used for the ramp up and no voltage was applied after 200 °C for the ramp down. These ramps produced a heating ramp up of 0.5 °C/sec (30 °C/min) and a ramp down of -0.8 °C/sec (-48 °C/min).

Equation 17: Ramp up equation to control voltage based on temperature (°C)

Equation 18: Ramp down equation to control voltage based on temperature (°C)

Example screen shots of the LabVIEW front panel and block diagram used to collect data and control the heating/cooling of the test specimens is shown in Figure 63 and Figure 64 of Appendix A.

Material Characterization

Shape memory effect and superelastic tests (loading paths 3 and 2 in Figure 6 respectively) were performed to characterize the material's response before thermomechanical training. The SME and superelastic tests were loaded and unloaded at a rate of 0.15 mm/min. The loadings started at 300 MPa and increased to 600 MPa in 100 MPa intervals. All testing was performed on the same specimen. The SME test was loaded and unloaded at room temperature, and then heated to approximately 40 °C degrees above the observed austenite finish temperature to ensure a complete transformation. The superelastic tests for the Hf alloy were loaded and unloaded at a constant 290 °C, while the HfCu was tested at a constant 260 °C. Both SME and superelastic tests started with a pre-load of 15 MPa to ensure a tight fit with the test specimens and the machine's grips.

Thermomechanical Training

The characterization results (SME and superelastic tests) were used to determine the appropriate stresses and temperatures for training. The specimens were thermomechanically trained by running thermal cycles at a specific constant training stress; also known as isobaric training (loading path 1 in Figure 6). For more information on isobaric training, see the Thermomechanical Training section of the Background. For isobaric training, the best results are achieved by using a max training stress above the martensite detwinnig stress, but below the austenite yield stress. Yielding of the material at any point is detrimental to the training results. The superelastic tests determine the

maximum training temperatures as well and if stress induced martensite will form during training because it has similar results as yielding on the training results.

Isobaric training was performed until TrIP became negligible or "saturated." The load used to reach the training stress was based on the initial diameter of the specimen. When TrIP started to decrease substantially, the test was stopped and the bar diameter re-measured. The load was then adjusted to account for changes in bar diameter from training. The initial training temperature was chosen to be just above the austenite finish temperature to ensure a complete transformation. A specimen of the same alloy was then trained at a temperature 50°C higher to investigate the effects training temperature had on TrIP and actuation strains. Once the samples were trained, they were cycled at lower constant stress values to characterize the materials transformation strains and phase transformation temperatures at different stresses. The phase transformation temperatures were determined by the method of intersecting tangents. A test matrix listing each test specimen and the test that was performed on it is shown in Table 2. There were a limited number of bars supplied, so some bars were used in more than one test.

Table 2: Test Matrix

Identifier	Material	Test Performed	Dia. (mm)	Additional Bar Info
H1	$NiTi_{29.7}Hf_{20}$	Shape Memory Effect	6.43	Used for SME test, then training at 600 MPa, 350 °C
H2	$NiTi_{29.7}Hf_{20}$	Superelastic	6.27	Used for SE test first, then failed during training at 600 MPa
H3	$NiTi_{29.7}Hf_{20}$	Training 300 MPa, As-Received	6.21	Training at 300 MPa first, then at 600 MPa, 400 °C
H4	$NiTi_{29.7}Hf_{20}$	Training 300 MPa - Annealed	6.29	Trained at 300 MPa only
H5	$NiTi_{29.7}Hf_{20}$	Training 600 MPa, 350 °C	6.27	Used for SME test, then training at 600 MPa, 350 °C
H6	$NiTi_{29.7}Hf_{20}$	Training 600 MPa, 400 °C	6.29	Training at 300 MPa first, then at 600 MPa, 400 °C
HC1	$NiCu_5Ti_{29.7}Hf_{20}$	Shape Memory Effect	6.27	Used for SME test, then training at 600 MPa, 350 °C
HC2	$NiCu_5Ti_{29.7}Hf_{20}$	Superelastic	6.27	Used only for SE test
HC3	$NiCu_5Ti_{29.7}Hf_{20}$	Training 600 MPa, 300 °C	6.36	Training at 600 MPa, 300 °C only
HC4	$NiCu_5Ti_{29.7}Hf_{20}$	Training 600 MPa, 350 °C	6.26	Used for SME test, then training at 600 MPa, 350 °C

RESULTS

Shape Memory Effect Tests

Shape memory effect tests were performed on each alloy to determine the detwinning stresses and shape recovery strain after loading. The 300 to 600 MPa test results for the $NiTi_{29.7}Hf_{20}$ alloy (bar H1) are shown in Figure 22 where the solid line along zero stress is the shape recovery.

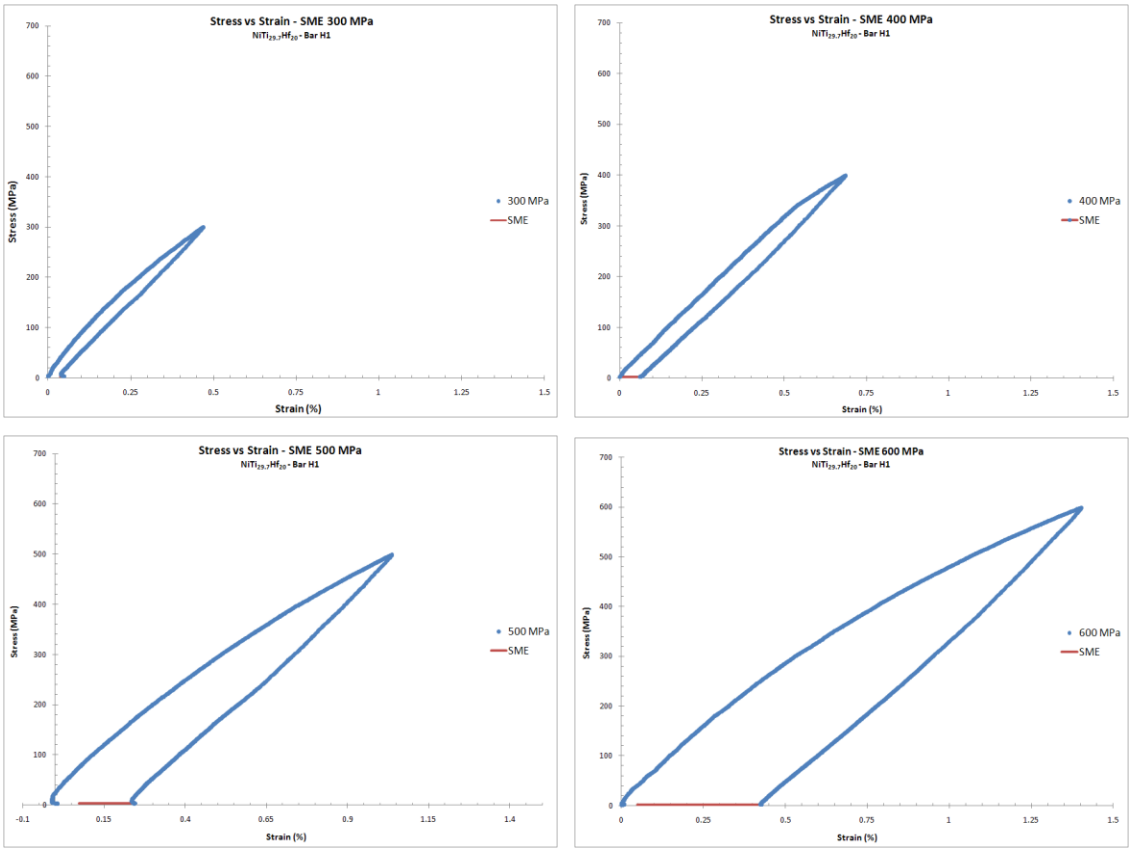

Figure 22: SME stress vs. strain curves from 300 to 600 MPa ($NiTi_{29.7}Hf_{20}$, Bar H1)

All stress levels show some amount of shape recovery, but none completely recover the entire deformation caused by loading. Also each loading is non-linear and no detwinning

plateau is observed like that of typical NiTi SMAs. Figure 23 compares the 300 and 600 MPa loading. Both seem to follow the same loading path and similar unloading slopes.

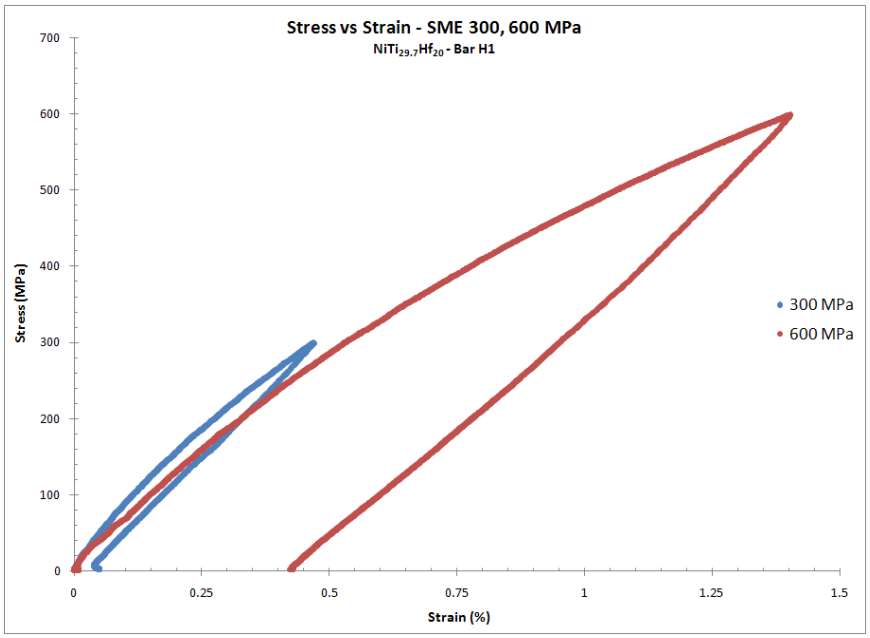

Figure 23: SME stress vs. strain comparison for 300 and 600 MPa ($NiTi_{29.7}Hf_{20}$, bar H1)

The results of the SME tests for the $NiCu_5Ti_{29.7}Hf_{20}$ (bar HC1) alloy are shown in Figure 24 with the solid again representing the shape recovery. Interestingly in the 300 MPa test, there is a positive shape recovery upon heating above the A_f temperature. This behavior is attributed to the internal stresses imparted into the material during forming and machining. The heating above A_f relieved the internal stresses and generated the positive SME. Again, none of the stress levels completely recovered the entire deformation caused by loading and no detwinning plateau is observed. Figure 25 compares the 300 and 600 MPa loading where again the loading and unloading curves follow similar slopes.

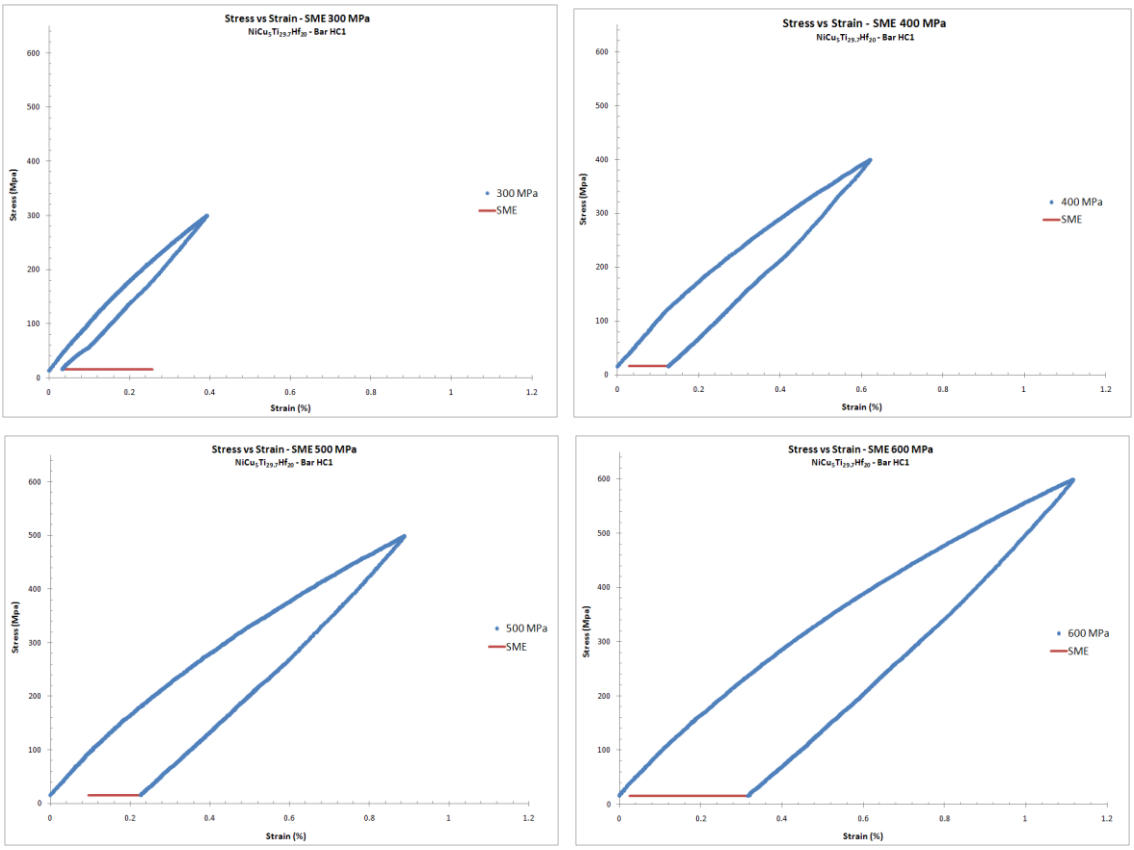

Figure 24: SME stress vs. strain curves from 300 to 600 MPa (HfCu alloy, Bar H1)

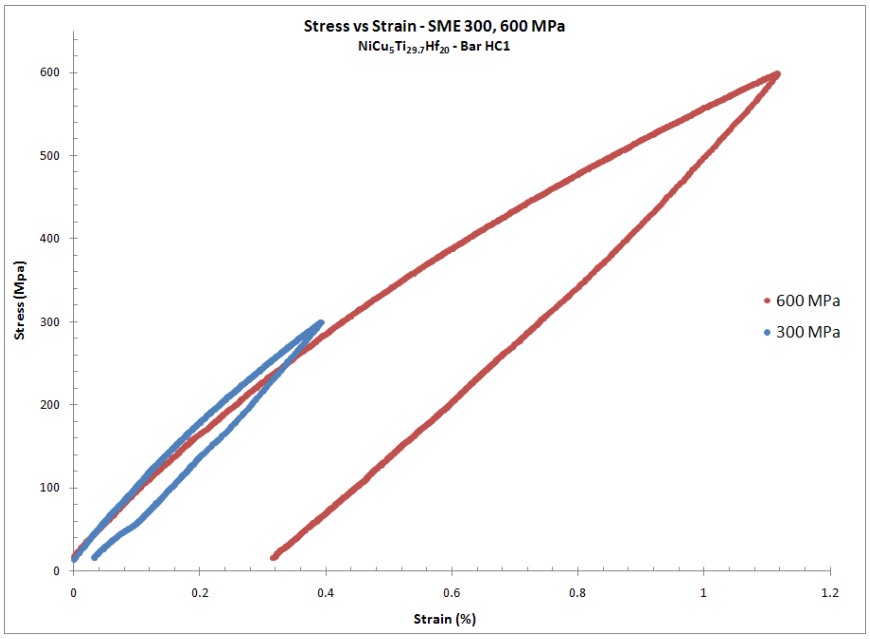

Figure 25: SME stress vs. strain comparison for 300 and 600 MPa ($NiCu_5Ti_{29.7}Hf_{20}$ alloy, Bar H1)

Figure 26 compares the SME tests of both alloys at 600 MPa. The $NiTi_{29.7}Hf_{20}$ alloy has a higher amount of strain at 600 MPa compared to the $NiCu_5Ti_{29.7}Hf_{20}$ alloy. The shape of the loading and unloading for both alloys is almost identical though. In conclusion, both alloys have similar results when loading in martensite and achieve comparable SME recovery strains upon reheating at no load.

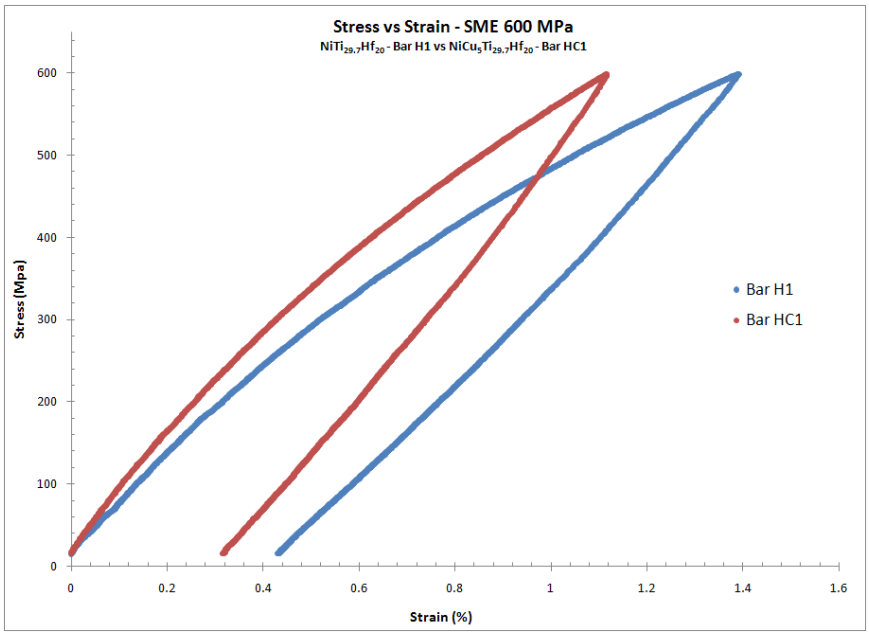

Figure 26: SME stress vs. strain curve comparison of $NiTi_{29.7}Hf_{20}$ (bar H1) and $NiCu_5Ti_{29.7}Hf_{20}$ (bar HC1) at 600 MPa

Superelastic Tests

The individual superelastic tests for the 300, 400, 500, and 600 MPa loadings of the $NiTi_{29.7}Hf_{20}$ and $NiCu_5Ti_{29.7}Hf_{20}$ alloys are show in Figure 52 and Figure 53 in Appendix A respectively. These results are condensed into Figure 27 and Figure 28; the test results of the 300 and 600 MPa loading for the $NiTi_{29.7}Hf_{20}$ and $NiCu_5Ti_{29.7}Hf_{20}$ alloy respectively. The austenite phase of both alloys is linear-elastic with the austenitic modulus of 81.5 GPa for $NiTi_{29.7}Hf_{20}$ and 76.1 GPa for $NiCu_5Ti_{29.7}Hf_{20}$. During these loadings, no stress induced martensite is formed and no yielding occurs. Figure 29 compares the austenite loading for both alloys up to 600 MPa.

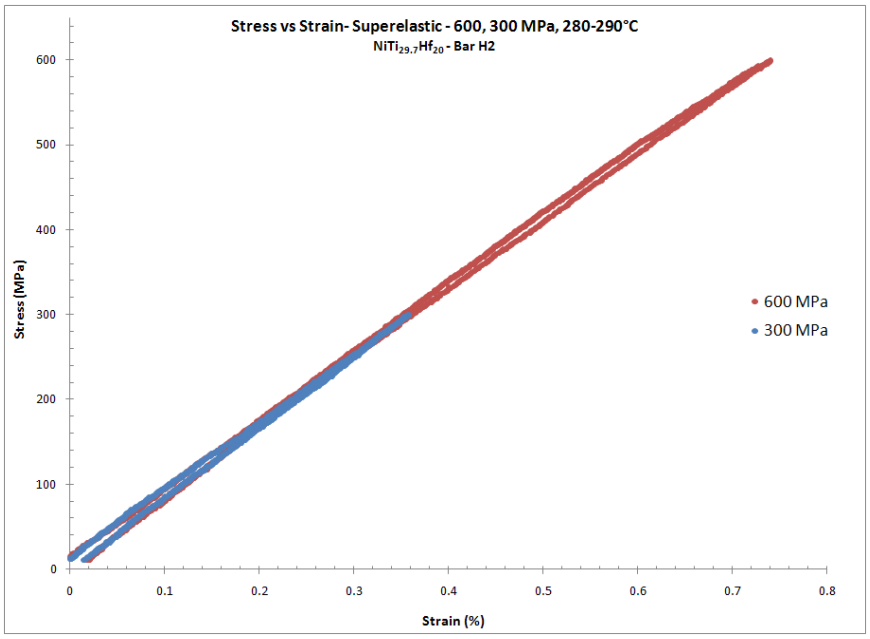

Figure 27: Superelastic stress vs. strain curve comparison for 300 and 600 MPa (Hf alloy, Bar H2)

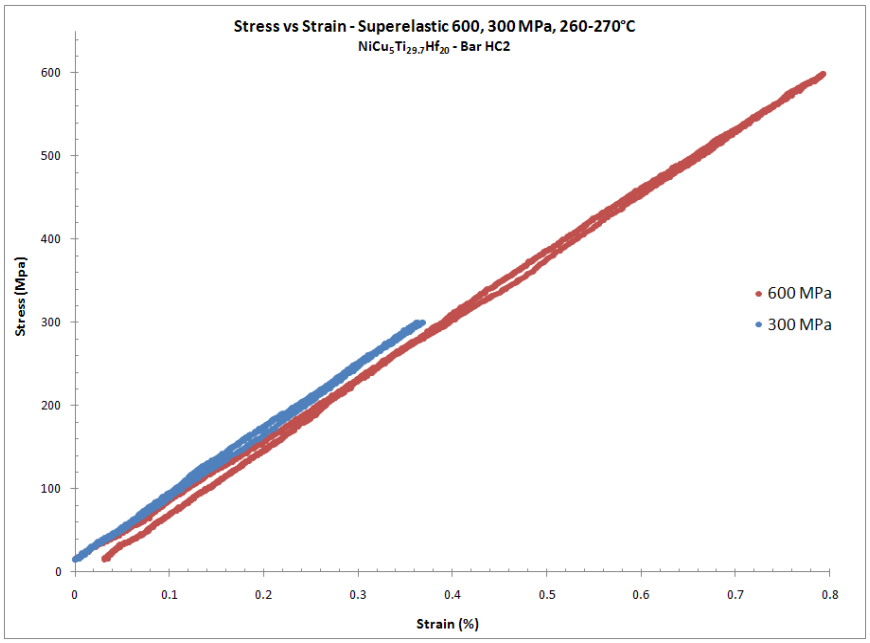

Figure 28: Superelastic stress vs. strain curve comparison for 300 and 600 MPa (HfCu alloy, Bar HC2)

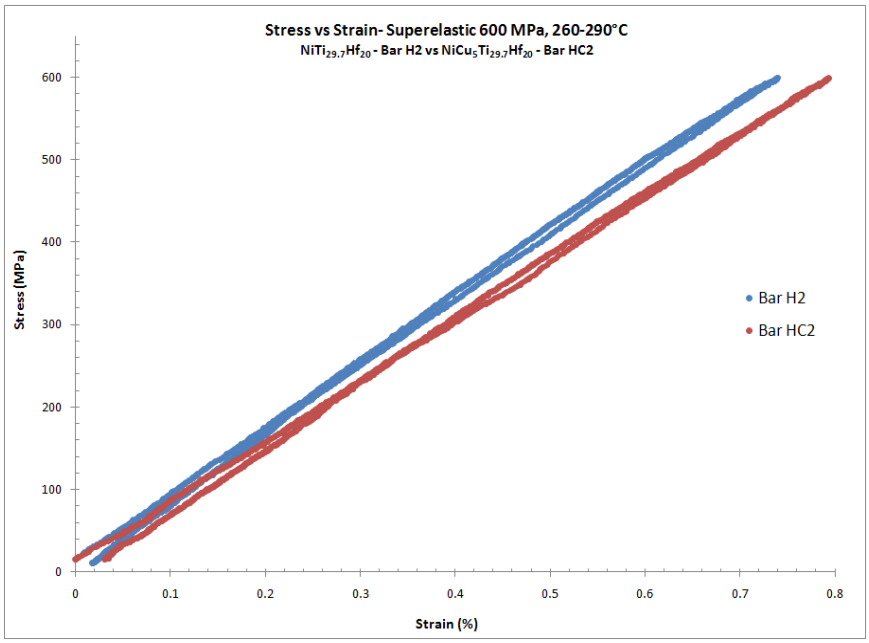

Figure 29: Superelastic stress vs. strain curve comparison of $NiTi_{29.7}Hf_{20}$ (bar H2) and $NiCu_5Ti_{29.7}Hf_{20}$ (bar HC2) at 600 MPa (Bar H2 at 280-290°C and Bar HC2 at 260-270°C)

Thermomechanical Training and Actuation Strains

$NiTi_{29.7}Hf_{20}$ 300 MPa, 290 °C Training and Actuation Results

The SME and superelastic tests revealed any stress up to 600 MPa was suitable for training stress both high temperature alloys. No yielding of martensite or austenite occurred below 600 MPa, and no stress induced martensite formed in the austenitic phase. The first thermomechancial training was performed on $NiTi_{29.7}Hf_{20}$ (bar H3) at max training stress and temperature of 300 MPa and 290 °C to ascertain if TrIP occurred in the high temperature alloys at lower stress levels. The results of the 300 MPa training are shown in the strain vs. temperature plot in Figure 30. The training showed almost no TrIP after several thermal cycles.

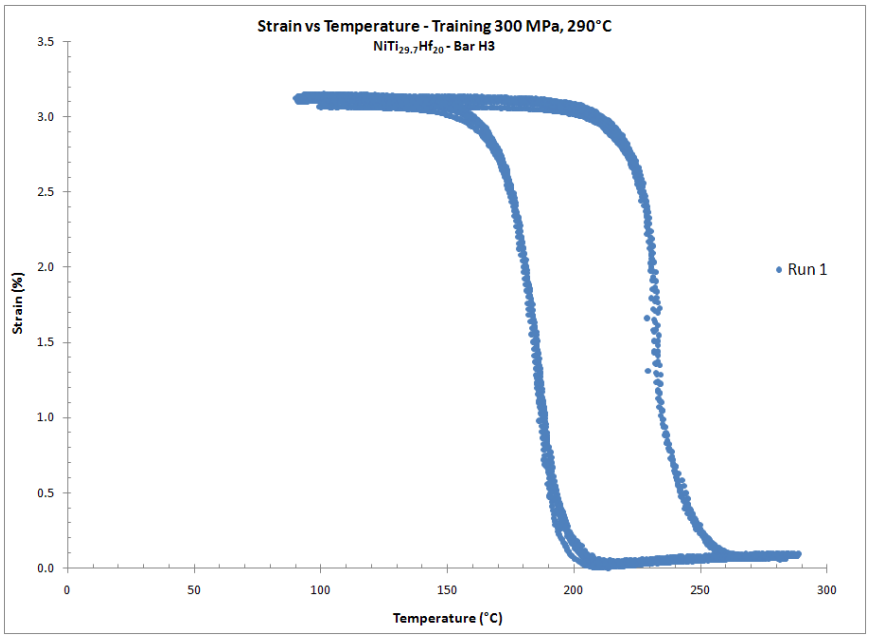

Figure 30: Strain vs. temperature curve for isobaric training of $NiTi_{29.7}Hf_{20}$ (bar H3) at 300 MPa, max temperature 290°C

Even though only a small amount of TrIP occurred during training at 300 MPa, some amount of TWSME was achieved. After training, the specimen was thermally actuated at stress levels from 300 to 0 MPa in 50 MPa steps to characterize the action strains. Figure 54 in Appendix A shows the temperature vs. strain plots for each individual stress level. The amount of actuation strain for each stress level is shown in Figure 31.

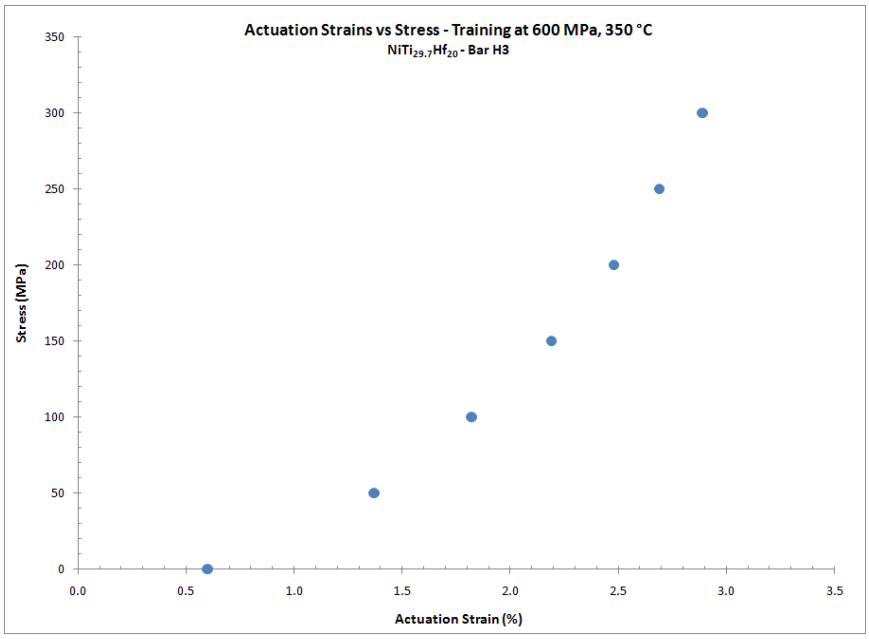

Figure 31: Actuation strains vs. stress for $NiTi_{29.7}Hf_{20}$ (bar H3) trained at 300 MPa, 290°C

$NiTi_{29.7}Hf_{20}$ 600 MPa, 350°C and 400°C Training

Training at 300 MPa produced very little TrIP, so the max training stress for the other specimens was increased to 600 MPa. The higher stress resulted in TrIP for the $NiTi_{29.7}Hf_{20}$ alloy as shown in Figure 32 and Figure 33. The training in Figure 32 was performed on bar H5 and used a max temperature of 350°C which was just high enough to ensure a complete transformation to austenite. To observe the effects training temperature has on TrIP, bar H3 was trained at 600 MPa and 400°C as seen in Figure 33. The higher training temperature resulted in a higher amount of TrIP; 0.579% permanent strain for training at 400°C compare to 0.514% permanent strain at 350°C.

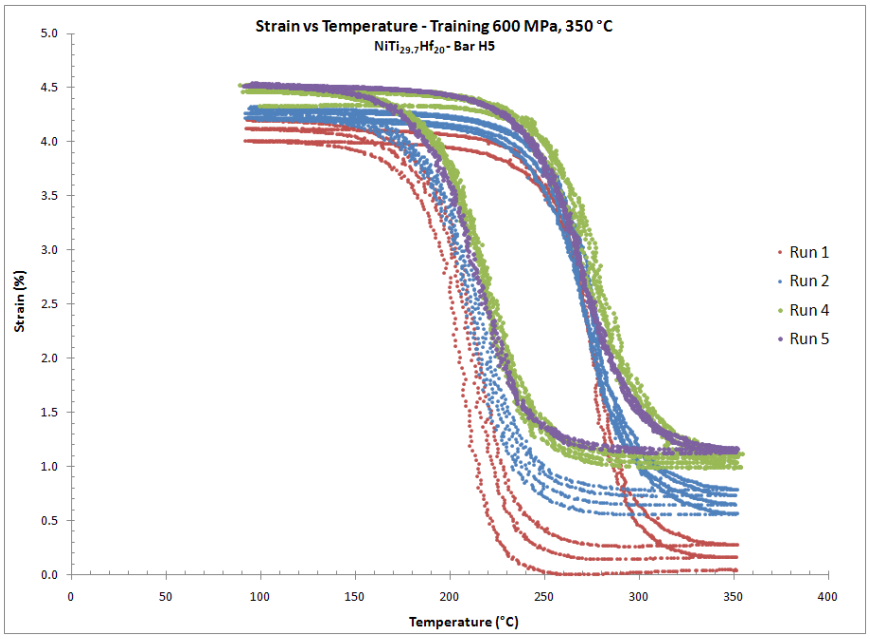

Figure 32: Strain vs. temperature curve for isobaric training of NiTi29.7Hf20 (bar H5) at 600 MPa, max temperature 350°C

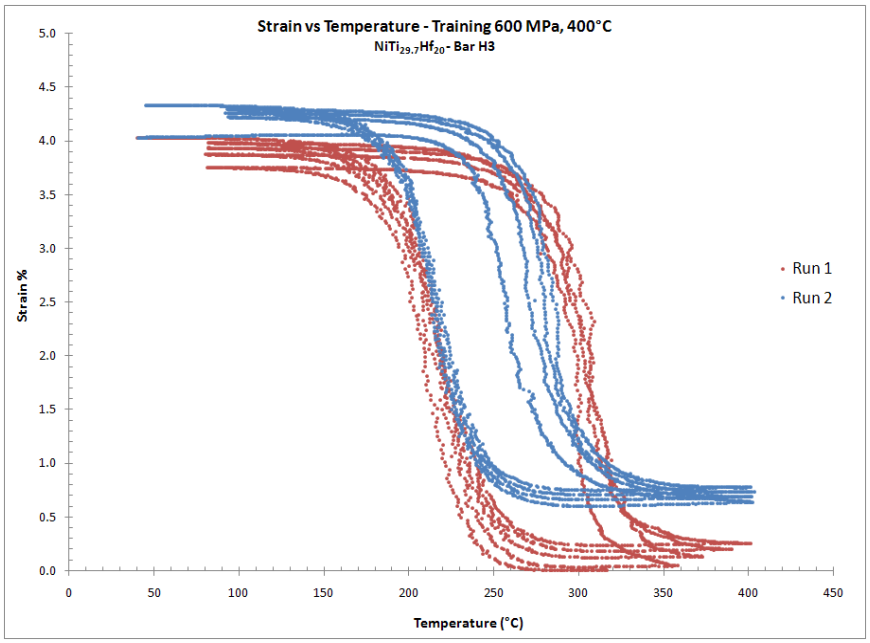

Figure 33: Strain vs. temperature curve for isobaric training of NiTi29.7Hf20 (bar H5) at 600 MPa, max temperature 400°C

$NiCu_5Ti_{29.7}Hf_{20}$ 600 MPa, 300°C and 350°C Training

Bars HC3 and HC4 of the $NiCu_5Ti_{29.7}Hf_{20}$ alloy were trained at a max stress of 600 MPa and 300°C and 350°C respectively. Both bars experience TrIP as seen in Figure 34 and Figure 35. Training at 300°C resulted in a permanent strain of 0.183% while training at 350°C resulted in 0.264%. Again the higher training temperature resulted in higher plastic strain growth.

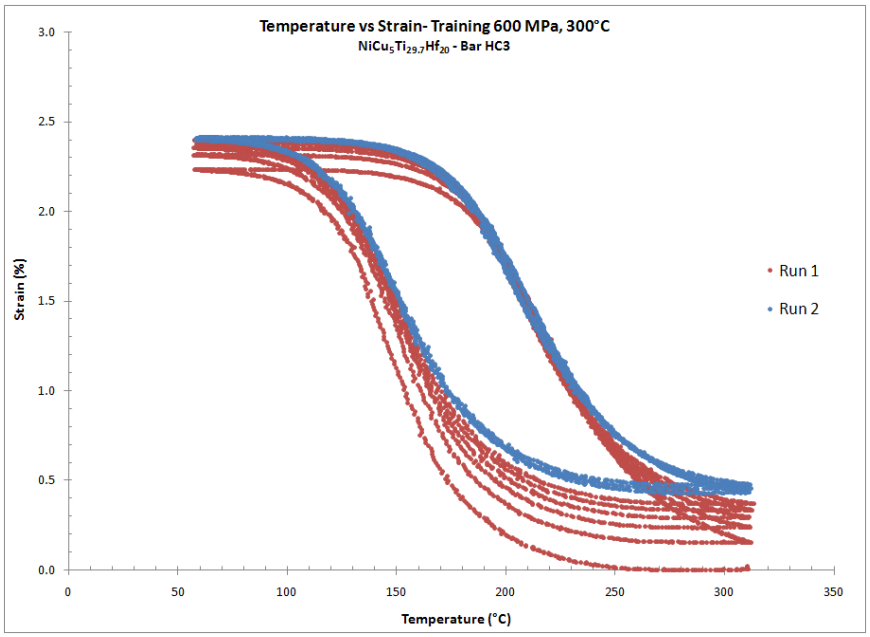

Figure 34: Strain vs. temperature curve for isobaric training of NiCu5Ti29.7Hf20 (bar HC3) at 600 MPa, max temperature 300°C

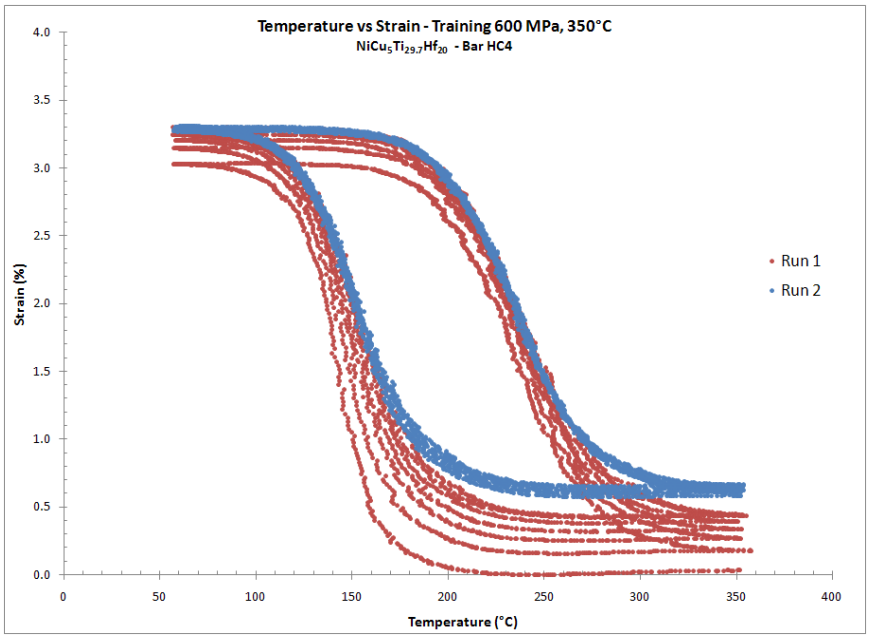

Figure 35: Strain vs. temperature curve for isobaric training of NiCu5Ti29.7Hf20 (bar HC4) at 600 MPa, max temperature 350°C

$NiTi_{29.7}Hf_{20}$ and $NiCu_5Ti_{29.7}Hf_{20}$ Actuation Strains

After each bar specimen was trained, they were thermally actuated three to four times from 600 MPa to 0 MPa in 100 MPa steps to determine actuation strains at different stresses. To show the difference in the actuation hysteresis of the $NiTi_{29.7}Hf_{20}$ and $NiCu_5Ti_{29.7}Hf_{20}$ alloys, actuation strains for bar H5 and bar HC3 are shown in strain vs. temperature plots for 600, 300 and 0 MPa in Figure 36. The $NiTi_{29.7}Hf_{20}$ alloy achieved higher actuation strains and a lower hysteresis between martensite and austenite than the $NiCu_5Ti_{29.7}Hf_{20}$ alloy. The $NiCu_5Ti_{29.7}Hf_{20}$ alloy requires a larger temperature range for the forward and reverse transformation. The complete strain (%) vs. temperature plots for bar H5, H6, HC3, and HC4 are shown in Figure 55, Figure 57, Figure 59, and Figure 61 respectively of Appendix A.

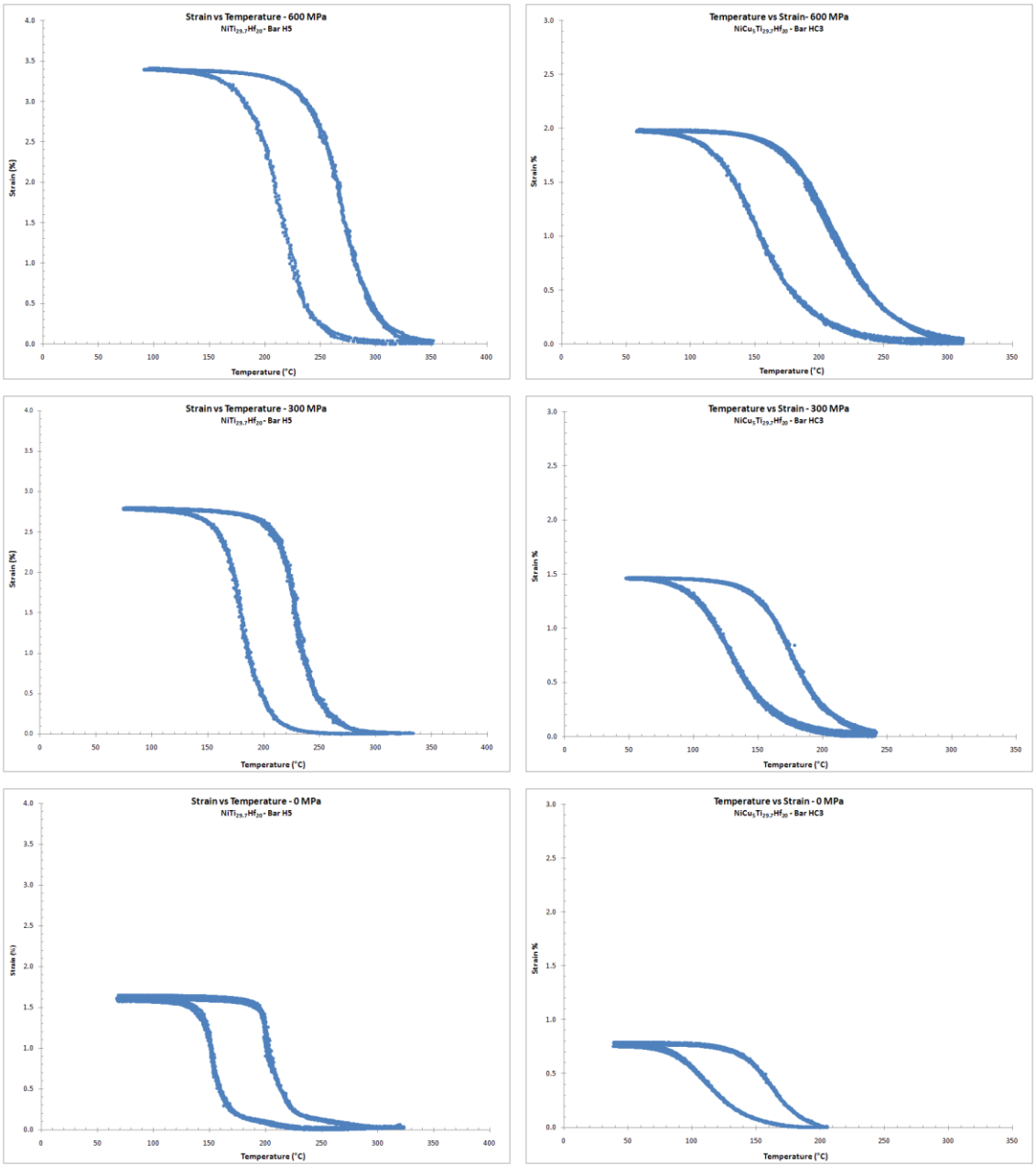

Figure 36: Left column - actuation strains for NiTi29.7Hf20, trained at 600 MPa, 350°C
Right column - actuation strains for NiCu5Ti29.7Hf20 trained at 600 MPa, 300°C

The results of all the actuation strains from training are listed in Table 3 and displayed graphically in Figure 37. The addition of copper to the high temperature alloys

reduces the amount of actuation strain from training. The $NiCu_5Ti_{29.7}Hf_{20}$ alloy does show a stronger dependence on training temperature than the $NiTi_{29.7}Hf_{20}$ alloy though. The curves of the $NiCu_5Ti_{29.7}Hf_{20}$ alloy have almost the exact same trend, just with a different axis intercept. The $NiTi_{29.7}Hf_{20}$ alloy on the other hand shows less of a dependence on training temperature. As the stress increases, the difference in training temperature becomes more apparent, but the zero stress actuation strain of bar H5 (trained at 350°C) is actually greater than that of bar H6 (trained at 400°C).

Table 3: Actuation strains (%) for each alloy – Training at 600 MPa and all training temperature

		Actuation Strain (%)			
Bar		H5	H6	HC3	HC4
Stress (MPa)	0	1.56	1.48	0.78	1.24
	100	2.14	2.16	0.98	1.60
	200	2.49	2.59	1.20	1.90
	300	2.79	2.89	1.46	2.13
	400	3.00	3.20	1.64	2.33
	500	3.19	3.34	1.80	2.50
	600	3.35	3.50	1.93	2.65

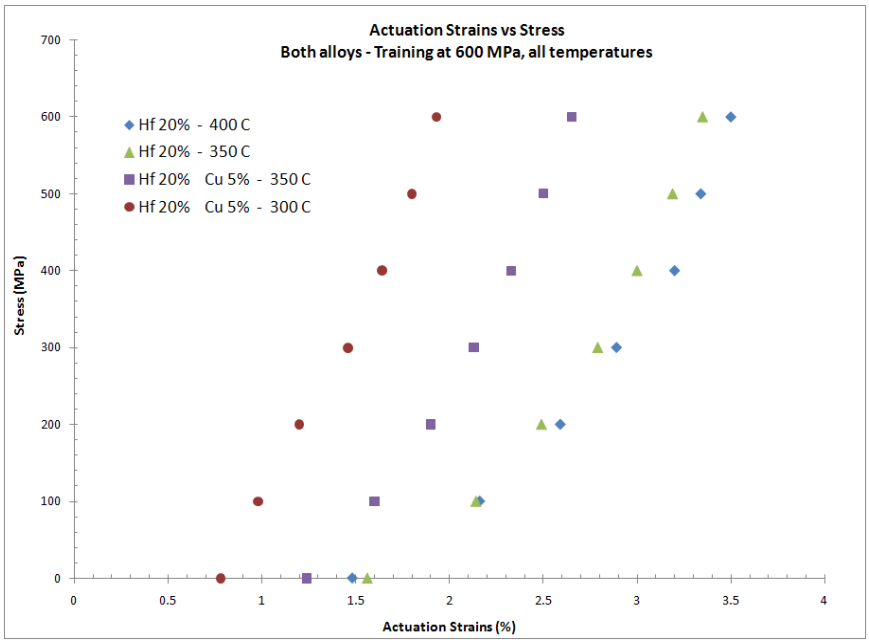

Figure 37: Actuation strains (%) vs. stress for both alloys trained at 600 MPa, all training temperatures

Back Stress Model Results

The resulting actuation strains were modeling using the Bo & Lagoudas model to assess the model's usefulness to high temperature alloys containing hafnium and copper (see Background for more information on model). The curve fit of interest is for the actuation strain (%) vs. stress. From these plots, the parameters of Equation 16 were determined by using MatLab's curve fitting tool. The tool allows for the input of a user defined equation and fits the parameters using a least squares regression. Equation 16 represents the back stress when the martensitic volume fraction (ξ) is one. Fitting this equation is useful because with the correct parameters, the actuation strain at any stress can be computed as seen in the following figures. The model fits for bar H5, H6, HC3, and HC4 are shown in Figure 38, Figure 39, Figure 40, and Figure 41 respectively. For

these fits, the parameters m_1 was set to 1.8 and D_2 to zero (see the Modeling TWSM section of the Background). The back stress equation fits very well to the data. The values of the calculated parameters are shown in Table 4.

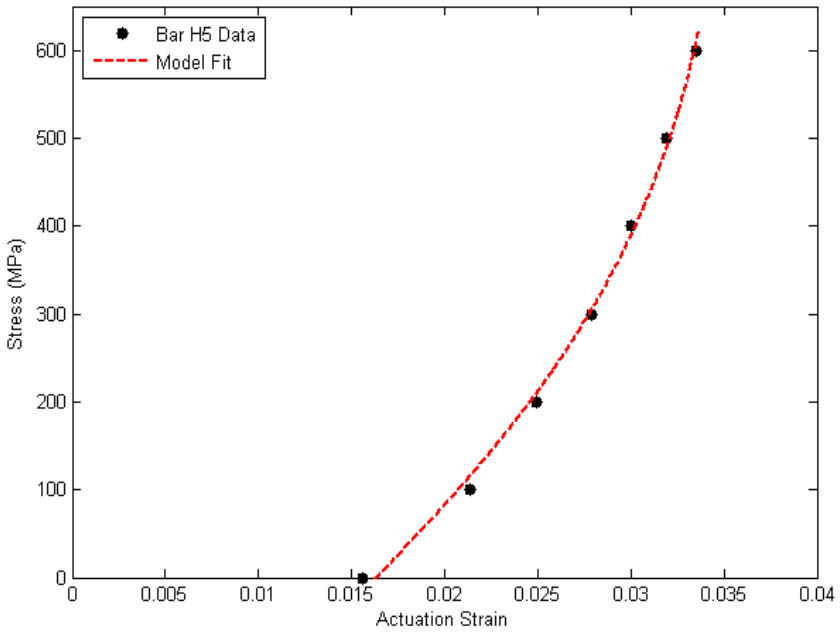

Figure 38: Model results for $NiTi_{29.7}Hf_{20}$ (Bar H5), trained at 600 MPa, 350°C

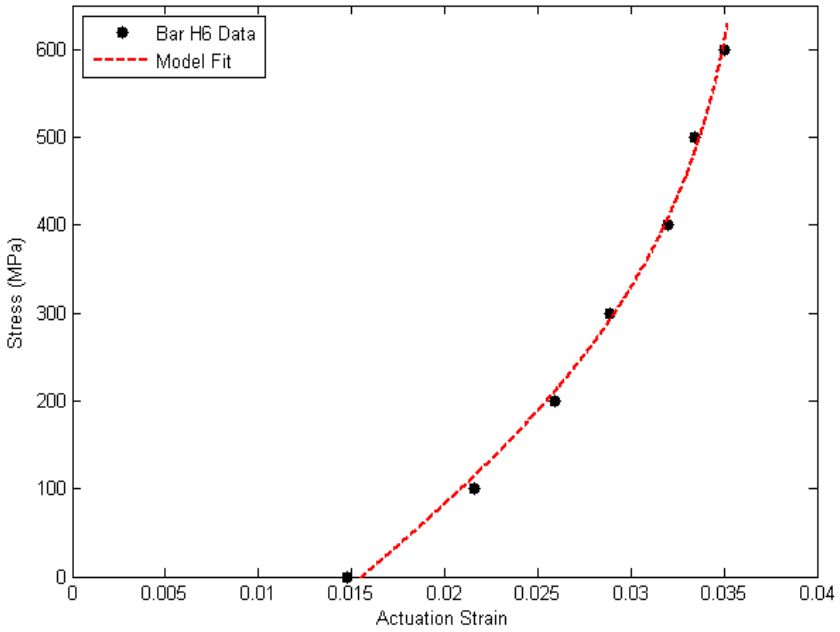

Figure 39: Model results for $NiTi_{29.7}Hf_{20}$ (Bar H6), trained at 600 MPa, 400°C

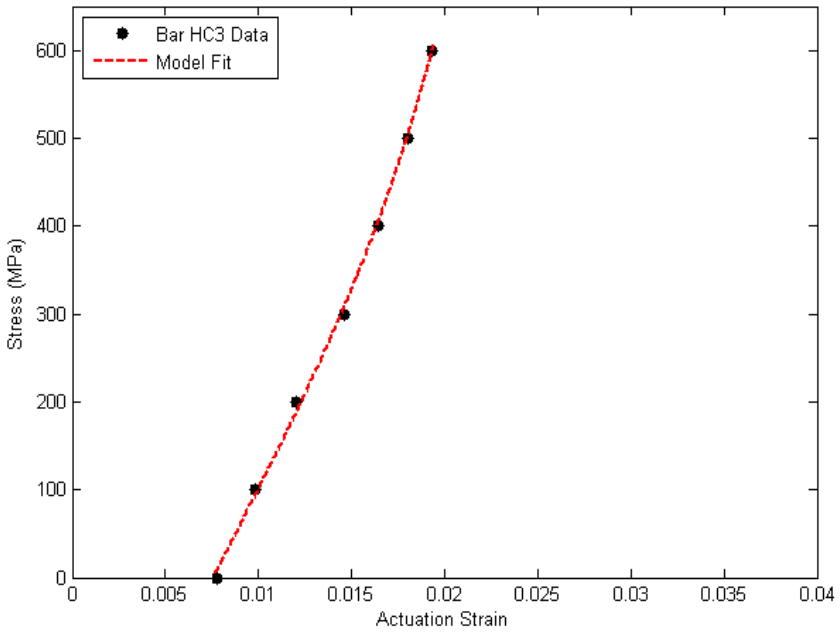

Figure 40: Model results for $NiCu_5Ti_{29.7}Hf_{20}$ (Bar HC3), trained at 600 MPa, 300°C

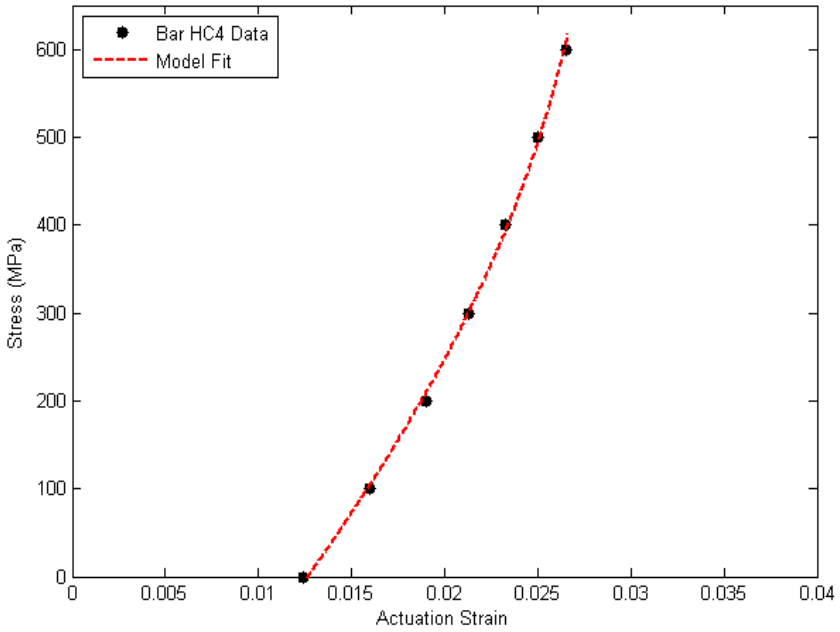

Figure 41: Model results for $NiCu_5Ti_{29.7}Hf_{20}$ (Bar HC4), trained at 600 MPa, 350°C

Table 4: Parameter results for high temperature alloy back stress model

Bar	D_1 (MPa)	D_3 (MPa)	H
H5	464.80	612.70	0.0358
H6	378.30	526.10	0.0367
HC3	464.40	785.50	0.0235
HC4	520.00	721.30	0.0297

Transformation Temperatures

The transformation temperatures for each stress level were determined using the method of intersecting tangents from the temperature vs. actuation strain plots of each alloy (see Appendix A). Figure 42 and Figure 43 are the transformation temperature for the $NiTi_{29.7}Hf_{20}$ and $NiCu_5Ti_{29.7}Hf_{20}$ alloy respectively. The dotted lines in both figures

represent the bars using the lower training temperatures. The addition of copper to $NiTi_{29.7}Hf_{20}$ alloy lowered each transformation temperatures by approximately 50°C. The bars subjected to the higher training temperatures resulted in raising the M_f and A_f transformation temperatures.

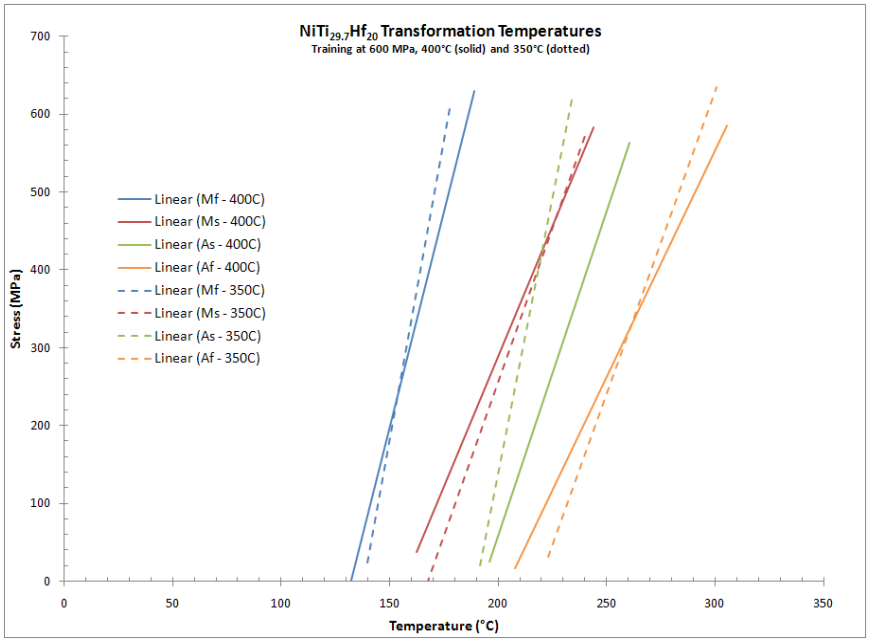

Figure 42: Transformation temperatures for $NiTi_{29.7}Hf_{20}$, both training temperatures included (350°C and 400°C)

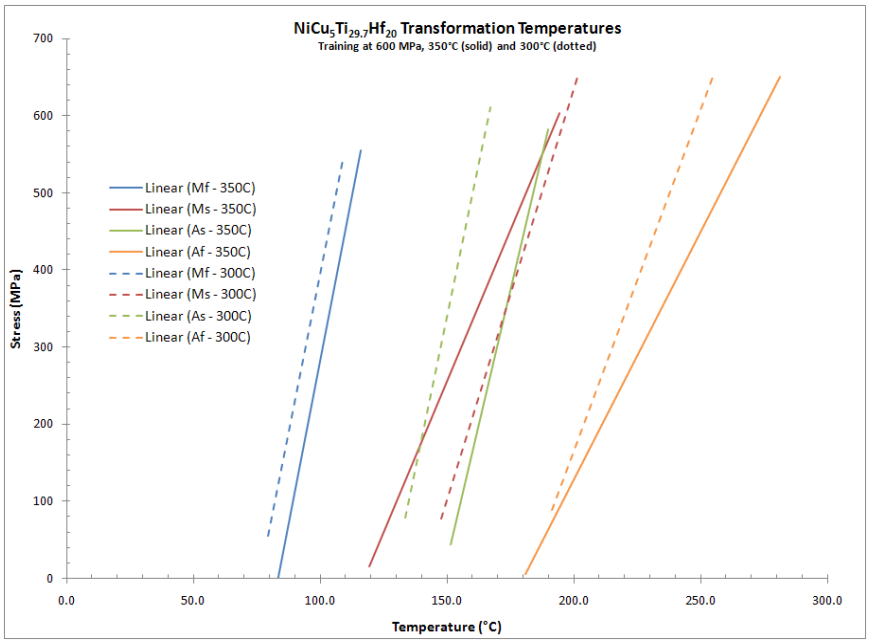

Figure 43: Transformation temperatures for $NiCu_5Ti_{29.7}Hf_{20}$, both training temperatures included (300°C and 350°C)

Annealing Effects

Up to this point there has been little information on how annealing the high temperature alloys affects their behaviors. As mentioned in the Experimental Procedure, a bar of each alloy was annealed at 450°C for 1 hour and allowed to cool in ambient air. The annealed $NiTi_{29.7}Hf_{20}$ bar was trained at 300 MPa, but only made it through four of the thermal cycles before failure. A picture of the failure surface for the annealed bar is shown in Figure 44. The annealed bar failed in a brittle manner with a flat failure surface. A closer look at the center of the bar reveals faint fatigue lines radiating from the center. This leans towards the conclusion a void formed in the center of the bar and each thermal cycle under the constant stress grew the void. Because of this failure at the lower training stress, further testing of the annealed specimens was abandoned.

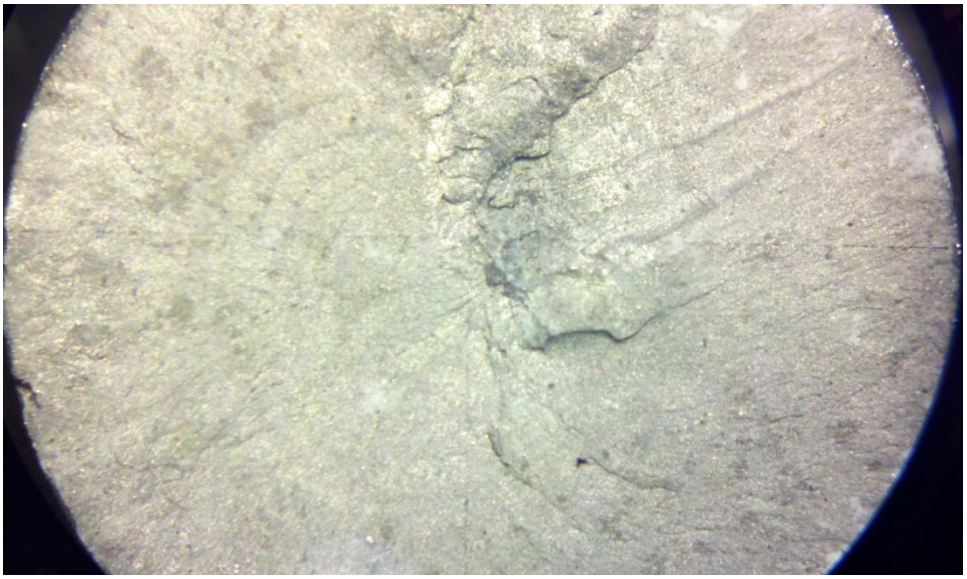

Figure 44: Annealed failure of $NiTi_{29.7}Hf_{20}$ - bar H4 trained at 300 MPa

This type of brittle failure during training was seen again on the $NiTi_{29.7}Hf_{20}$ as-received bar H2. This bar was initially used for superelastic testing. It later failed during isobaric training at 600 MPa and a max training temperature of 400°C in an attempt to obtain a better characterization of the actuation strains for these training parameters. The failure surface, Figure 45, has a similar brittle fracture to that of the annealed bar except for the appearance of fatigue lines. Before the thermomechanical training, the superelastic test subjected this bar to high temperatures, 280-290°C, for several hours. The time duration and high temperature was enough to form the same phenomenon in the annealed bar.

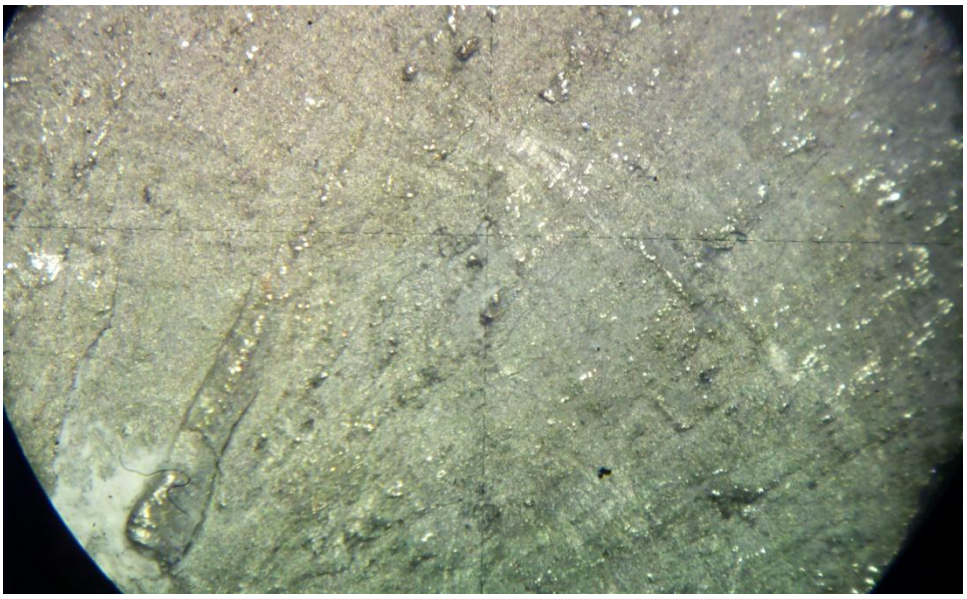

Figure 45: As-received failure of $NiTi_{29.7}Hf_{20}$ - bar H2 trained at 600 MPa

DISCUSSION

Training Characterization

Shape Memory Effect Tests

The results for the high temperature SME tests in Figure 23 and Figure 24 are different from typical NiTi in that the martensite did not detwinn and there were only small amounts of shape recovery on reheating. The loading was also non-linear at the lowest loading of 300 MPa and resulted in some amount of permanent strain. This information implies that both high temperature alloys experience slip and martensite reorientation at the same time. In the Ternary and High Temperature Shape Memory Alloys section of the Background, this behavior is attributed mainly to the matrix of NiTiHf alloys having a low resistance to slip where dislocation slip and martensite variant reorientation to occur almost simultaneously in the martensitic state (Chastaing, et al., 2006; Meng, et al., 2008). The occurrence of slip with the deformation is also the reason why the shape recovery after reheating is so low. Recovery comes from the reversibility of the detwinning (reorientation) deformation of the martensite variants. When slip occurs at the same time, some permanent strain is still present even with recovery of all the martensite variants.

The absence of detwinning is explained by the presence of $(Ti,Hf)_2Ni$ and $(Ti,Hf)_3Ni_4$ precipitates that formed during the three hour, 500°C aging process each bar experienced. The precipitates create an internal stress field that strengthens the matrix and is resistant to detwinning. Even with the precipitates strengthening the matrix, the

martensite phase still has a low resistance to slip due to slip plane distortion. This is shown best in Figure 46 where the martensitic response of the high temperature alloys are compared to 55NiTi ($NiTi_{50.1}$ at wt.%). The 55NiTi shows the characteristic plateau of detwinning while the high temperature alloys do not.

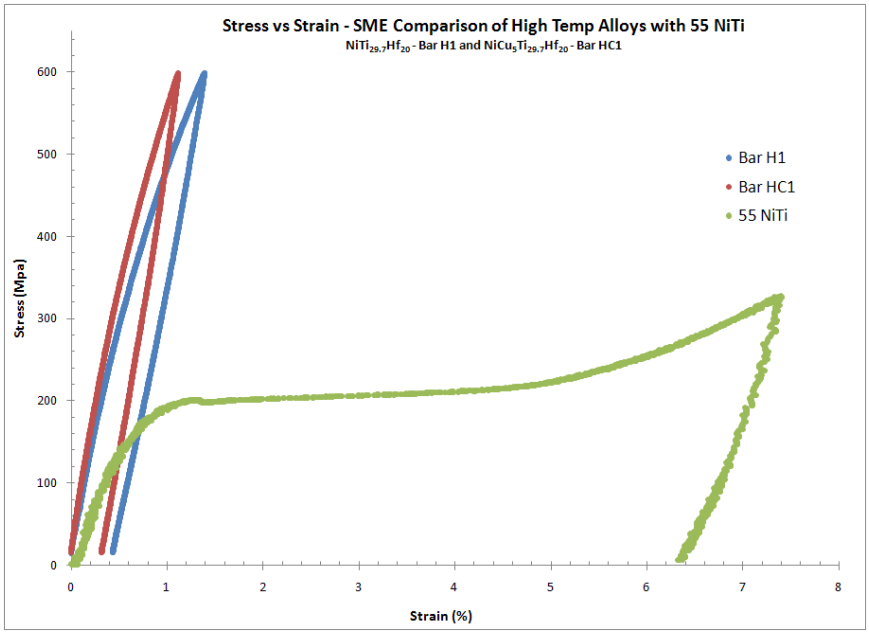

Figure 46: Stress vs. strain comparison of the martensite loading for the high temperature alloys and 55NiTi (55NiTi data provided by (Becker, 2010)

Superelastic Tests

The results of the superelastic tests at 600 MPa show no formation of stress induced martensite. The curves have a linear elastic loading up to 600 MPa and no yielding of the austenite occurs. The austenite matrix of the high temperature alloys exhibits more strength that that of 55NiTi which begins yielding around 300 MPa as seen in Figure 47. The reason for the high strength is the (Hf,Ti)Ni particulates also exist in the austenitic phase. The austenitic phase has a more ordered cubic structure than that of

martensite. In martensite, the addition of hafnium makes slip easier by distorting the slip planes of certain variants. In austenite, the (Ti,Hf)Ni particulates cause a precipitate hardening of the material and impede dislocation motion. This is why the high temperature alloys can reach such a high stress without yielding.

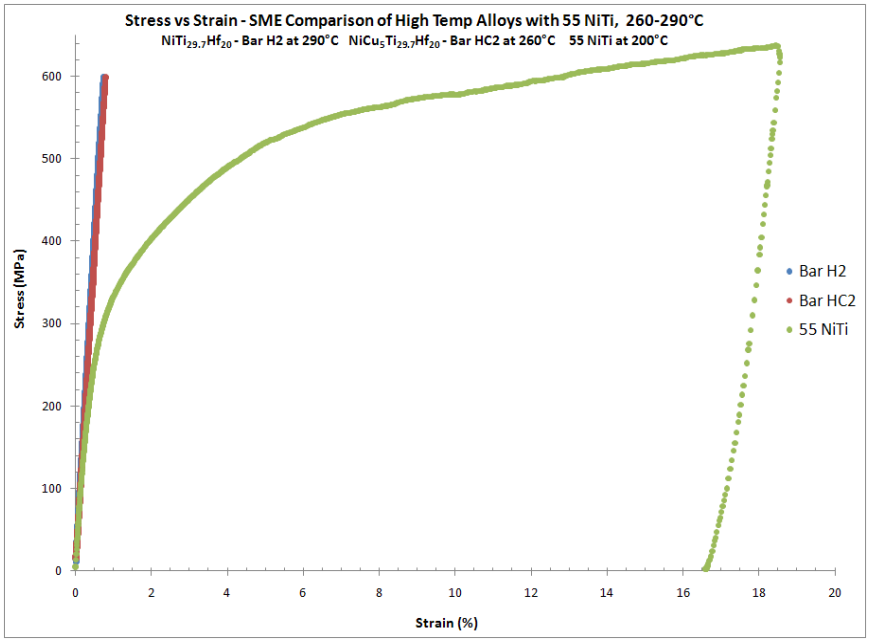

Figure 47: Stress vs. strain comparison of superelastic loading for the high temperature alloys and 55NiTi (55NiTi data provided by (Becker, 2010)

Training Parameters

The training temperatures and stresses used were based on the results of the SME and superelastic tests. Avoiding yielding it either phase and stress inducing martensite is ideal for the best isobaric training results. The SME and superelastic tests showed that up to 600 MPa neither of these would occur. The superelastic tests also revealed training temperatures above 290°C and 270°C were needed for $NiTi_{29.7}Hf_{20}$ and $NiCu_5Ti_{29.7}Hf_{20}$

respectively. With 600 MPa set as the max training stress, a bar was also trained at 300 MPa to determine if this stress was high enough to induce any TWSM.

Thermomechanical Training of High Temperature SMAs

The training results of each high temperature alloy in this study show minimal TrIP. This seems counter-intuitive since the stress to cause slip in the martensite phase is very low. Dislocation slip does occur in the first cycles of training and creates high internal stresses field in the material. This early stress field develops TWSM in the material within the first cycles, but it also work hardens the material. This work hardening limits further grain movement which in turn limits the TrIP achieved during training. The difference is very clearly seen by comparing the training of $NiTi_{29.7}Hf_{20}$ with 55NiTi as in Figure 48. The grains of 55NiTi are not hindered by early slip and develop a much higher amount of TrIP.

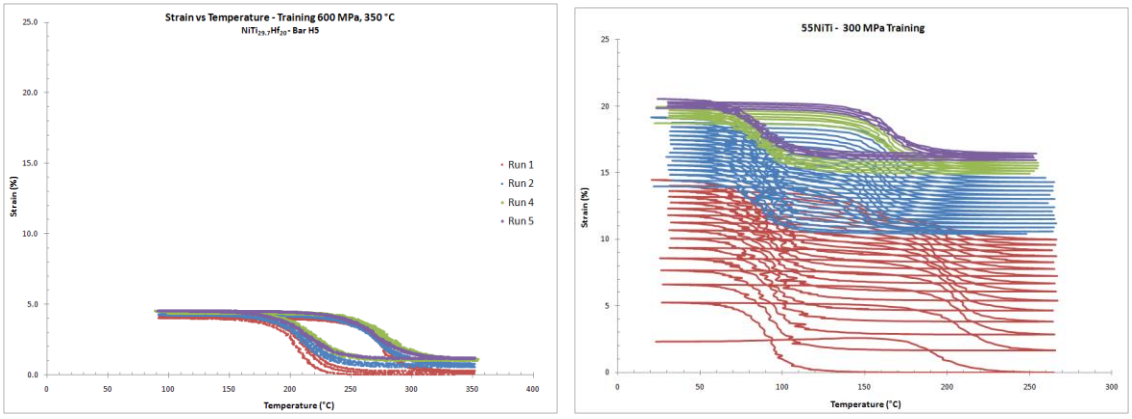

Figure 48: Training Comparison for high temperature $NiTi_{29.7}Hf_{20}$ alloy and 55NiTi, training performed on bars of similar diameter (55NiTi data provided by (Becker, 2010)

Actuation Strains

The results of the actuation strains in Figure 37 show that the high temperature SMAs $NiTi_{29.7}Hf_{20}$ and $NiCu_5Ti_{29.7}Hf_{20}$ can be trained into actuators. While the addition of copper provides some benefits, overall it decreases the amount of TrIP and possible actuation strain. The increase in temperature hysteresis of the $NiCu_5Ti_{29.7}Hf_{20}$ alloy is also not ideal for an actuator. The hysteresis also represents how long it takes the actuator to move between its on and off position. A larger temperature hysteresis means the actuator has to be heated and cooled in a larger window which slows the actuator's response time.

The training temperature had a substantial effect on the actuation strains for the $NiCu_5Ti_{29.7}Hf_{20}$, but not for the $NiTi_{29.7}Hf_{20}$. As explained in the Thermomechanically Training section of the Background, the actuation strains of NiTi are increased by increasing training temperature to a certain extent. Other studies have suggested this is from less retained martensite being present at the higher temperatures and allows for more TrIP to develop (Padula, et al.). From this explanation, the $NiTi_{29.7}Hf_{20}$ alloy not resulting in higher actuation strains at higher temperatures seems unusual because it too would retain less martensite at higher temperatures. One explanation is the training history of the bar. The actuation strain results for training at 600 MPa, 400°C came from bar H6. But before the 600 MPa training, the bar was trained at 300 MPa labeled as bar H3 (bar H6 and H3 are the same bar, just with different labels for different training). It's

possible this prior training created path dependence in the material. This is supported by comparing the actuation strains between bar H3 and H6 in Table 5 and Figure 49.

Table 5: Actuation strains (%) comparison for $NiTi_{29.7}Hf_{20}$ - trained at 300 MPa as bar H3, then and 600 MPa as bar H6

Stress (MPa)	$NiTi_{29.7}Hf_{20}$ (Bar H3) 300 MPa Training	$NiTi_{29.7}Hf_{20}$ (Bar H3) 600 MPa Training
0	0.6	1.48
100	1.82	2.16
200	2.48	2.59
300	2.89	2.89
400	-	3.20
500	-	3.34
600	-	3.50

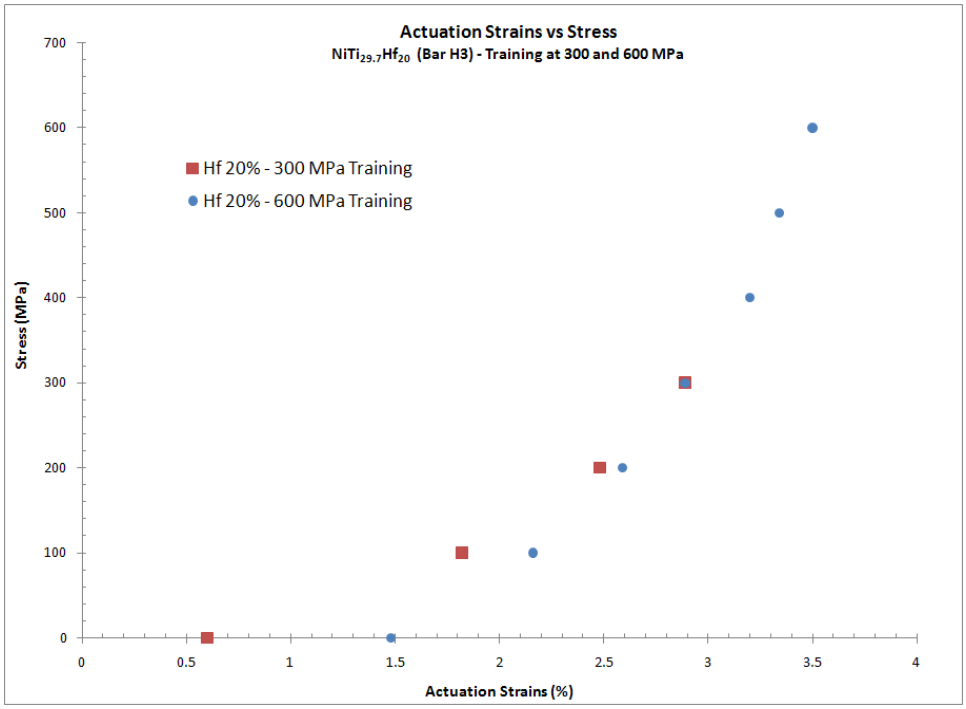

Figure 49: Actuation strain vs. stress for $NiTi_{29.7}Hf_{20}$ - trained at 300 MPa as bar H3, then and 600 MPa as bar H6

The 300 and 600 MPa training start to converge at the actuation strains around 200 MPa. The 600 training developed higher actuation strains at the lower stresses, but it appears that the lower training stress of 300 MPa performed on the bar first has limited the maximum actuation strains possible. An effort was made to train bar H2, used only in the superelastic test, at 600 MPa, 400°C, but after thermal cycles at constant stress this bar failed in a brittle as reported in the results. The explanation of this brittle failure is discussed in following sections. The failure of bar H2 during this training was the last $NiTi_{29.7}Hf_{20}$ test specimen available so another attempt couldn't be made.

The actuation strains developed in the high temperature alloys are lower than that of typical NiTi actuation strains for this same training procedure. Figure 50 compares the highest actuation strains of both high temperature alloys to that of 55NiTi. Important to note is 55NiTi was trained at 300 MPa, not 600 MPa like the high temperature alloys, and 55NiTi's actuation strains are still higher. Like other results reported in literature, high temperature alloys using the addition of another element to NiTi do not achieve actuation strains as high as regular NiTi.

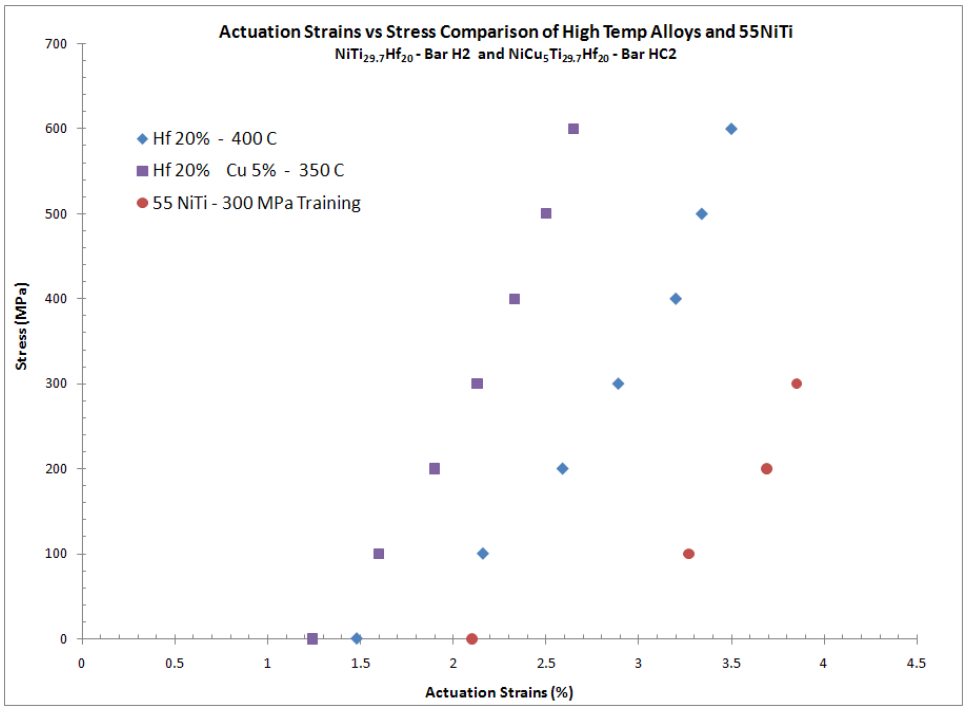

Figure 50: Actuation strain comparison for high temperature $NiTi_{29.7}Hf_{20}$ alloy and 55NiTi, training performed on bars of similar diameter (55NiTi data provided by (Becker, 2010)

Model Fits and Predictions

The Bo & Lagoudas model resulted in a very good fit to the high temperature SMA actuation strain data and is capable of predicting the actuation strains at other stresses. Prior to this study, this model was only used to fit NiTi and NiTiCu data. This research shows the model is also capable of fitting and predicting the behavior of hafnium based high temperature SMAs. One noticeable trend in the table is the maximum transformation strain, H, increases with increasing training temperature. This further reinforces that higher training temperatures result in higher actuation strains. Also D_3, the heterogeneity back stress, decreases with increasing training temperature in all instances.

Varying the temperature while keeping the training stress constant sheds light on how the material parameters of the model behave when changing the stress and temperature. The end goal of fitting experimental data to this model is to understand what controllable variable (temperature, stress, alloy composition, etc) effects which material parameter. The research performed prior to this study showed the material parameters are independent of size, i.e. a bar and wire results are the same. This research extends the model to SMAs other than NiTi and that H and D_3 are affected by training temperature. This information can lead to further testing of an alloy to determine an expected range of values for these material parameters based on training temperature. In this way, the model is now used to predict actuation strains, instead of fitting action strains to the model.

Transformation Temperatures vs. Creep and Annealing Temperatures

The transformation temperatures of the both high temperature alloys were higher than what is possible with typical NiTi SMAs. Figure 51 compares the transformation temperatures of the $NiTi_{29.7}Hf_{20}$ alloy to 55NiTi. The transformation temperatures for both $NiTi_{29.7}Hf_{20}$ and $NiCu_5Ti_{29.7}Hf_{20}$ are actually almost ideally suited to avoid many of the problems encountered when using high temperature SMAs. If the transformation temperatures are too high, creep and annealing of the dislocations that cause TWSM can occur. A general rule is creep becomes problematic when the temperature reaches $0.35T_{melting}$ for metals (Ashby, Hugh, & Cebon, 2007). The melting temperature of equiatomic NiTi is approximately 1300°C. So using this melting temperature and this

general rule, the problematic creep temperature can be estimated to occur somewhere around 450°C in the high temperature SMAs. The highest transformation temperatures found in this study do not exceed this limit, and are below the temperatures used for annealing. This makes the $NiTi_{29.7}Hf_{20}$ and $NiCu_5Ti_{29.7}Hf_{20}$ alloy systems perfect candidates for high temperature actuators.

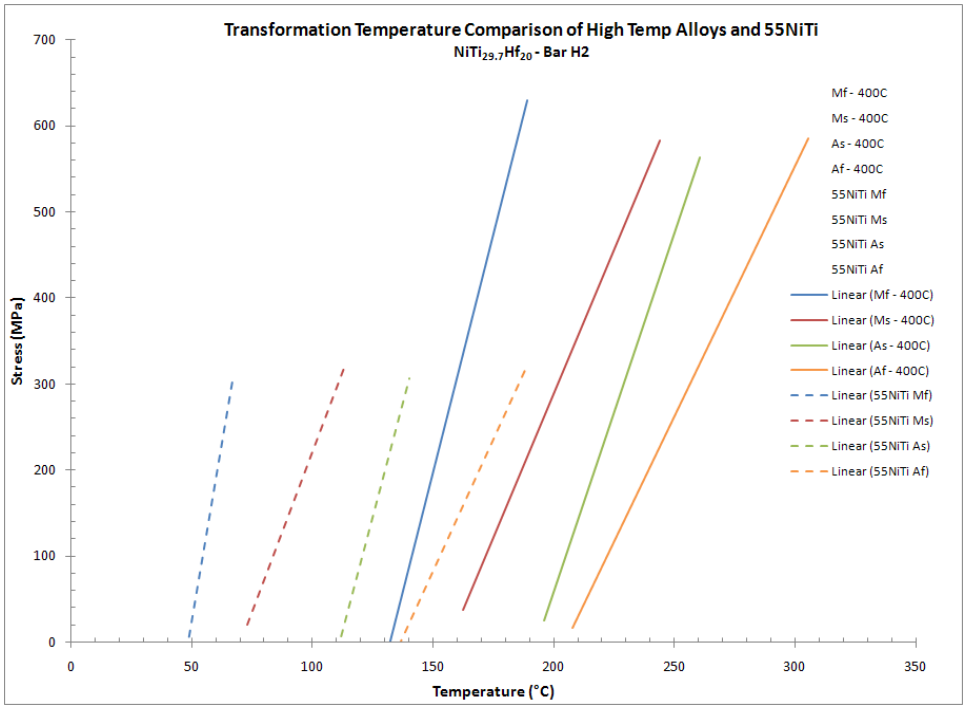

Figure 51: Transformation temperatures for high temperature $NiTi_{29.7}Hf_{20}$ alloy and 55NiTi, for bars of similar diameter (55NiTi data provided by (Becker, 2010)

Causes of Test Specimen Failures

The failures of two $NiTi_{29.7}Hf_{20}$ test specimens during the thermomechanical training is attributed to the formation of (TiHf)Ni particulates during annealing or during an extending exposure to high temperatures. See Ternary and High Temperature Shape Memory Alloys section in the Background for more information on (TiHf)Ni precipitate

formation. The precipitates act to strength the matrix of the material, but as the strength increases the toughness decreases. Both failures occurred in a brittle like nature during training. The slip and martensite reorientation occurring around the precipitates during training was enough for the material to fail.

The failure of the bar H4, annealed for one hour at 450°C, is conceivable because the annealing process allows more than enough time for (TiHf)Ni particulates to form throughout the bar. The failure of bar H2 though, which was used for the superelastic test only, is worrisome because it was exposed to a lower temperature of 290°C for two to three hours. Because of the failure, it can be concluded this exposure was enough to also form (TiHf)Ni particulates through the bar. In an actual application, a high temperature SMA actuator could easily be kept in the austenite state for an extended period of time. (TiHf)Ni particulates could easily form in this period and lead to degradation and failure of the actuator.

CONCLUSION

This work was a continuation of a previous study by Becker (2010) to characterize and train SMAs into 1-D actuators in an effort to standardize training procedures for SMAs. The characterization and training procedure was extended from NiTi to two high temperature SMAs: $NiTi_{29.7}Hf_{20}$ and $NiCu_5Ti_{29.7}Hf_{20}$. The initial characterization was successfully at determining the SME and superelastic response of the two alloys. The information from the above tests was then used to determine appropriate training stresses and temperatures. Two bars of each alloy were trained at a constant stress of 600 MPa, and at two different maximum training temperatures to determine the effect training temperature has on actuation results. The $NiTi_{29.7}Hf_{20}$ alloy was trained at 350°C and 400°C, and the $NiCu_5Ti_{29.7}Hf_{20}$ alloy at 300°C and 350°C.

The SME and superelastic tests reveal a strengthened matrix compared to NiTi, but also one where slip and martensite reorientation occur simultaneous in the martensitic phase. From past literature, the cause of this behavior is attributed to the formation of $(Ti,Hf)_2Ni$ particulates that form during aging and annealing of the materials. The precipitates strengthen the matrix by blocking large dislocation motion while providing the martensite phase with a slip plane through lattice distortions. Because of martensite slip and variant reorientation occurring simultaneously, a high internal stress field quickly forms in the material during training. This limits the permanent strain developed by TrIP during isobaric training and is considerable less than typical NiTi. This also leads to the development of less actuation strain. The addition of copper to the $NiTi_{29.7}Hf_{20}$ alloy also further lowered the actuation strains and transformation temperatures.

The different maximum training temperatures had a significant effect on the amount of actuation strain developed for each bar. The increased training temperatures increased the amount of plastic strain from TrIP and the achieved actuation strains in almost all instances; especially for the $NiCu_5Ti_{29.7}Hf_{20}$ alloy. The one instance in the $NiTi_{29.7}Hf_{20}$ alloy where the actuation strain was not higher for the higher training temperature is attributed to the past training history of the bar.

The stress vs. action strain data was fit to the model by Bo & Lagoudas. This was the first time high temperature SMA data was fit to this model, but the model showed a very strong fit to the data. It is now possible to predict the action strains at other stresses using the model. The use of two different training temperatures also revealed the material parameters H and D_3 increase and decrease respectively for an increase in training temperature. Now it is known H and D_3 are at least functions of temperature, and further testing can be used to better define this relationship.

The two high temperature alloys use in this research are ideally suited for development as high temperature actuators due to the position of their transformation temperatures. The transformation temperatures of both alloys are higher than what can be usefully achieved by NiTi, and low enough to avoid rapid actuator degradation from creep and annealing of dislocations. However, the actuators may not be suited to extended periods of high temperatures as the failures of two test specimens has shown. The extended exposure of high temperatures encourages the formation of $(TiHf)_2Ni$ particulates which embrittle the material. The embrittlement can lead to degradation and failure during the phase transformations of the actuators.

FUTURE WORK

The next step in this research is to characterize the degradation of the actuation strains after numerous actuation cycles. Because of the development of $(TiHf)_2Ni$ in both alloys, the questions is how many transformation cycles can occur before the particulates start to seriously affect the actuator's performance. The effect higher transformation temperatures have on the annealing of dislocations can also be examined in this type of test. This test could require hundreds of on/off cycles for the actuator. This test would also answer several other questions including cycles to actuator failure.

A second challenge for the high temperature alloys is an understanding of how their performance changes with extended periods of high temperatures. This information could be obtained through a thermal fatigue tests. This would include using the same training procedure on the high temperature alloys as discussed in the work, and then subject the actuators to a high constant stress and temperature for an extend period of time. Follow this by several actuation cycles and repeat. After a certain number of cycles, the material's actuation strains and microstructure is examined to gage how the extended high temperatures are affecting its behavior and composition.

REFERENCES

Ashby, M., Hugh, S., & Cebon, D. (2007). *Materials Engineering, Science, Processing, and Design*: Elservier.

Auricchio, F. (2001). A robust integration-algorithm for a finite-strain shape-memory-alloy superelastic model. *International Journal of Plasticity, 17*(7), 971-990.

Becker, M. (2010). *Thermomechanical Training and Characterization of Shape Memory Alloy Axial Actuators.* Montana State University, Bozeman.

Bo, Z. H., & Lagoudas, D. C. (1999a). Thermomechanical modeling of polycrystalline SMAs under cyclic loading, Part I: theoretical derivations. *International Journal of Engineering Science, 37*(9), 1089-1140.

Bo, Z. H., & Lagoudas, D. C. (1999b). Thermomechanical modeling of polycrystalline SMAs under cyclic loading, Part III: evolution of plastic strains and two-way shape memory effect. *International Journal of Engineering Science, 37*(9), 1175-1203.

Chastaing, K., Vermaut, P., Ochin, P., Segui, C., Laval, J. Y., & Portier, R. (2006). Effect of Cu and Hf additions on NiTi martensitic transformation. *Materials Science and Engineering a-Structural Materials Properties Microstructure and Processing, 438*, 661-665. doi: 10.1016/j.msea.2006.02.114

Fuentes, J. M. G., Gumpel, P., & Strittmatter, J. (2002). Phase change behavior of nitinol shape memory alloys - Influence of heat and thermomechanical treatments. *Advanced Engineering Materials, 4*(7), 437-451.

Gao, X. J., & Brinson, L. C. (2002). A simplified Multivariant SMA model based on invariant plane nature of martensitic transformation. *Journal of Intelligent Material Systems and Structures, 13*(12), 795-810. doi: 10.1177/104538902032786

Govindjee, S., & Miehe, C. (2001). A multi-variant martensitic phase transformation model: formulation and numerical implementation. *Computer Methods in Applied Mechanics and Engineering, 191*(3-5), 215-238.

Juhasz, L., Schnack, E., Hesebeck, O., & Andra, H. (2002). Macroscopic modeling of shape memory alloys under non-proportional thermo-mechanical loadings. *Journal of Intelligent Material Systems and Structures, 13*(12), 825-836. doi: 10.1177/104538902032789

Kauffman, G. B., & Mayo, I. (1996). The Story of Nitinol: The Serendipitous Discovery of the Memory Metal and Its Applications. *The Chemical Educator, 2*(2), 1-21.

Kumar, P. K., & Lagoudas, D. C. (2010). Experimental and microstructural characterization of simultaneous creep, plasticity and phase transformation in Ti50Pd40Ni10 high-temperature shape memory alloy. [Article]. *Acta Materialia, 58*(5), 1618-1628. doi: 10.1016/j.actamat.2009.11.006

Lagoudas, D. C., & Bo, Z. H. (1999). Thermomechanical modeling of poly-crystalline SMAs under cyclic loading, Part II: material characterization and experimental results for a stable transformation cycle. *International Journal of Engineering Science, 37*(9), 1141-1173.

Lagoudas, D. C., & Entchev, P. B. (2004). Modeling of transformation-induced plasticity and its effect on the behavior of porous shape memory alloys. Part I: constitutive model for fully dense SMAs. *Mechanics of Materials, 36*(9), 865-892.

Lagoudas, D. C., Entchev, P. B., Popov, P., Patoor, E., Brinson, L. C., & Gao, X. J. (2006). Shape memory alloys, Part II: Modeling of polycrystals. *Mechanics of Materials, 38*(5-6), 430-462. doi: 10.1016/j.mechmat.2005.08.003

Lagoudas, D. C., & Shu, S. G. (1999). Residual deformation of active structures with SMA actuators. *International Journal of Mechanical Sciences, 41*(6), 595-619.

Lahoz, R., Gracia-Villa, L., & Puertolas, J. A. (2002). Training of the two-way shape memory effect by bending in NiTi alloys. *Journal of Engineering Materials and Technology-Transactions of the Asme, 124*(4), 397-401. doi: 10.1115/1.1495001

Lexcellent, C., Leclercq, S., Gabry, B., & Bourbon, G. (2000). The two way shape memory effect of shape memory alloys: an experimental study and a phenomenological model. *International Journal of Plasticity, 16*(10-11), 1155-1168.

Lim, T. J., & McDowell, D. L. (1994). *Degradation of an Ni-Ti Alloy During Cyclic Loading.* Paper presented at the 1994 North American Conference on Smart Structures and Materials, Orlando, Florida.

Liu, Y., & Xiang, H. (1998). Apparent modulus of elasticity of near-equiatomic NiTi. *Journal of Alloys and Compounds, 270*(1-2), 154-159.

Liu, Y. N., Liu, Y., & Van Humbeeck, J. (1998). Two-way shape memory effect developed by martensite deformation in NiTi. *Acta Materialia, 47*(1), 199-209.

Liu, Y. O., & McCormick, P. G. (1990). FACTORS INFLUENCING THE DEVELOPMENT OF 2-WAY SHAPE MEMORY IN NITI. *Acta Metallurgica Et Materialia, 38*(7), 1321-1326.

Lu, Z. K., & Weng, G. J. (1998). A self-consistent model for the stress-strain behavior of shape-memory alloy polycrystals. *Acta Materialia, 46*(15), 5423-5433.

Lubliner, J. (1990). *Plasticity Theory*: Macmillan Publishing Company.

Luo, H. Y., & Abel, E. W. (2007). A comparison of methods for the training of NiTi two-way shape memory alloy. *Smart Materials & Structures, 16*(6), 2543-2549. doi: 10.1088/0964-1726/16/6/058

McCormick, P. G., & Liu, Y. N. (1994). THERMODYNAMIC ANALYSIS OF THE MARTENSITIC-TRANSFORMATION IN NITI .2. EFFECT OF TRANSFORMATION CYCLING. *Acta Metallurgica Et Materialia, 42*(7), 2407-2413.

Meng, X. L., Cai, W., Fu, Y. D., Li, Q. F., Zhang, J. X., & Zhao, L. C. (2008). Shape-memory behaviors in an aged Ni-rich TiNiHf high temperature shape-memory alloy. [Article]. *Intermetallics, 16*(5), 698-705. doi: 10.1016/j.intermet.2008.02.005

Meng, X. L., Fu, Y. D., Cai, W., Li, Q. F., & Zhao, L. C. (2009). Microstructure and martensitic transformation behaviors of a Ti-Ni-Hf-Cu high-temperature shape memory alloy ribbon. *Philosophical Magazine Letters, 89*(7), 431-438. doi: 10.1080/09500830903019004

Mertmann, M., & Vergani, G. (2008). Design and application of shape memory actuators. *European Physical Journal-Special Topics, 158*, 221-230. doi: 10.1140/epjst/e2008-00679-9

Miller, D. (2000). *Thermomechanical Characterization of Plastic Deformation and Transformation Fatigue in NiTi Shape Memory Alloys.* Texas A&M University.

Miller, D. A., & Lagoudas, D. C. (2000). Thermomechanical characterization of NiTiCu and NiTi SMA actuators: influence of plastic strains. *Smart Materials & Structures, 9*(5), 640-652.

Miller, D. A., & Lagoudas, D. C. (2001). Influence of cold work and heat treatment on the shape memory effect and plastic strain development of NiTi. *Materials Science and Engineering a-Structural Materials Properties Microstructure and Processing, 308*(1-2), 161-175.

Miyazaki, S., Imai, T., Igo, Y., & Otsuka, K. (1986). EFFECT OF CYCLIC DEFORMATION ON THE PSEUDOELASTICITY CHARACTERISTICS OF TI-NI ALLOYS. *Metallurgical Transactions a-Physical Metallurgy and Materials Science, 17*(1), 115-120.

Otsuka, K., & Ren, X. B. (1999). Recent developments in the research of shape memory alloys. *Intermetallics, 7*(5), 511-528.

Otsuka, K., & Shimizu, K. (1986). Pseudoelasticity and shape memory effects in alloys. *International Metals Reviews, 31*(3), 94-113. Retrieved from

Otsuka, K., & Wayman, C. M. (1998). *Shape Memory Materials*: Press Syndicate of the University of Cambridge.

Padula, S. I., Qiu, S., Gaydosh, D., Noebe, R., Bigelow, G., Garg, A., & Vaidyanathan, R. Effect of Upper-Cycle Temperature on the Load-baised, Strain-Temperature Response of NiTi.

Panduranga, M. K., Shin, D. D., & Carman, G. P. (2006). Shape memory behavior of high temperature Ti-Ni-Pt thin films. *Thin Solid Films, 515*(4), 1938-1941. doi: 10.1016/j.tsf.2006.07.153

Pappas, P., Bollas, D., Parthenios, J., Dracopoulos, V., & Galiotis, C. (2007). Transformation fatigue and stress relaxation of shape memory alloy wires. [Article]. *Smart Materials & Structures, 16*(6), 2560-2570. doi: 10.1088/0964-1726/16/6/060

Patoor, E., Eberhardt, A., & Berveiller, M. (1996). Micromechanical modelling of superelasticity in shape memory alloys. *Journal De Physique Iv, 6*(C1), 277-292.

Patoor, E., Lagoudas, D. C., Entchev, P. B., Brinson, L. C., & Gao, X. J. (2006). Shape memory alloys, Part I: General properties and modeling of single crystals. *Mechanics of Materials, 38*(5-6), 391-429. doi: 10.1016/j.mechmat.2005.05.027

Qidwai, M. A., & Lagoudas, D. C. (2000). Numerical implementation of a shape memory alloy thermomechanical constitutive model using return mapping algorithms. *International Journal for Numerical Methods in Engineering, 47*(6), 1123-1168.

Reed-Hill, R. E., & Abbaschian, R. (1992). *Physical Metallurgy Principles* (3rd ed.): PWS-Kent Publishing Company.

Tanaka, K., Kobayashi, S., & Sato, Y. (1986). THERMOMECHANICS OF TRANSFORMATION PSEUDOELASTICITY AND SHAPE MEMORY EFFECT IN ALLOYS. *International Journal of Plasticity, 2*(1), 59-72.

Tanaka, K., Nishimura, F., Hayashi, T., Tobushi, H., & Lexcellent, C. (1995). PHENOMENOLOGICAL ANALYSIS ON SUBLOOPS AND CYCLIC BEHAVIOR IN SHAPE-MEMORY ALLOYS UNDER MECHANICAL AND OR THERMAL LOADS. *Mechanics of Materials, 19*(4), 281-292.

Tobushi, H., Ohashi, Y., Saida, H., Hori, T., & Shirai, S. (1992). RECOVERY STRESS AND RECOVERY STRAIN OF TINI SHAPE MEMORY ALLOY - (CYCLIC PROPERTIES UNDER CONSTANT RESIDUAL STRAIN AND CONSTANT MAXIMUM STRESS). *Jsme International Journal Series I-Solid Mechanics Strength of Materials, 35*(1), 84-90.

Volk, B., & Lagoudas, D. C. (2005). Characterization of High Temperature Shape Memory Alloys: Texas Institute for Intelligent Bio-Nano Materials and Structures for Aerospace Vehicles.

Wada, K., & Liu, Y. (2008). Thermomechanical training and the shape recovery characteristics of NiTi alloys. *Materials Science and Engineering a-Structural Materials Properties Microstructure and Processing, 481*, 166-169. doi: 10.1016/j.msea.2007.02.143

Wojcik, C. C. (2009). Properties and Heat Treatment of High Transition Temperature Ni-Ti-Hf Alloys. *Journal of Materials Engineering and Performance, 18*(5-6), 511-516. doi: 10.1007/s11665-009-9357-2

Yoon, S. H., & Yeo, D. J. (2008). Experimental investigation of thermo-mechanical Behaviors in Ni-Ti shape memory alloy. *Journal of Intelligent Material Systems and Structures, 19*(3), 283-289. doi: 10.1177/1045389x07083623

Zhou, B., & Yoon, S. H. (2006). A new phase transformation constitutive model of shape memory alloys. *Smart Materials & Structures, 15*(6), 1967-1973. doi: 10.1088/0964-1726/15/6/053

APPENDIX A

FIGURES

APPENDIX A

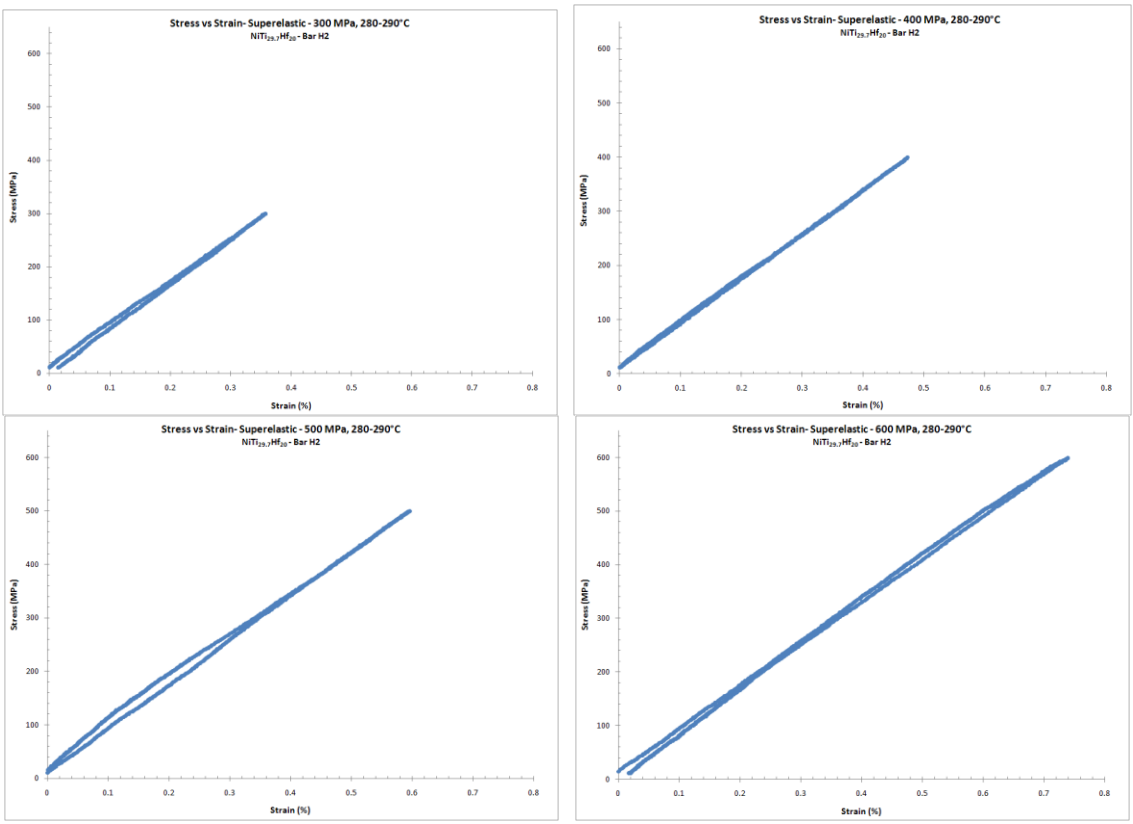

Figure 52: Superelastic stress vs. strain curves from 300 to 600 MPa ($NiTi_{29.7}Hf_{20}$ alloy, Bar H2)

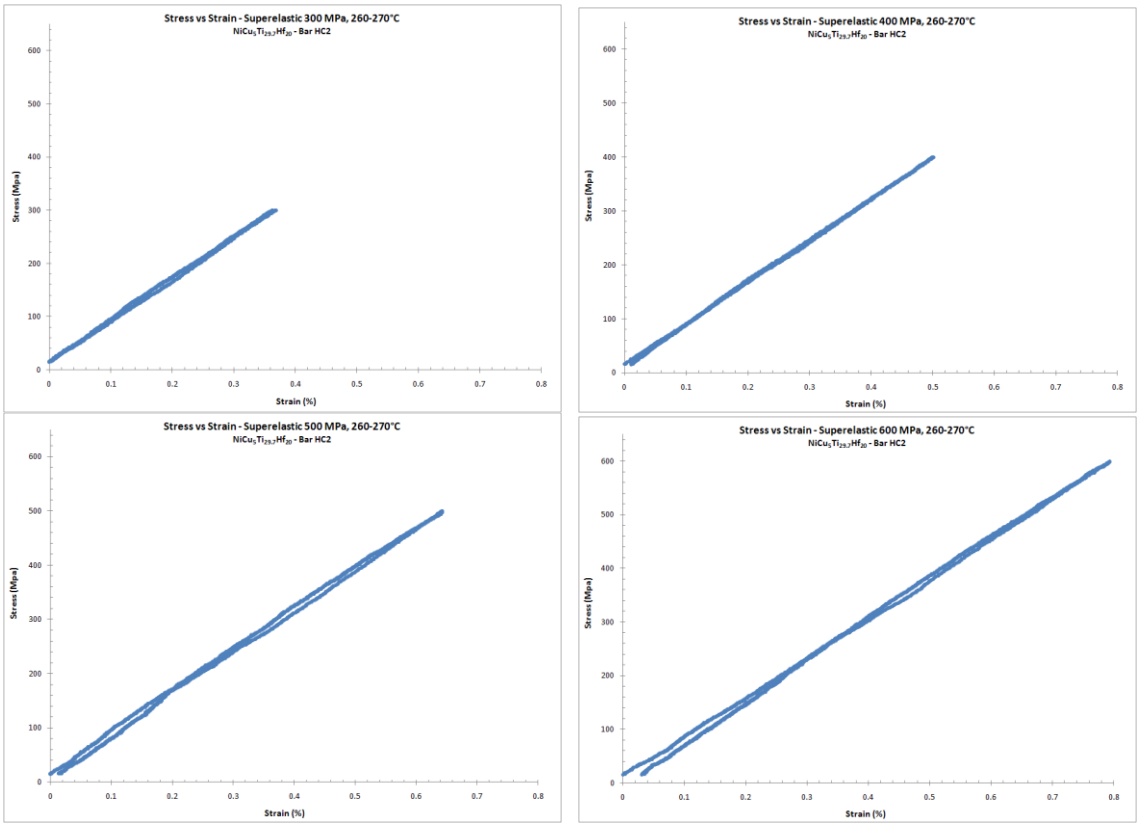

Figure 53: Superelastic stress vs. strain curves from 300 to 600 MPa ($NiCu_5Ti_{29.7}Hf_{20}$ alloy, Bar HC2)

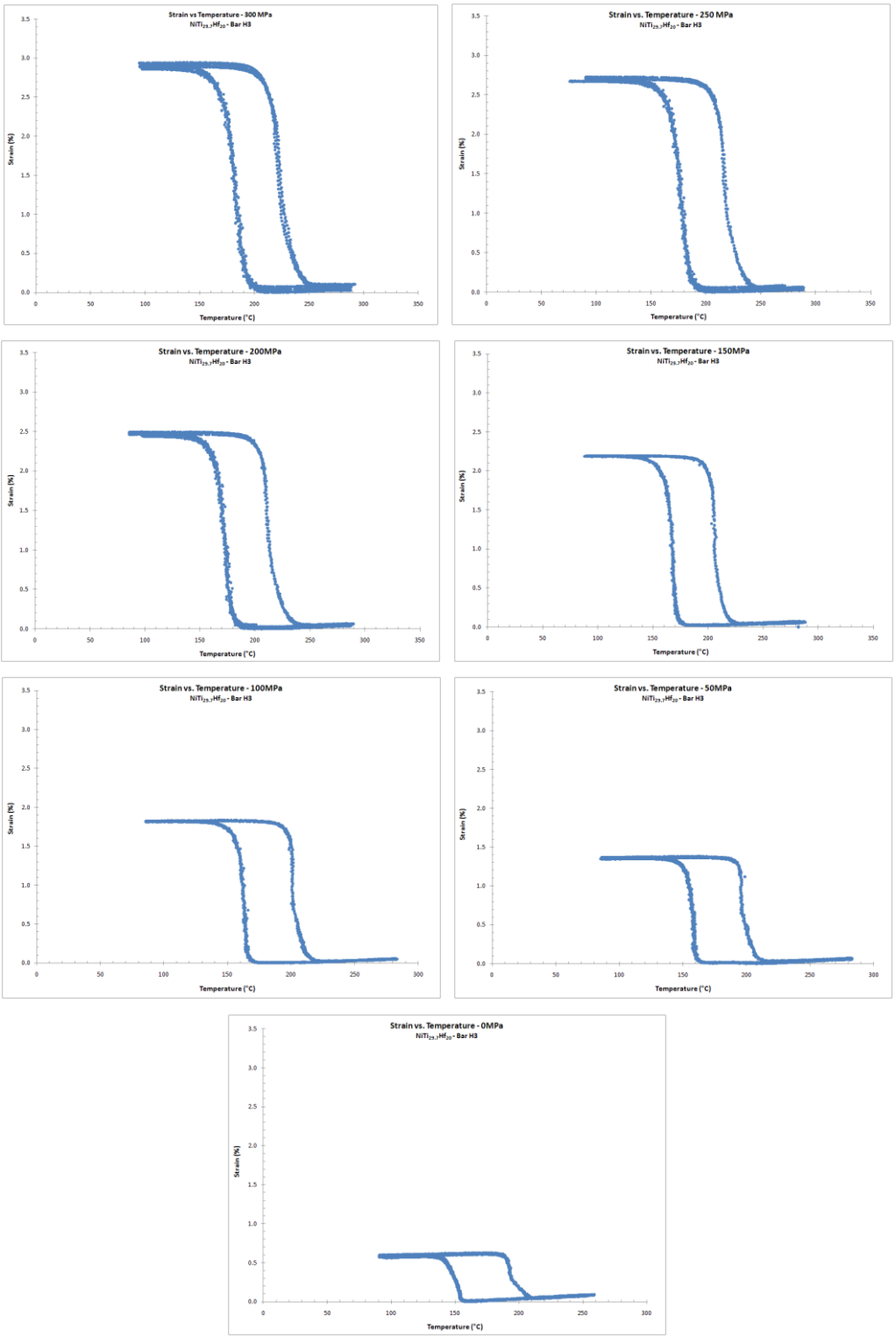

Figure 54: Actuation strains of $NiTi_{29.7}Hf_{20}$ (bar H3) trained at 300 MPa, 290°C; stress levels vary from 300 to 0 MPa

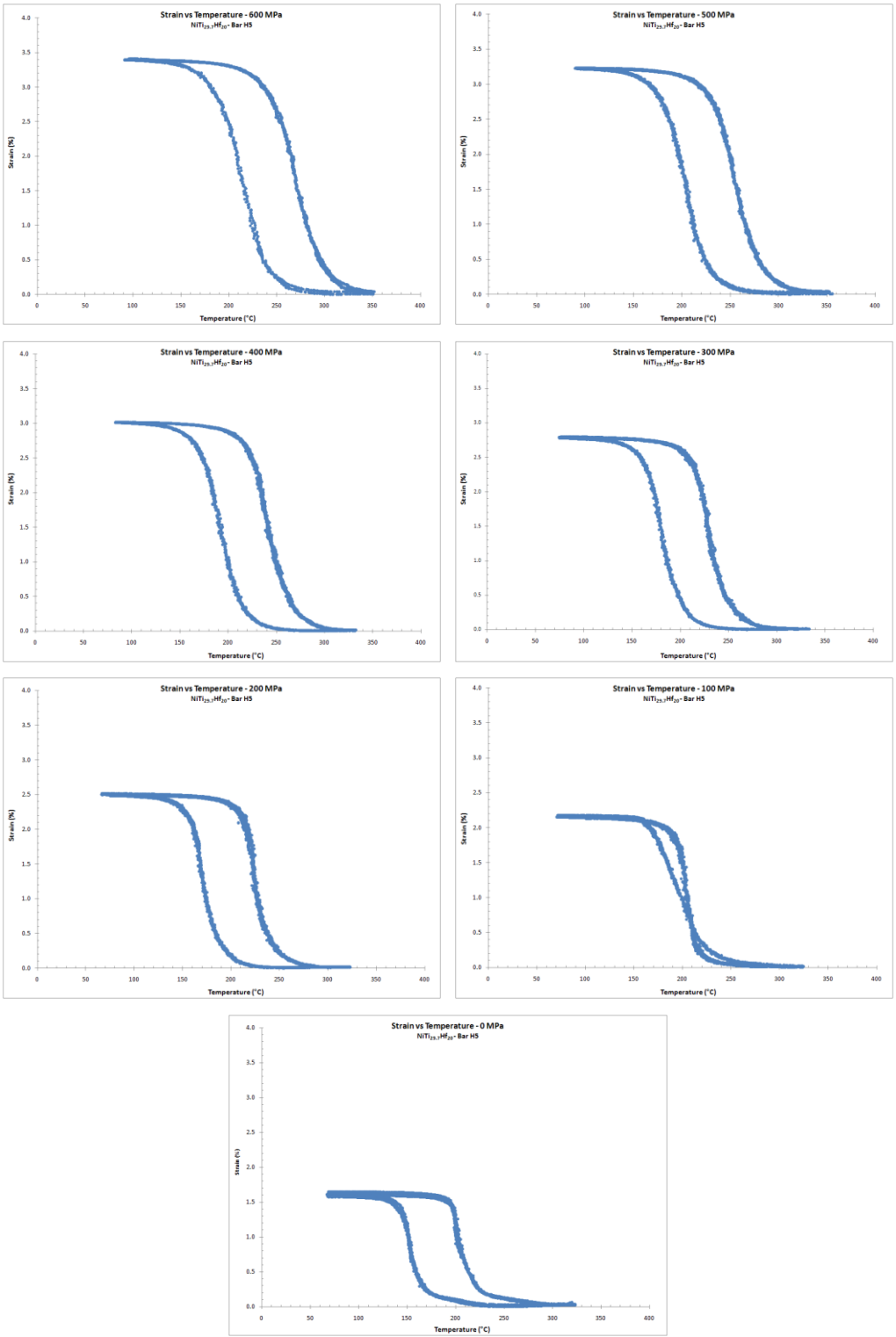

Figure 55: Actuation strains of $NiTi_{29.7}Hf_{20}$ (bar H5) trained at 600 MPa, 350°C; stress levels vary from 600 to 0 MPa

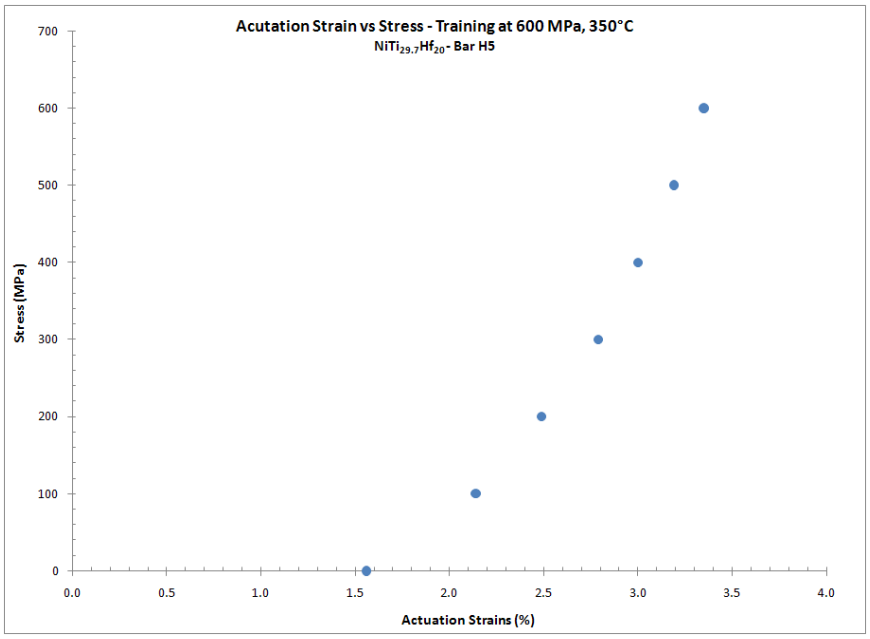

Figure 56: Actuation strains vs. stress for $NiTi_{29.7}Hf_{20}$ (bar H5) trained at 600 MPa, 350°C

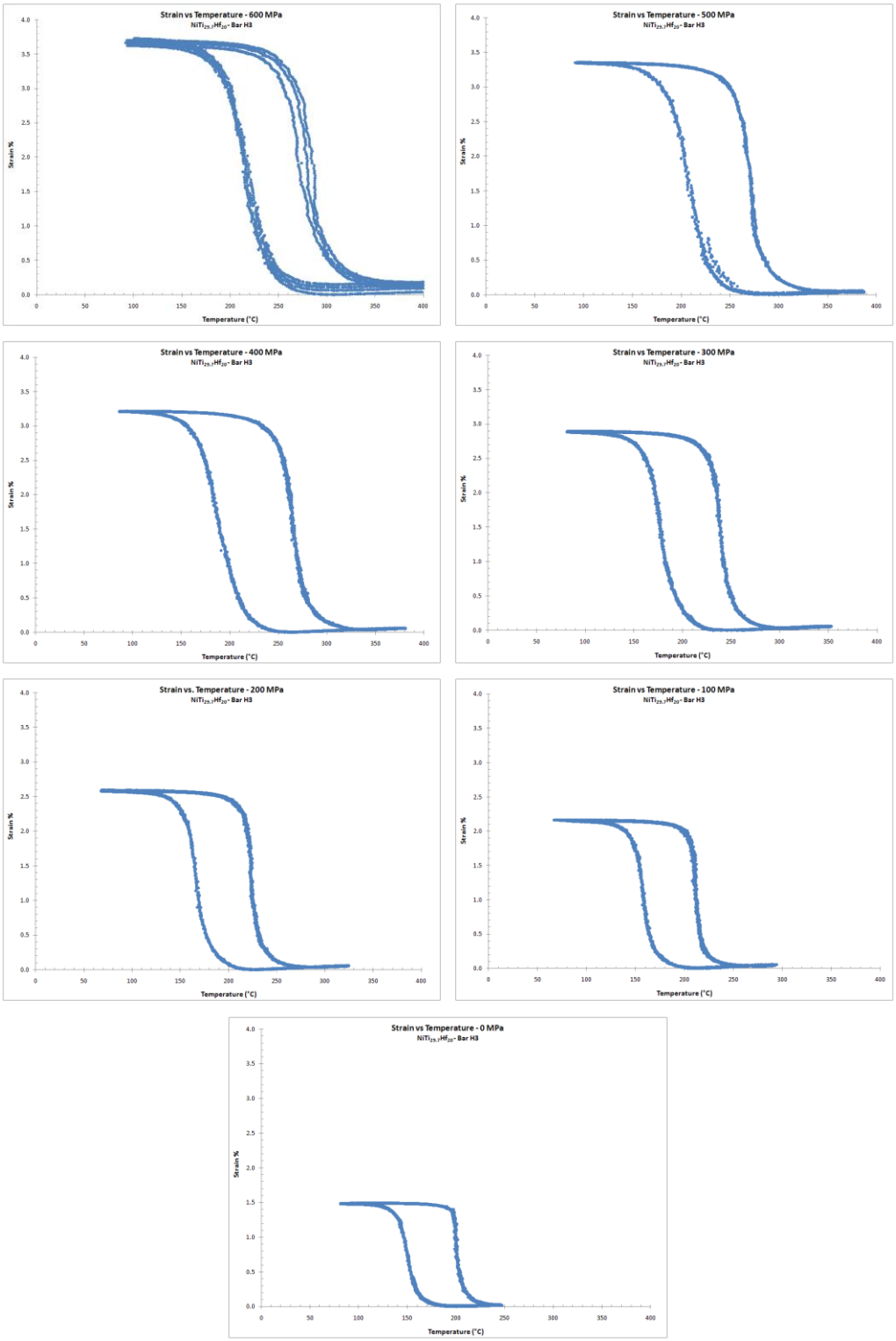

Figure 57: Actuation strains of $NiTi_{29.7}Hf_{20}$ (bar H6) trained at 600 MPa, 400°C; stress levels vary from 600 to 0 MPa

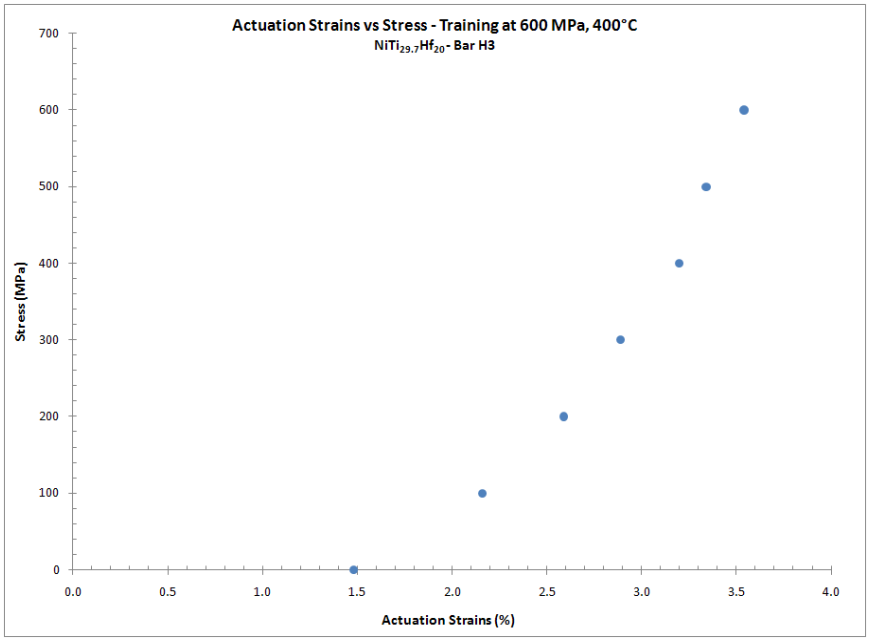

Figure 58: Actuation strains vs. stress for $NiTi_{29.7}Hf_{20}$ (bar H5) trained at 600 MPa, 400°C

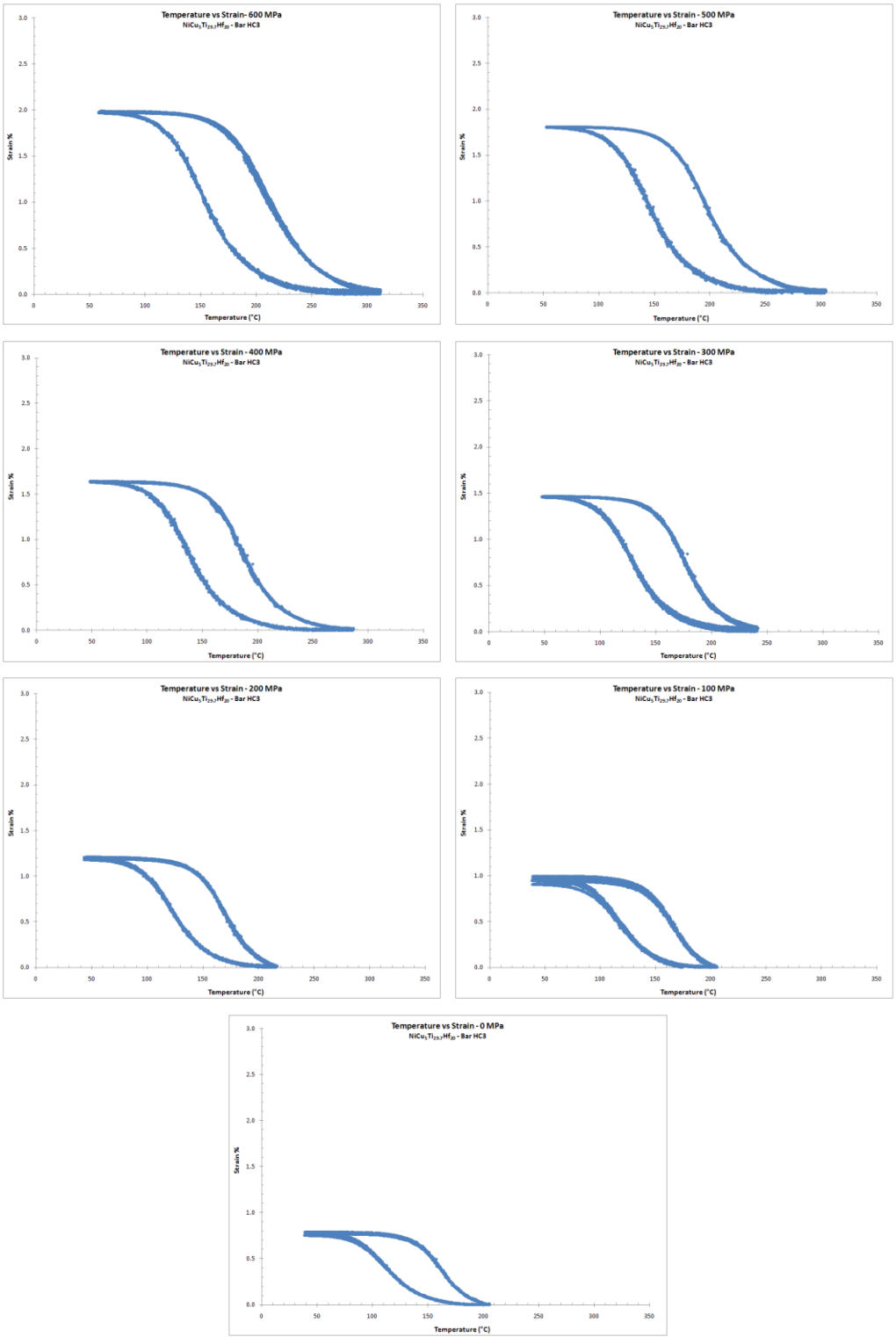

Figure 59: Actuation strains of $NiCu_5Ti_{29.7}Hf_{20}$ (bar HC3) trained at 600 MPa, 300°C; stress levels vary from 600 to 0 MPa

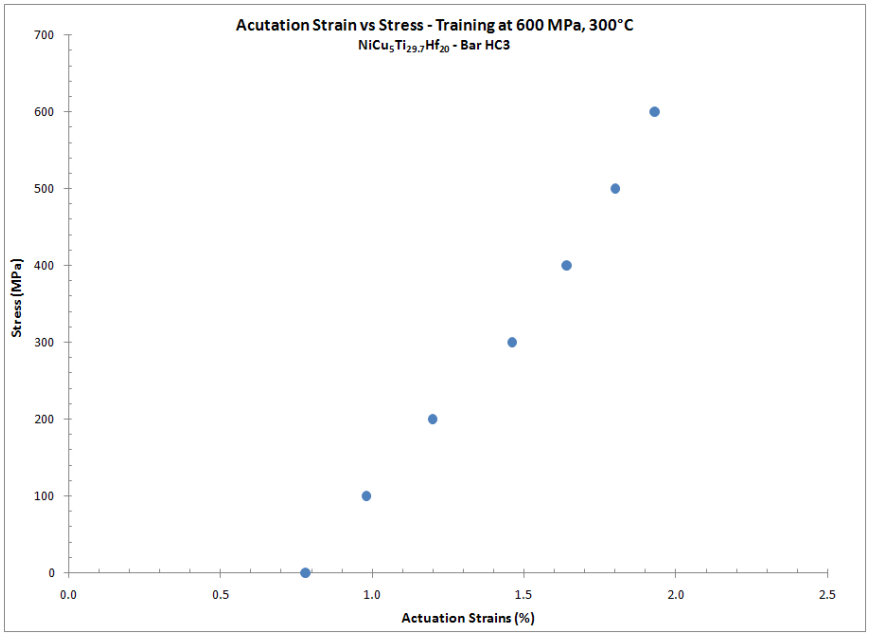

Figure 60: Actuation strains vs. stress for $NiCu_5Ti_{29.7}Hf_{20}$ (bar HC3) trained at 600 MPa, 300°C

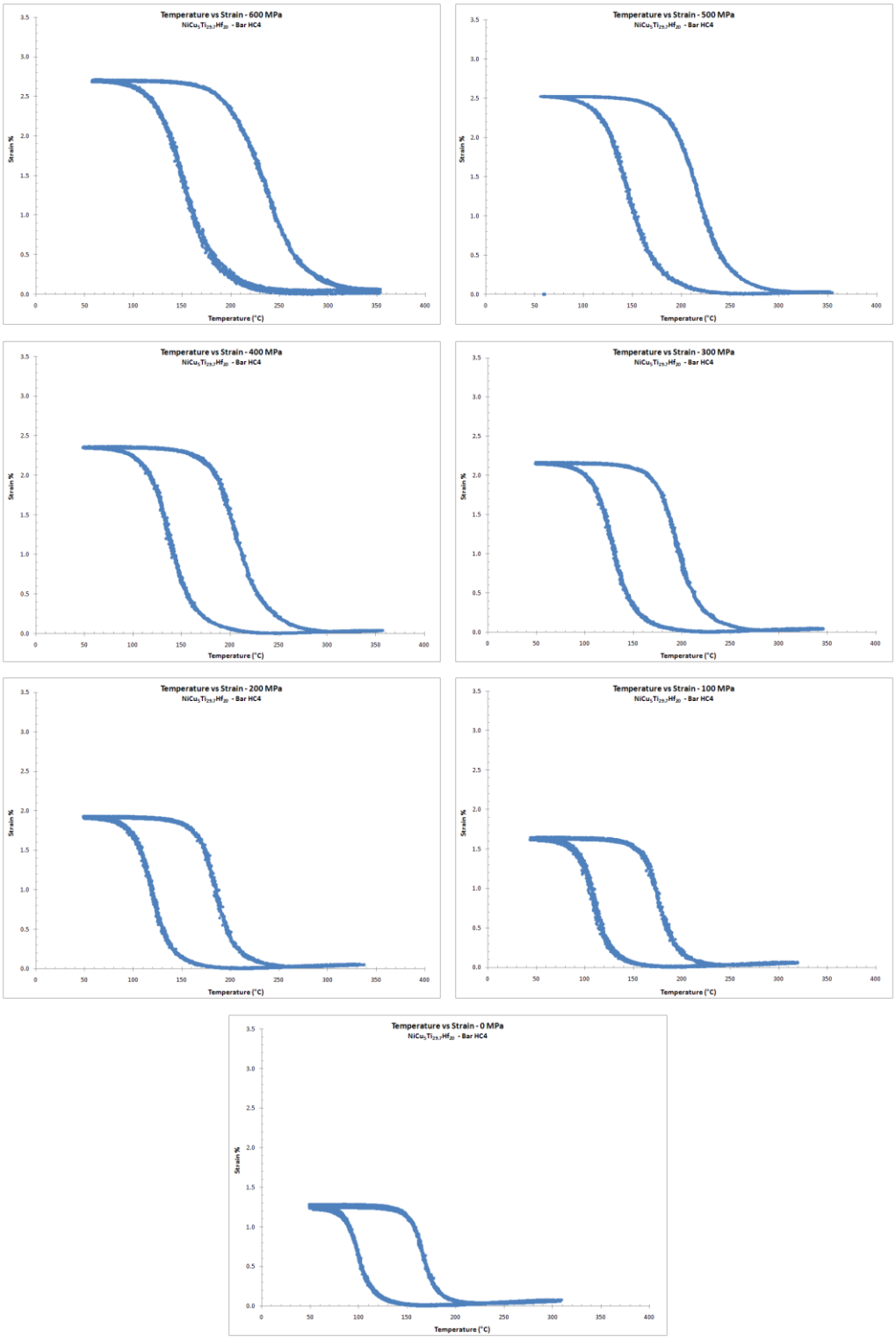

Figure 61: Actuation strains of $NiCu_5Ti_{29.7}Hf_{20}$ (bar HC4) trained at 600 MPa, 350°C; stress levels vary from 600 to 0 MPa

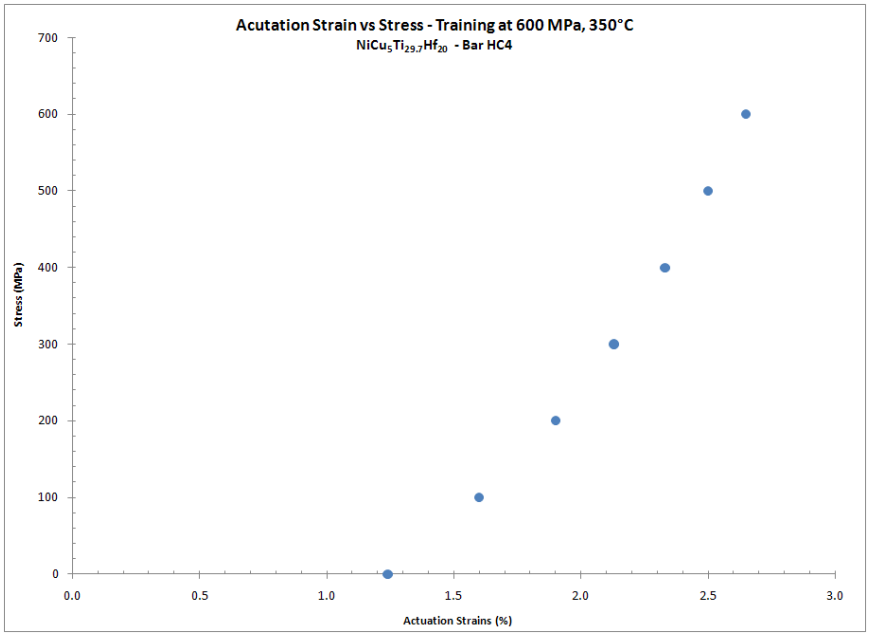

Figure 62: Actuation strains vs. stress for $NiCu_5Ti_{29.7}Hf_{20}$ (bar HC5) trained at 600 MPa, 350°C

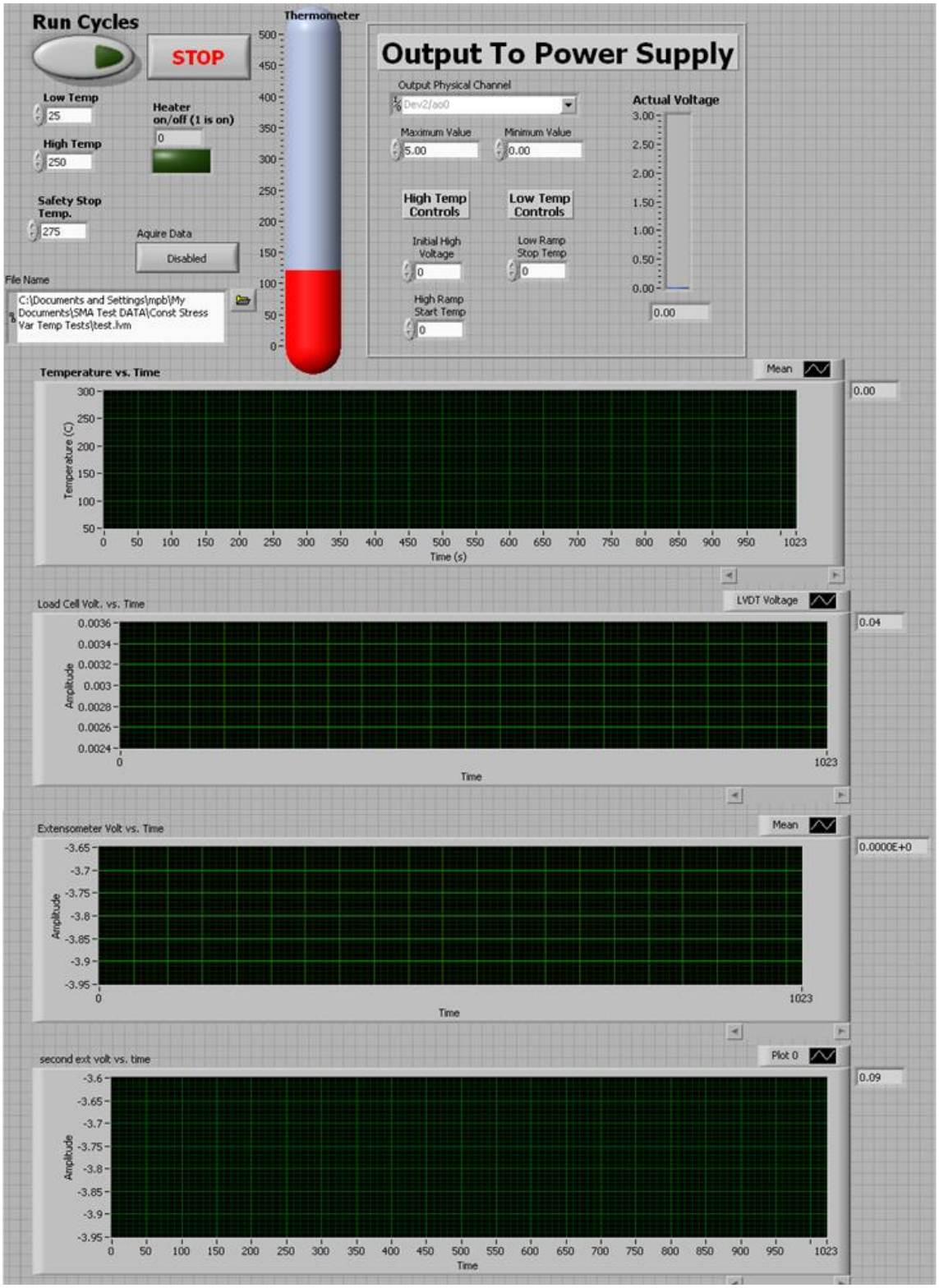

Figure 63: Example screenshot of LabVIEW front panel

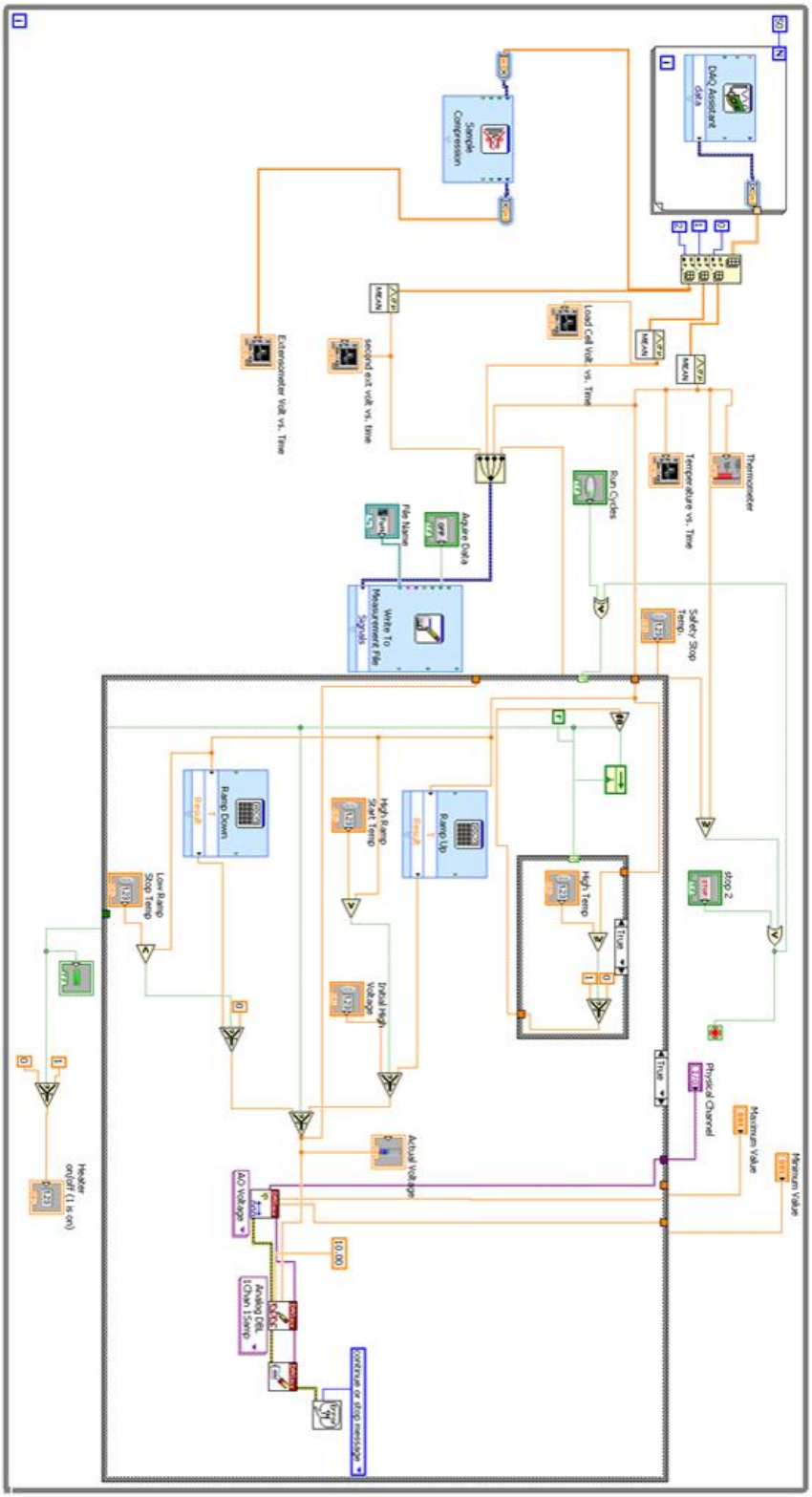

Figure 64: Example screenshot of LabVIEW block diagram